

Matrix Isolation Spectroscopy of Small Molecules: An *ab initio* Modeling Study

Inaugural-Dissertation
to obtain the academic degree
Doctor rerum naturalium (Dr. rer. nat.)

submitted to the Department of Biology, Chemistry, Pharmacy
of Freie Universität Berlin

by

Frederik Bader

June 2021

The work described in this dissertation was done under the supervision of Prof. Dr. Beate Paulus at the Institute of Chemistry and Biochemistry of Freie Universität Berlin starting from April 2018 until June 2021.

First Reviewer: Prof. Dr. Beate Paulus

Second Reviewer: Prof. Jean Christophe Tremblay, Ph.D.

Date of defense: July 22, 2021

Selbstständigkeitserklärung

Hiermit erkläre ich, dass ich die vorliegende Dissertation selbstständig und nur mit den angegebenen Hilfsmitteln und Quellen angefertigt habe. Alle Stellen, die wörtlich oder sinngemäß aus anderen veröffentlichten Arbeiten stammen, sind entsprechend gekennzeichnet. Des Weiteren versichere ich, dass die vorliegende Arbeit, weder im Ganzen noch in Teilen, für eine andere Prüfung angefertigt wurde.

Danksagung

Zuerst möchte ich mich bei meiner Betreuerin Prof. Dr. Beate Paulus bedanken, für die Möglichkeit, diese Arbeit in ihrer Gruppe anzufertigen, für die inhaltliche und finanzielle Unterstützung und auch für die Freiheit, das Projekt ganz nach meinen Vorstellungen zu gestalten. Abgesehen davon haben ihre Lehrveranstaltungen, an denen ich als Student und Tutor teilgenommen habe, mein Interesse an der theoretischen Chemie geweckt und meine Kenntnisse maßgeblich geprägt.

An zweiter Stelle bedanke ich mich bei Prof. Jean Christophe Tremblay, Ph.D., für die Übernahme des Zweitgutachtens, aber viel mehr für die Zusammenarbeit während des zweiten Abschnitts des Projekts. Unsere Diskussionen führten stets zu neuen Impulsen für meine Arbeit sowie gehobener Laune und neuer Hoffnung.

Ich möchte mich ebenfalls bei Prof. Dr. Sebastian Riedel, Dr. habil. Helmut Beckers, Dr. Carsten Müller und Dr. Frenio Redeker für die experimentelle Basis meines Projekts sowie für gelegentlich anfallende Gespräche zu meinen Rechnungen bedanken.

Vielen Dank an die Zentraleinrichtung für Datenverarbeitung (ZEDAT) der Freien Universität Berlin für das Bereitstellen von Rechenkapazitäten und Beantworten meiner Fragen.

Das Land Berlin hat meine Arbeit mit dem Elsa-Neumann-Stipendium gefördert - dafür vielen Dank.

Bei den Arbeitsgruppen der theoretischen Chemie bedanke ich mich für das freundliche Arbeitsumfeld. Insbesondere Tilen Lindic möchte ich für seinen Beitrag zu meiner Arbeit danken, den er in einem Forschungspraktikum geleistet hat.

Dann wäre da noch mein Büropartner Dr. Tobias Serwatka zu nennen. Während der letzten Jahre war er immer bereit über Sinn und Unsinn verschiedenster Art zu diskutieren und fungierte zuverlässig als Wegbereiter für gehobene Blutzuckerspiegel um Ostern und Weihnachten. Vielen Dank für den angenehmen Alltag.

Meinen Freunden bin ich sehr dankbar für ihre Geduld und Nachsicht mit mir, sowie ihr gutes Zureden, für die Freude, die sie mir bereiten, und nicht zuletzt für die Zerstreuung, die sie mir ermöglichen. Das alles gilt auch für Julia, die dieses Kunststück seit etwa drei Jahren fast täglich zu vollbringen vermag. Zuletzt möchte ich mich bei meiner Familie, besonders aber bei meinen Eltern bedanken, die mich seit jeher in allem unterstützen und ermutigen.

Abstract

Matrix isolation spectroscopy refers to experimental techniques that consist of trapping chemical compounds in inert frozen matrices and examining them with spectroscopic methods. As matrix isolation is commonly used to investigate very reactive species not stable outside of the matrices, theoretical modeling is often key to understanding the measured spectra. It is also crucial to comprehend the effect of the environment on the guest species, which expresses itself in experiment through matrix effects.

The objective of this thesis is implementing a workflow that allows for highly accurate modeling of small molecules in rare gas environments. The procedure facilitates the analysis of matrix isolation experiments on a microscopic level by associating observed vibrational signals with particular structural environments. Through that, additional insights provided by theory can be used to further characterize the experimental situation.

The first part of the work consists of assessing the requirements for structural cluster models to faithfully describe extended guest-matrix systems. To this end, carbon dioxide in argon matrices is investigated with density functional theory methods. The comparison of calculations using periodic boundary conditions with cluster models shows the importance of including multiple shells of host atoms around the guest. After that, a modeling procedure is established, which is used to examine the vibrational properties of trifluoride anions in neon and argon matrices. Based on truncated forms of many-body expanded potential energy surfaces, optimized guest-host environments are isolated from extended trifluoride-rare gas clusters. These are used to determine anharmonic vibrational properties of the entrapped trifluoride. For particular guest-host structures the results produced by the workflow are in almost quantitative agreement with experimental observations, indicating that these are the environments present in experiment. Beyond that, the analyses of the models with respect to structure, stability and vibrations reveal the effect of certain guest-host and host-host interaction types in the trifluoride-matrix systems.

Kurzzusammenfassung

Matrixisolationsspektroskopie beschreibt experimentelle Techniken, die daraus bestehen, chemische Verbindungen in inerten festen Matrizen zu isolieren und mit spektroskopischen Methoden zu charakterisieren. Da Matrixisolation typischerweise dazu genutzt wird, hochreaktive Verbindungen zu untersuchen, welche außerhalb der Matrizen nicht stabil sind, ist theoretische Modellierung oftmals entscheidend, um die gemessenen Spektren zu verstehen. Außerdem ist sie notwendig, um den Einfluss der Umgebung auf die Gastspezies, der sich im Experiment durch sogenannte Matrix-Effekte äußert, nachzuvollziehen.

Das Ziel dieser Arbeit ist es, ein Schema einzuführen, welches das hochgenaue Modellieren kleiner Moleküle in Edelgas-Matrizen erlaubt. Diese Prozedur ermöglicht die Analyse von Matrixisolationsexperimenten auf der mikroskopischen Ebene, indem sie beobachtete Schwingungsübergänge bestimmten strukturellen Umgebungen zuweist. Dadurch können die zusätzlichen der Theorie zugänglichen Informationen genutzt werden, um das Experiment gründlicher zu charakterisieren.

Der erste Teil dieser Arbeit befasst sich mit den Anforderungen an strukturelle Cluster-Modelle im Hinblick auf deren Beschreibung eines ausgedehnten Gast-Matrix-Systems. Dazu wird Kohlenstoffdioxid in Argon-Matrizen mit Methoden der Dichtefunktional-Theorie untersucht. Der Vergleich von Rechnungen, die periodische Randbedingungen ausnutzen, mit Cluster-Modellen verdeutlicht die Notwendigkeit, mehrere Schalen der den Gast umgebenden Wirt-Atome zu berücksichtigen. Im Anschluss daran wird eine Modellierungsprozedur aufgebaut, die dazu genutzt wird, die Schwingungseigenschaften eines Trifluorid-Anions in Neon- und Argon-Matrizen zu untersuchen. Basierend auf Mehrkörperentwicklungen der Potentialhyperflächen werden optimierte Gast-Wirt-Umgebungen aus größeren Trifluorid-Edelgas-Clustern bestimmt. Mit diesen wird das anharmonische Schwingungsverhalten des eingeschlossenen Trifluorids berechnet. Für bestimmte Gast-Wirt-Strukturen liefert die Modellierung Ergebnisse in quantitativer Übereinstimmung mit den experimentellen Beobachtungen. Das deutet darauf hin, dass diese Umgebungen im Experiment beobachtet werden. Darüber hinaus offenbaren die Analysen der Modelle im Hinblick auf Struktur, Stabilität und Schwingungen die Wirkung bestimmter Gast-Wirt- und Wirt-Wirt-Wechselwirkungsmuster in den Trifluorid-Matrix-Systemen.

Contents

List of Figures	XIII
List of Tables	XV
List of Abbreviations	XVII
List of Publications	XIX
1 Introduction	1
2 Theoretical Basics	7
2.1 The Molecular Schrödinger Equation	8
2.2 The Electronic Schrödinger Equation	10
2.3 The Nuclear Schrödinger Equation	31
3 Summary	47
3.1 Carbon Dioxide in Argon - Preparation Phase	47
3.2 Trifluoride in Neon - Establishing the Model	52
3.3 Trifluoride in Argon - Extending the Model	58
3.4 Conclusion and Outlook	61
4 Publications	65
Bibliography	119

List of Figures

2.1	Rotation of coordinate systems	33
3.1	CO ₂ -argon model structures	49
3.2	Trifluoride-neon models	55
3.3	Trifluoride-argon environments	59

List of Tables

2.1	Coordinate systems for internal coordinates	36
-----	---	----

List of Abbreviations

B3LYP - Becke-3-Lee-Yang-Parr
BF - body-fixed (coordinate system)
BOA - Born-Oppenheimer approximation
CCSD - coupled cluster with single and double excitations
CCSDT - coupled cluster with single, double and triple excitations
CCSD(T) - coupled cluster with single, double and perturbative triple excitations
CI - configuration interaction
CIS - configuration interaction with single excitations
CISD - configuration interaction with single and double excitations
CSF - configuration state function
DCRW - dynamic cell rigid wall
DFT - density functional theory
DVR - discrete variable representation
FBR - finite basis representation
GGA - generalized gradient approximation
HF - Hartree-Fock
KS - Kohn-Sham
LCAO - linear combination of atomic orbitals
LDA - local density approximation
LYP - Lee-Yang-Parr
MBE - many-body expansion
MH - minima hopping
MP2 - second-order Møller-Plesset perturbation theory
PBE - Perdew-Burke-Ernzerhof
PBE0 - Perdew-Burke-Ernzerhof hybrid functional
PES - potential energy surface

PIP - permutationally invariant polynomials
PW91 - Perdew-Wang 91
RHHF - Roothaan-Hall-Hartree-Fock
TI - translationally invariant
UV/vis - ultra-violet and visible
VBR - variational basis representation
VCC - vibrational coupled cluster
VCI - vibrational configuration interaction
VPT2 - second-order vibrational perturbation theory
VRT - vibration-rotation-translation
VSCF - vibrational self-consistent field

List of Publications

Main Publications

Paper A

F. Bader, T. Lindic and B. Paulus

"A Validation of Cluster Modeling in the Description of Matrix Isolation Spectroscopy"

J. Comput. Chem., 2020, **41**, 751–758.

Paper B

F. Bader, J. C. Tremblay and B. Paulus

"A pair potential modeling study of F_3^- in neon matrices"

Phys. Chem. Chem. Phys., 2021, **23**, 886–899.

Paper C

F. Bader, J. C. Tremblay and B. Paulus

"Theoretical modeling of molecules in weakly interacting environments: Trifluoride anions in argon"

manuscript submitted to *Physical Chemistry Chemical Physics* on May 26, 2021

Additional Publications

Paper E1

F. Bader, S. Riedel, H. Beckers, C. Müller, J. C. Tremblay and B. Paulus

"The Peculiar Interaction of Trifluoride Anions with Cryogenic Rare Gas Matrices"

manuscript submitted to *The Journal of Physical Chemistry Letters* on May 19, 2021

Chapter 1

Introduction

The functionality of a variety of chemical systems is rooted in non-covalent interactions.^[1] For instance, in protein folding dynamics the non-covalent interactions within the peptide chain as well as the solvent drive the formation of the native state of the protein.^[2,3] Likewise, they affect the assembly of supermolecular aggregates in the field of molecular machines^[4] and can influence regio- and enantioselectivity in catalytic reactions.^[5-7] Compared to covalent bonds, the non-covalent interactions are more delicate. Their individual influence reaches farther, but is less strong and directional.^[5] Accordingly, when aiming for specific manipulations of large systems through these weak interactions, a firm comprehension of the underlying physical forces on a fundamental level is crucial. With respect to the latter, rare gases are of a peculiar significance, because their interactions are predominantly non-covalent and dispersive. As a result weakly bound di- or trimers involving rare gas atoms are well suited to study the subtleties of interactions with non-covalent character.^[8-10] In extended rare gas environments enclosed chemical systems are perturbed solely by weak dispersive forces. This can be used to approximate industrially relevant solute-solvent systems and study corresponding solute reactions in reduced complexity.^[11-13] Moreover, the inert character of the environments can be exploited to effectively stabilize and subsequently examine even very unstable guest species, such as weakly interacting molecular aggregates or highly reactive molecules. An experimental procedure based on this notion is matrix isolation.

Introduced in 1954 by George Pimentel, the matrix isolation technique consists of trapping chemical compounds in inert frozen materials at very low temperatures.^[14] Embed-

ded in the matrices, the isolated guest systems are protected from other reactive molecules. Moreover, due to the low temperatures diffusion and internal decomposition reactions are mostly avoided.^[14-16] Correspondingly, the entrapped compounds are stabilized compared to other environments, allowing for the synthesis of new highly reactive species, molecular aggregates as well as reaction intermediates and facilitating an in-depth study of the molecular properties. Various experimental schemes can be deployed to influence the guest species and the matrix environment: The degree of interactions among the guest molecules can be tuned through the ratio of concentrations of the matrix material and the investigated species, potentially effecting oligomerizations.^[17,18] Moreover, the formation of matrix environments is affected by the deposition conditions.^[19] Temperature annealing is used to investigate the stability of guests and matrix environments and to initiate intramolecular conversions and reactions among neighboring entrapped species.^[17,20-26] In a similar way, photo excitations can be exploited to probe the stability of the investigated species and evoke conversion, dissociation and recombination reactions.^[20-28] Another helpful procedure is isotopic labeling of the guest, as the resulting isotope effects may help to identify the entrapped species.^[18,29,30] The characterization of the guest molecule is typically achieved by spectroscopic methods. Vibrational properties are commonly obtained by infra-red and Raman spectroscopy. Also, UV/vis spectroscopy^[31,32] and electron paramagnetic resonance measurements^[33,34] are used to characterize molecules entrapped in matrices. The present work, however, concerns only vibrational matrix isolation spectroscopy.

Regarding the investigation of molecular motion through vibrational spectroscopy, the presence of a matrix environment and the experimental conditions have several ramifications. The low temperatures in the matrix isolation experiments result in guest molecules in their vibrational and electronic ground state.^[35] As was mentioned before, molecular translations are strongly hindered, leaving most guest species strictly isolated after the formation of the guest-host environment. Likewise, because of the confinement in the matrix overall rotations of the guest molecules are in many cases quenched. Exceptions to this are small molecules such as water and methane, but even for them only a small number of rovibrational transitions are observed due to the low temperatures.^[36,37] Aside from these general effects, the particular interactions between the guest molecule and the matrix environment may affect intrinsic properties of the guest, for instance the molecular geometry and vibrational excitation energies. In order to reduce this influence and ascertain weak guest-host interactions, typically used matrix materials are rare gases.^[15] Due to their inertness and the dispersive character of their interactions, the rare gas atoms' in-

fluence on guest molecules is rather delicate. Accordingly, the properties of the entrapped species are in many cases altered only to a small extent compared to the gas phase at very low concentrations. Because of an increased polarizability of the matrix atoms stronger guest-host interactions are found in matrices of heavier rare gases.^[35] In principle, all of the aforementioned effects on the guest species should lead to comprehensible spectra with rather sharp signals, which are appropriate for investigating processes such as isomerizations and intramolecular tunneling.^[27,38–40]

Yet, actual vibrational spectra of matrix-isolated species are often complicated by the appearance of matrix effects, caused by the influence of the environment on the guest.^[15,41] Most straightforwardly, the guest-host interactions in a particular matrix environment may perturb the vibrational excitations of the guest molecule. Typically, this results in small signal shifts compared to (experimental or calculated) reference data for the free molecule, which by themselves do not complicate the spectra significantly.^[35,41] However, the occurrence of multiple trapping sites characterized by different guest-host interaction patterns and therefore matrix shifts may introduce additional spectral signals; these are the commonly observable site effects. Likewise, the presence of an environment can cause a signal splitting of degenerate molecular vibrations due to a reduced symmetry of the entrapped species compared to the free one.^[18,19] Additional complexity in the spectra can be the result of oligomerizations of the guest species or, for a few small molecules, rovibrational transitions.^[17,41] It was mentioned before that oligomerizations of the guest and the occurrence of guest-host environments can be affected by the experimental conditions during the matrix condensation as well as schemes such as temperature annealing. Correspondingly, these measures may be used to systematically study the behaviour of the entrapped species through the spectroscopic matrix effects. At first glance the latter may seem undesirable, as they produce more complex spectroscopic signatures and obscure the rather clear spectra expected for individual molecules isolated in a particular type of inert environment at very low temperatures. However, the matrix effects also grant the opportunity to gain a more detailed understanding of the matrix environment, the guest-host interactions and their effect on the entrapped species.

The matrix isolation technique is particularly useful for the investigation of very unstable and sometimes novel species, for which reference data of the free compounds does not necessarily exist. Especially in these cases the origin of the experimental observations is not always obvious from the experiment alone. Thus, it is a natural approach to complement the information provided by the matrix isolation experiments with a corresponding

theoretical study. Generally, the key to connecting reality, that is experiment, to the vast range of information accessible to theoretical methods is the reproduction of the measured properties. For instance, by finding a model that reliably yields vibrational frequencies in agreement with the experimentally observed ones, insights on the corresponding structural and thermodynamical properties become available.

The complexity of a theoretical investigation of matrix isolation experiments is strongly tied to its objective and the examined species. If the product of the experimental procedure is unknown, but several likely candidates exist, the initial goal of the modeling is the identification of the entrapped species. With regards to that, it often suffices to disregard the matrix environment and investigate the free molecules.^[30,41–43] Concerning vibrational matrix isolation spectroscopy, the relevant properties for free molecules and smaller molecular aggregates may be assessed by a normal mode analysis or a more involved scheme on the basis of accurate quantum chemical calculations within the Born-Oppenheimer approximation. For compounds of small to moderate size and relatively simple electronic structure the complexity as well as the numerical expense of these calculations are manageable. Therefore, these types of quantum chemical schemes are very suitable companions for the matrix isolation experiments.

In contrast to that, an accurate theoretical investigation of complete guest-matrix systems and observed matrix effects is typically associated with significantly greater efforts. Different aspects factor into this. A thorough modeling approach of the matrix environment requires the description of not only a small number, but several shells of host atoms around the guest species. Only then the models are able to provide matrix environments, where the guest-host and host-host interactions are regarded in a balanced way. The result of considering a sizable number of matrix atoms is a drastically increased number of electronic and nuclear degrees of freedom in the quantum chemical calculations of electronic structure and nuclear motion¹. Naturally, this restricts the range of quantum chemical methods, which can be employed to describe the full system.

Concerning electronic structure, further important aspects of the theoretical description of matrix-isolated molecules are the treatment of the guest-host interactions as well as the guest itself. The former usually correspond to weak dispersive interactions, which are crucial to accurate modeling, but require further attention in electronic structure calculations. With respect to the latter aspect, molecules, for which matrix isolation can be particularly important – for instance weakly bound or radical compounds – may demand high-level

¹Note that nuclear motion may refer to nuclear properties obtained from either static, that is time-independent, calculations or dynamic schemes, where the system is propagated through time.

methods, which are intractable for extended systems as a whole. However, these obstacles can be reconciled by applying fragmentation-based quantum chemical methods relying on a decomposition of the compound systems' electronic energy, such as the method of increments^[44,45] and other many-body expansion or embedding schemes.^[46–48]

For the description of nuclear motion in extended guest-host systems, several questions arise. Regarding the guest, the relevance of vibrational anharmonicity, intermode coupling as well as uniform rotations and translations of the molecule in the matrix has to be assessed. If these aspects are key to obtaining results approaching high accuracy, a scheme beyond a normal mode analysis is required. This greatly increases the conceptual and numerical demands. Secondly, the effect of the matrix environment on the motion of the guest species needs to be considered. This influence may be split in two parts for a given matrix environment, that is a static and a dynamic contribution. The former describes the influence of a rigid host environment on the entrapped molecule and should comprise a large fraction of the matrix atoms' effect. On the other hand, the dynamic contribution to the matrix effect comprises the coupling of molecular to environmental motion. In order to grasp this part the host atoms have to be treated as moving particles. Moreover, for lighter matrix materials, such as *para*-H₂^[49,50] or helium in helium nano droplet isolation spectroscopy,^[51–53] a quantum treatment of the matrix environment may be necessary to approach physically sound results. Finally, the nuclear, in particular vibrational, properties can be determined from solving time-independent static problems, but also extracted from trajectories yielded by time-dependent, dynamic simulations.

In view of that, it is clear that the modeling of matrix effects can become quite complicated and is not suited to accompany every matrix isolation experiment. Nevertheless, it is very valuable to the development of insights on matrix isolation and the effect of weak guest-host interactions on different types of molecules, as the modeling may unlock information unavailable from experiment, provided it is accurate enough.

The aim of this work is to establish and apply a modeling procedure for the description of small molecules in cryogenic rare gas environments. The purpose of the modeling workflow is to determine vibrational excitation energies of the investigated molecule in different matrix structures. Through the calculated values the observations from matrix isolation experiments may be connected with particular guest-host environments. Based on this assignment, the structural and vibrational properties as well as the relative stabilities of the identified models can be further investigated. This should complement the experimental data for the investigated systems and supply additional insights on the

formation of the guest-host environments and the peculiarities of guest-host interactions involving rare gas atoms. In order to facilitate the assignment of a structural model to the experimental observations, the latter have to be reproduced to great accuracy. Correspondingly, the modeling procedure will be based upon electronic structure calculations with high-level quantum chemical correlation methods, extended cluster models of guest-host structures and vibrational analyses that account for anharmonicity and intermode coupling in the guest as well as the influence of the rare gas environment. With this foundation, the modeling procedure should be able to provide accurate vibrational excitations in a reliable and systematically improvable way.

In the next chapter the theoretical foundations of the quantum chemical methods relevant to this thesis are outlined. Then, in Chapter 3 the insights gained in the course of this work are summarized and discussed in the general context of theoretical modeling of matrix isolation experiments. Chapter 4 comprises the publications on which this thesis is based.

Chapter 2

Theoretical Basics

This chapter outlines the quantum chemical theory and methodology, on which this thesis is based. Starting from the time-independent Schrödinger equation, the widely used procedure of a separated treatment of electronic and nuclear degrees of freedom is motivated. Ensuingly, various schemes to solve the electronic part of the Schrödinger equation are described. The chapter is concluded with an account of important aspects of treating the nuclear Schrödinger equation. Equations are given in atomic units.

Several sections of this chapter follow the outlines given elsewhere. The presentation of the time-independent Schrödinger equation and Born-Oppenheimer approximation is similar to the ones in *Modern Quantum Chemistry* by Szabo and Ostlund^[54] and *Introduction to Quantum Mechanics: A Time-Dependent Perspective* by Tannor.^[55] The former book is also used for the description of Hartree-Fock theory, quantum chemical correlation and Møller-Plesset perturbation theory. To outline the coupled cluster and explicit correlation approaches *Electronic Structure Theory* by Helgaker, Jorgensen and Olsen^[56] and reviews by Bartlett *et al.*,^[57] Valeev *et al.*^[58] as well as Ten-no and Noga^[59] were considered. *A Chemist's Guide to Density Functional Theory* by Koch and Holthausen^[60] and *Theoretical Surface Science* by Groß^[61] served as guides to the illustration of density functional theory and calculations of periodic systems. The account of the nuclear Schrödinger equation is based on the Lennard-Jones lecture by Sutcliffe,^[62] the Perspective article by Császár *et al.*,^[63] the aforementioned book by Tannor^[55] and review articles by Light and collaborators.^[64,65] Finally, for the description of the vibrational self-consistent field method the works of Bowman *et al.*^[66,67] and Rauhut^[68] have been used.

2.1 The Molecular Schrödinger Equation

The starting point for this foray into the depths of quantum chemistry is the non-relativistic time-independent Schrödinger equation of a molecule in field-free space

$$\mathbf{H} \Psi(\vec{X}) = E \Psi(\vec{X}) \quad , \quad (2.1)$$

where \mathbf{H} and Ψ are the molecular Hamilton operator and wave function (or state), respectively, and the total energy is given by E . The coordinate vector \vec{X} contains the electronic and nuclear spatial and spin coordinates. For an unperturbed system the Hamiltonian comprises operators describing the kinetic energies of electrons and nuclei, \mathbf{T}_e and \mathbf{T}_n , as well as the Coulomb interactions among these particles, that is \mathbf{V}_{e-e} , \mathbf{V}_{e-n} and \mathbf{V}_{n-n} . The operators are defined in Equations (2.2) in atomic units with respect to a system of N nuclei and n electrons. M_α , Z_α , \vec{R}_α , \vec{r}_i refer to the mass of nucleus α , its charge and position as well as the position of electron i .

$$\mathbf{H} = \mathbf{T}_n + \mathbf{V}_{n-n} + \mathbf{T}_e + \mathbf{V}_{e-e} + \mathbf{V}_{n-e} \quad , \quad (2.2a)$$

$$\mathbf{T}_n = - \sum_{\alpha=1}^N \frac{1}{2M_\alpha} \Delta_\alpha \quad , \quad (2.2b)$$

$$\mathbf{V}_{n-n} = \sum_{\alpha=1}^N \sum_{\beta>\alpha}^N \frac{Z_\alpha Z_\beta}{|\vec{R}_\alpha - \vec{R}_\beta|} \quad , \quad (2.2c)$$

$$\mathbf{T}_e = -\frac{1}{2} \sum_{i=1}^n \Delta_i \quad , \quad (2.2d)$$

$$\mathbf{V}_{e-e} = \sum_{i=1}^n \sum_{j>i}^n \frac{1}{|\vec{r}_i - \vec{r}_j|} \quad , \quad (2.2e)$$

$$\mathbf{V}_{n-e} = - \sum_{\alpha=1}^N \sum_{i=1}^n \frac{Z_\alpha}{|\vec{R}_\alpha - \vec{r}_i|} \quad . \quad (2.2f)$$

Solving the time-independent Schrödinger equation is very complicated and once the investigated system contains multiple electrons or nuclei analytically intractable. Then, the solutions have to be approximated by taking purposeful steps to simplify the problem. Typically, at the start of solving the time-independent Schrödinger equation is the separation into an electronic and a nuclear problem. This approach is physically motivated in the sense that electrons move significantly faster than nuclei due to their smaller mass. In

accordance to that, the electrons should adapt to nuclear motion immediately, rendering the nuclear coordinates parameters in the electronic problem. On the formal level, this is incorporated into the molecular wave function through

$$\Psi(\vec{r}, \vec{R}) = \xi(\vec{R}) \Phi(\vec{r}; \vec{R}) \quad , \quad (2.3)$$

meaning that Ψ is considered to be separable into nuclear and electronic wave functions, $\xi(\vec{R})$ and $\Phi(\vec{r}; \vec{R})$. In Equation (2.3) and the remaining section, the dependence on the electronic and nuclear spin coordinates is neglected for simplicity. Notably, the electronic part depends on the nuclear coordinates only parametrically. Moreover, an electronic Schrödinger equation,

$$H_{\text{el}} \Phi(\vec{r}; \vec{R}) = (T_{\text{e}} + V_{\text{e-e}} + V_{\text{n-e}} + V_{\text{n-n}}) \Phi(\vec{r}; \vec{R}) = E_{\text{el}}(\vec{R}) \Phi(\vec{r}; \vec{R}) \quad , \quad (2.4)$$

can be formulated. Herein, the nuclei are considered frozen, resulting in an electronic Hamiltonian with $T_{\text{n}} = 0$ and constant $V_{\text{n-n}}$. This is called the clamped nuclei approximation. Equation (2.4) yields the electronic energy E_{el} for a given electronic state Φ depending on the nuclear configuration \vec{R} . The complete set of electronic energies (including the contribution of the $V_{\text{n-n}}$ potential) for all nuclear configurations and a given electronic state is called a potential energy surface (PES). It represents an average potential affecting the nuclear motion. Principally, there are different solutions to the electronic problem, that is various electronic states. In fact, the molecular wave function may be expressed by means of the complete set of electronic states for any nuclear configuration according to the expansion

$$\Psi(\vec{r}, \vec{R}) = \sum_k \xi_k(\vec{R}) \Phi_k(\vec{r}; \vec{R}) \quad . \quad (2.5)$$

To obtain approximations of the full molecular wave functions and total energies the nuclei have to be treated as well. After inserting the electronic Schrödinger equation and the expansion in Equation (2.5) into Equation (2.1),

$$H \Psi(\vec{r}, \vec{R}) = E \Psi(\vec{r}, \vec{R}) = \sum_k \left(T_{\text{n}} + E_{\text{el},k}(\vec{R}) \right) \xi_k(\vec{R}) \Phi_k(\vec{r}; \vec{R}) \quad , \quad (2.6)$$

projecting Equation (2.6) onto an electronic state Φ_j^* and integrating over the electronic

coordinates the nuclear problem is defined as

$$\begin{aligned}
 E \xi_j(\vec{R}) = & \sum_k (\mathbf{T}_n + E_{\text{el},k}) \xi_k(\vec{R}) \delta_{jk} \\
 & - \sum_k \sum_\alpha \frac{1}{M_\alpha} \left(\int \Phi_j^*(\vec{r}; \vec{R}) \vec{\nabla}_\alpha \Phi_k(\vec{r}; \vec{R}) d\vec{r} \right) \vec{\nabla}_\alpha \xi_k(\vec{R}) \\
 & - \sum_k \sum_\alpha \frac{1}{2M_\alpha} \left(\int \Phi_j^*(\vec{r}; \vec{R}) \Delta_\alpha \Phi_k(\vec{r}; \vec{R}) d\vec{r} \right) \xi_k(\vec{R}) .
 \end{aligned} \tag{2.7}$$

The last two lines in Equation (2.7) describe the non-adiabatic coupling between electronic states through nuclear motion. The complete neglect of these coupling elements corresponds to the Born-Oppenheimer approximation (BOA).^[69] It often is a sensible approach if the electronic states are well separated. Within the Born-Oppenheimer approximation the nuclear Schrödinger equation is

$$(\mathbf{T}_n + E_{\text{el},k}(\vec{R})) \xi_k(\vec{R}) = E \xi_k(\vec{R}) . \tag{2.8}$$

Thus, for a given electronic state with a potential energy surface $E_{\text{el},k}(\vec{R})$ nuclear wave functions and properties can be determined independently from other electronic states.

Up to this point effective measures have been described that allow for an approximate solution of the molecular time-independent Schrödinger equation: Electrons and nuclei are treated successively. In a first step the electronic Schrödinger equation is solved for selected nuclear configurations to obtain potential energy surfaces for the investigated electronic states. Then, these may be used to solve the nuclear Schrödinger equation in the adiabatic (Born-Oppenheimer) approximation. Even though the molecular problem is greatly facilitated by this workflow, the electronic and nuclear Schrödinger equations remain challenging obstacles in their own right.

2.2 The Electronic Schrödinger Equation

This section deals with the treatment of the electronic Schrödinger equation. Starting with wave function-based procedures, general aspects of the electronic wave function are described. Then, the variational principle, Hartree-Fock (HF) theory and several quantum chemical correlation methods are accounted for. To conclude the section, an overview of

the foundations of density functional theory (DFT) for isolated and extended systems is given.

2.2.1 Electronic Wave Functions

Analogously to the molecular Schrödinger equation, the electronic problem cannot be solved analytically for many-electron systems. The difficulties arise mainly from the Coulomb interaction between the electrons (V_{e-e} in Equation (2.5)). This term couples the coordinates of different electrons, producing an *interacting* system and preventing any kind of analytical solution via a product ansatz for the wave function. Thus, to approach the electronic Schrödinger equation approximations are necessary. Another important aspect of the electronic problem is the nature of the particles. As electrons are fermions, a wave function describing an electronic system has to comply with the antisymmetry (or Pauli) principle. Accordingly, the electronic wave function has to be antisymmetric with respect to the exchange of the spin and spatial coordinates of two electrons,

$$\Phi(\vec{x}_1, \dots, \vec{x}_i, \dots, \vec{x}_j, \dots, \vec{x}_n) = -\Phi(\vec{x}_1, \dots, \vec{x}_j, \dots, \vec{x}_i, \dots, \vec{x}_n) \quad , \quad (2.9)$$

with Φ as the wave function of an n -electron system and \vec{x}_i as the spatial and spin coordinates of electron i , $\vec{x}_i = (\vec{r}_i, \omega_i)$. Thus, any approximation of the electronic wave function has to regard the electrons' spatial coordinates as well as their spin, even though the electronic Hamiltonian is only a function of the electronic spatial coordinates.

So how can the electronic wave function be approached? A suitable functional form is identified by considering the electronic problem in reduced complexity by disregarding the electron-electron interaction. Such a non-interacting system may be described by a simple product of one-electron wave functions. This is the Hartree product, which, however, is not applicable, as it is not antisymmetric upon exchange of two sets of electron coordinates. A different approach for electronic wave functions is the Slater determinant. For its construction, a set of orthonormal single-electron wave functions is arranged in a determinant,

$$\Phi(\vec{x}_1, \dots, \vec{x}_n) = \frac{1}{\sqrt{n!}} \begin{vmatrix} \chi_1(\vec{x}_1) & \chi_1(\vec{x}_2) & \dots & \chi_1(\vec{x}_n) \\ \chi_2(\vec{x}_1) & \chi_2(\vec{x}_2) & \dots & \chi_2(\vec{x}_n) \\ \vdots & \vdots & \dots & \vdots \\ \chi_n(\vec{x}_1) & \chi_n(\vec{x}_2) & \dots & \chi_n(\vec{x}_n) \end{vmatrix} . \quad (2.10)$$

The one-electron functions χ_i are called spin orbitals and may be written as a product of a spatial function $\varphi(\vec{r})$ and a spin function $g(\omega)$,

$$\chi_i(\vec{x}_k) = \varphi_i(\vec{r}_k) g_i(\omega_k) \quad , \quad (2.11)$$

where the spin function may represent α - or β -spin. The Slater determinant is a solution to the non-interacting system and – unlike the Hartree product – in accord with the anti-symmetry principle. Therefore, it is a valid approach to representing the electronic wave function in investigations including the interaction between electrons.

2.2.2 Variational Principle

In the course of solving the electronic Schrödinger equation another important scheme occurs, namely the variational principle. While this principle is integral to approximating solutions of the electronic (and also the nuclear) problem, its applicability to eigenvalue problems is far more general. Regarding quantum chemical theory, the notion at the core of the variational principle is

$$\langle \tilde{\Phi} | H | \tilde{\Phi} \rangle \geq E_0 \quad , \quad (2.12)$$

where H is a Hamiltonian with a non-degenerate ground state of energy E_0 and $\tilde{\Phi}$ is a normalized trial wave function ($\langle \tilde{\Phi} | \tilde{\Phi} \rangle = 1$). Accordingly, the expectation value of H with respect to the trial function must be greater than or equal to E_0 , if E_0 is the true ground state energy. The equality holds only if the trial wave function and the true ground state wave function are equal. As a consequence, the ground state can be approached systematically by minimizing the expectation value of the Hamiltonian through variation of the trial function. Typically, in actual applications the trial wave function is linearly expanded into a finite (and for simplicity orthonormal) basis $\{|\phi_i\rangle\}$

$$|\tilde{\Phi}\rangle = \sum_i c_i |\phi_i\rangle \quad . \quad (2.13)$$

In this case, a secular equation can be derived using the method of Lagrange multipliers under the condition that the trial wave function remains normalized. The states described by the Hamiltonian are then approximated by the solutions of the eigenvalue problem

$$\mathbf{HC} = \mathbf{EC} \quad , \quad (2.14)$$

where the Hamiltonian matrix consists of the matrix elements $H_{ij} = \langle \phi_i | \mathbf{H} | \phi_j \rangle$, the diagonal matrix \mathbf{E} contains the energies of the respective states and the matrix \mathbf{C} contains the corresponding expansion coefficients. Importantly, the properties obtained from variational methods typically represent bounded approximations to the true solutions. In accord with that the true values are monotonously approached with increasing quality of the approximation. The latter is dictated by the size and quality of the basis set. Thus, a linear variational procedure consists of the selection of an appropriate basis set, the construction of the Hamiltonian matrix in the selected basis and its subsequent diagonalization.

2.2.3 Hartree-Fock Theory

Equipped with the functional form for the electronic wave functions, that is the Slater determinant, and the variational principle, the electronic Schrödinger equation can be approached. In this regard, the foundation of a wave function-based investigation of a many-electron system is Hartree-Fock theory. Within its framework the electronic ground state wave function is approximated by a single Slater determinant or configuration state function¹ and the electronic problem is treated with the variational principle. The result is an iterative procedure where the interaction among electrons is described in a mean-field way.

The expectation value of the electronic Hamiltonian for n electrons with respect to a trial Slater determinant containing the spin orbitals $\{\chi_i\}$ is given by

$$\begin{aligned} E_{\text{HF}} &= \langle \tilde{\Phi}_{\text{SD}} | \mathbf{H}_{\text{el}} | \tilde{\Phi}_{\text{SD}} \rangle \\ &= \sum_{i=1}^n \langle \chi_i | \hat{h} | \chi_i \rangle + \frac{1}{2} \sum_{i,j}^n (\langle \chi_i \chi_j | \chi_i \chi_j \rangle - \langle \chi_i \chi_j | \chi_j \chi_i \rangle) \quad . \end{aligned} \quad (2.15)$$

In Equation (2.15), the non-interacting Hamiltonian \hat{h} comprises an electron's kinetic energy operator and its interaction with the nuclei,

$$\hat{h} = -\frac{1}{2}\Delta - \sum_{\alpha=1}^N \frac{Z_{\alpha}}{|\vec{r} - \vec{R}_{\alpha}|} \quad , \quad (2.16)$$

while the two-electron integrals in the double sum govern the electron-electron interac-

¹A configuration state function is a linear combination of Slater determinants that is used to account for spin symmetry.

tion. A two-electron integral $\langle \chi_i \chi_j | \chi_k \chi_l \rangle$ is defined by

$$\langle \chi_i \chi_j | \chi_k \chi_l \rangle = \int \mathbf{d}\vec{x}_1 \mathbf{d}\vec{x}_2 \chi_i^*(\vec{x}_1) \chi_j^*(\vec{x}_2) \frac{1}{r_{12}} \chi_k(\vec{x}_1) \chi_l(\vec{x}_2) \quad . \quad (2.17)$$

Through variation of the electronic energy with respect to the spin orbitals, while demanding that the latter remain orthonormal, the canonical Fock equations are derived:

$$\hat{f} \chi_i = \epsilon_i \chi_i \quad . \quad (2.18)$$

The (unitarily transformed) Lagrange multiplier ϵ_i corresponds to the energy of spin orbital χ_i and \hat{f} is the Fock operator. The latter is an effective one-electron operator described by

$$\hat{f} = \hat{h} + \sum_{i=1}^n \left(\hat{J}_i - \hat{K}_i \right) \quad , \quad (2.19)$$

where the action of the Coulomb and exchange operators \hat{J}_i and \hat{K}_i on the spin orbitals can be defined in terms of the integrals

$$\begin{aligned} \langle \chi_j | \hat{J}_i | \chi_k \rangle &= \int \mathbf{d}\vec{x}_1 \chi_j^*(\vec{x}_1) \left[\int \mathbf{d}\vec{x}_2 \chi_i^*(\vec{x}_2) \frac{1}{r_{12}} \chi_i(\vec{x}_2) \right] \chi_k(\vec{x}_1) \\ &= \langle \chi_j \chi_i | \chi_k \chi_i \rangle \quad , \end{aligned} \quad (2.20a)$$

$$\begin{aligned} \langle \chi_j | \hat{K}_i | \chi_k \rangle &= \int \mathbf{d}\vec{x}_1 \chi_j^*(\vec{x}_1) \left[\int \mathbf{d}\vec{x}_2 \chi_i^*(\vec{x}_2) \frac{1}{r_{12}} \chi_k(\vec{x}_2) \right] \chi_i(\vec{x}_1) \\ &= \langle \chi_j \chi_i | \chi_i \chi_k \rangle \quad . \end{aligned} \quad (2.20b)$$

The operator $\hat{J}_i(\vec{x}_1)$ represents the Coulomb interaction of electron 1 with a second electron in spin orbital χ_i averaged over the coordinates \vec{x}_2 of the second electron. In contrast to that, the exchange operator swaps the occupation for the involved spin orbitals, hindering the interpretation in terms of a regular Coulomb interaction between electrons. Still, the exchange interaction of electron 1 with the second electron is averaged over the coordinates of the latter as well. Correspondingly, the electron-electron interaction as a whole is treated such that an electron is affected by an average potential generated by the remaining electrons. The Hartree-Fock scheme is thus a mean-field theory. Notably, all spin orbitals enter the Fock operator through the Coulomb and exchange operators. Hence, the solutions to the Fock equation have to be identified iteratively until self-consistency is reached. A (spin-restricted) formulation of the canonical Fock equations in terms of only the spatial electronic coordinates and orbitals is possible.

With the HF approach, the electronic ground state wave function may be determined from solving n one-electron problems in an effective potential for the spin orbitals, instead of a complete n -electron problem. Although this greatly facilitates the solution of the electronic Schrödinger equation, a grid-based treatment of the one-electron problem remains demanding. In order to lower the numerical cost, Roothaan^[70] and Hall^[71] showed for spin-restricted HF theory that by introducing a linear expansion of the molecular orbitals into a finite set of basis functions the Fock equations can be restated as a numerically favorable matrix equation. To this end, a set of non-orthogonal atomic orbitals $\{\zeta_j\}$ is used to expand the spatial part (φ_i) of the molecular spin orbitals χ_i ,

$$\varphi_i = \sum_j c_{ji} \zeta_j \quad . \quad (2.21)$$

This linear combination of atomic orbitals is denoted the LCAO ansatz. After incorporating the basis set expansion into the Fock equation the Roothaan-Hall-Hartree-Fock matrix equation is accessible,

$$\mathbf{F}\mathbf{c} = \mathbf{S}\mathbf{c}\epsilon \quad , \quad (2.22)$$

with the diagonal matrix ϵ and the coefficient matrix \mathbf{c} containing the orbital energies and expansion coefficients, respectively. The elements of the Fock matrix \mathbf{F} and the overlap matrix \mathbf{S} are defined by

$$F_{ij} = \langle \zeta_i | \hat{f} | \zeta_j \rangle \quad , \quad (2.23a)$$

$$S_{ij} = \langle \zeta_i | \zeta_j \rangle \quad . \quad (2.23b)$$

In analogy to the original Hartree-Fock method, the expansion coefficients contribute to the Fock matrix. Thus, the Roothaan-Hall-Hartree-Fock equation has to be solved self-consistently as well. Starting from an initial guess of the coefficient matrix, the matrix equation is solved to obtain an improved set of coefficients. The latter are reinserted into the equation, which is then solved again. This is iterated until the energies and coefficients are considered converged. For spin-unrestricted HF theory a corresponding formalism based on the LCAO ansatz can be derived, leading to the Pople-Nesbet equations.^[72] Also, in actual calculations the radial part of atomic orbitals is typically expanded into a set of atom-centered Gaussian functions. This is done to further reduce the computational effort, as the Gaussians display properties favorable for numerical calculations, for instance analytical integrability.

2.2.4 Quantum Chemical Correlation Methods

Hartree-Fock theory is usually only the first step to a wave function based investigation of a chemical system. As in the scheme the electron-electron interaction is treated only in a mean-field way, there is obvious room for improvement in the description of the electronic structure. To advance, the interdependence of the electrons beyond the mean-field approximation, typically referred to as *dynamical* electron correlation², has to be regarded. In this spirit the quantum chemical correlation energy is defined as the difference between the exact non-relativistic electronic energy and the Hartree-Fock energy in the limit of a complete basis set,

$$E_{\text{corr}} = E_{\text{exact}} - E_{\text{HF}} \quad . \quad (2.24)$$

Various approaches to grasp *dynamical* electron correlation have been developed, each characterized by certain strengths and weaknesses. Among the properties, which determine the quality of a quantum chemical correlation method, accuracy and numerical expense are paramount. However, there are other, more subtle criteria, such as variational character and size-consistency, often used to describe correlation methods. Concerning the latter factors, a variational correlation method is formulated through a variational principle, as described in Section 2.2.2. Aside from conceptual simplicity, this ensures that within the selected basis the calculated correlation energies represent bounded approximations to the exact value. Size-consistency refers to the description of interactions between chemical fragments. Consider a chemical system with fragments A and B at large distances. In that case, the interaction between the fragments vanishes. Accordingly, the energy of the compound system should be equal to that of the isolated parts, that is $E(\text{AB}) = E(\text{A}) + E(\text{B})$. A size-consistent method is able to correctly describe a compound system with separated fragments.^[54]

Perturbation Theory

Although important, the contribution of the correlation energy to the total electronic energy is small compared to the Hartree-Fock part. Correspondingly, electron correlation may be interpreted as a perturbation to the Hartree-Fock system and thus be subjected

²On another note, there is also *static* correlation, which relates to systems with non-negligible multireference character. These are characterized by ground state wave functions not well described by a single Slater determinant or configuration state function. This kind of correlation is not regarded here.

to Rayleigh-Schrödinger perturbation theory. Herein, the Hamiltonian is divided into an unperturbed part H_0 and a perturbation V , yielding the Schrödinger equation

$$H |\Phi_i\rangle = (H_0 + V) |\Phi_i\rangle = E_i |\Phi_i\rangle \quad . \quad (2.25)$$

Moreover, the solutions of the unperturbed Hamiltonian, that is energies $E_i^{(0)}$ and wave functions $\Phi_i^{(0)}$, are known,

$$H_0 |\Phi_i^{(0)}\rangle = E_i^{(0)} |\Phi_i^{(0)}\rangle \quad . \quad (2.26)$$

Then, the effect of the perturbation on the energies and wave functions of the unperturbed system is broken down into small contributions. This is achieved by placing an ordering parameter λ into Equation (2.25) and expanding the energy of the perturbed system E_i and the perturbed wave function Φ_i into a power series of λ ,

$$H |\Phi_i\rangle = (H_0 + \lambda V) |\Phi_i\rangle \quad , \quad (2.27a)$$

$$E_i = E_i^{(0)} + \lambda E_i^{(1)} + \lambda^2 E_i^{(2)} + \dots \quad , \quad (2.27b)$$

$$|\Phi_i\rangle = |\Phi_i^{(0)}\rangle + \lambda |\Phi_i^{(1)}\rangle + \lambda^2 |\Phi_i^{(2)}\rangle + \dots \quad , \quad (2.27c)$$

with $E_i^{(p)}$ and $\Phi_i^{(p)}$ ($p > 0$) being the corrections of p -th order to the unperturbed energy and wave function. These corrective terms can be accessed by inserting the power series expansion into the Schrödinger equation including the perturbation (Equation (2.27a)) and isolating the expressions with matching order of λ . From the latter, the energy corrections of arbitrary order can be derived by assuming intermediate normalization $\langle \Phi_i^{(0)} | \Phi_i \rangle = 1$,

$$E_i^{(0)} = \langle \Phi_i^{(0)} | H_0 | \Phi_i^{(0)} \rangle \quad , \quad (2.28a)$$

$$E_i^{(1)} = \langle \Phi_i^{(0)} | V | \Phi_i^{(0)} \rangle \quad , \quad (2.28b)$$

$$E_i^{(2)} = \langle \Phi_i^{(0)} | V | \Phi_i^{(1)} \rangle \quad , \quad (2.28c)$$

...

$$E_i^{(p)} = \langle \Phi_i^{(0)} | V | \Phi_i^{(p-1)} \rangle \quad . \quad (2.28d)$$

The zeroth- and first-order energies are given by the expectation values of the unperturbed Hamiltonian and the perturbation with respect to the unperturbed wave function, respectively. Beyond that, the energy correction to the p -th order requires the wave function correction of $(p - 1)$ -th order. Generally, the latter corrections can be expressed via the eigenfunctions of the unperturbed problem, as these form a complete basis. The appli-

cation of this basis set expansion (and several orthogonality relations) allows for the formulation of expressions for the energy corrections involving only the unperturbed wave functions and energies. For instance, the second-order correction is determined via

$$E_i^{(2)} = \sum_{\substack{g \\ g \neq i}} \frac{\langle \Phi_i^{(0)} | \mathbf{V} | \Phi_g^{(0)} \rangle \langle \Phi_g^{(0)} | \mathbf{V} | \Phi_i^{(0)} \rangle}{E_i^{(0)} - E_g^{(0)}} = \sum_{\substack{g \\ g \neq i}} \frac{|\langle \Phi_i^{(0)} | \mathbf{V} | \Phi_g^{(0)} \rangle|^2}{E_i^{(0)} - E_g^{(0)}} . \quad (2.29)$$

When perturbation theory is applied to the problem of electron correlation it is typically referred to as Møller-Plesset perturbation theory. Within that framework the unperturbed system is taken to be the sum of the Fock operators for all electrons, while the perturbation comprises the electron-electron interaction without the Coulomb and exchange operators, which are included in the Fock operators. The operators are defined by

$$\mathbf{H}_0 = \sum_i \hat{f}(\vec{x}_i) = \sum_i \left[\hat{h}(\vec{x}_i) + \sum_j \left(\hat{J}_j(\vec{x}_i) - \hat{K}_j(\vec{x}_i) \right) \right] , \quad (2.30)$$

and

$$\mathbf{V} = \sum_{\substack{i,j \\ i < j}} \frac{1}{r_{ij}} - \sum_{i,j} \left(\hat{J}_j(\vec{x}_i) - \hat{K}_j(\vec{x}_i) \right) . \quad (2.31)$$

The required set of eigenstates of the unperturbed Hamiltonian consists of the Slater determinants (or CSFs) generated by the occupied and unoccupied (virtual) spin orbitals obtained in the Hartree-Fock procedure. The relevant excited Slater determinants are denoted Φ_i^a (or analogously Φ_{ij}^{ab} , Φ_{ijk}^{abc} , ...), where the indices indicate the replacement of the (originally occupied) spin orbital χ_i (lower index) in the Slater determinant by the (originally unoccupied) spin orbital χ_a (upper index). If the degree of excitation is unspecified, the excited determinants will be represented by Φ_g . The Hartree-Fock ground state is Φ_0 .

With this formulation of the problem the zeroth-order energy equals the sum of the orbital energies - but not the Hartree-Fock energy -, that is

$$\begin{aligned} E_0^{(0)} &= \langle \Phi_0 | \mathbf{H}_0 | \Phi_0 \rangle = \sum_i \epsilon_i \\ &= \sum_i \left[\langle \chi_i | \hat{h} | \chi_i \rangle + \sum_j \left(\langle \chi_i \chi_j | \chi_i \chi_j \rangle - \langle \chi_i \chi_j | \chi_j \chi_i \rangle \right) \right] . \end{aligned} \quad (2.32)$$

The first-order energy correction is determined by

$$E_0^{(1)} = \langle \Phi_0 | \mathbf{V} | \Phi_0 \rangle = -\frac{1}{2} \sum_{i,j} \left(\langle \chi_i \chi_j | \chi_i \chi_j \rangle - \langle \chi_i \chi_j | \chi_j \chi_i \rangle \right) . \quad (2.33)$$

Accordingly, the sum of $E_0^{(0)}$ and $E_0^{(1)}$ is the Hartree-Fock energy (Equation (2.15)) and the second-order energy correction is the first term to account for electron correlation. The second-order energies depend on matrix elements $\langle \Phi_0 | \mathbf{V} | \Phi_g \rangle$ coupling the Hartree-Fock ground state and the excited determinants. Luckily, in this case the constitution of the electronic problem allows for the neglect of most excited Slater determinants. To start off, all determinants with excitation levels of more than two can be neglected. This is because the perturbation features only two-electron operators. As a result, corresponding matrix elements between determinants differing by more than two spin orbitals must vanish. Moreover, if Φ_g is a singly excited determinant the matrix element will be zero as well, due to Brillouin's theorem. (A singly excited determinant corresponds to an off-diagonal element in the Fock matrix. For the canonical Fock equations, these are zero.) Therefore, for the matrix elements $\langle \Phi_0 | \mathbf{V} | \Phi_g \rangle$ the only relevant determinants are doubly excited. With this the second-order energy correction is readily formulated as

$$E_0^{(2)} = \frac{1}{4} \sum_{a,b,i,j} \frac{|\langle \chi_a \chi_b | \chi_i \chi_j \rangle - \langle \chi_a \chi_b | \chi_j \chi_i \rangle|^2}{(\epsilon_i + \epsilon_j - \epsilon_a - \epsilon_b)} , \quad (2.34)$$

where the indices i and j refer to occupied orbitals and a and b represent virtual ones. The corrections of higher orders feature products of matrix elements of the $\langle \Phi_0 | \mathbf{V} | \Phi_g \rangle$ type and matrix elements coupling excited determinants to each other ($\langle \Phi_{g'} | \mathbf{V} | \Phi_g \rangle$). Although the restrictions due to the two-electron operators in the perturbation still apply, this drastically increases the complexity of the problem.

Møller-Plesset perturbation theory is a commonly applied method in quantum chemistry. It is size-consistent at any order of corrections. Also, at the level of second-order corrections (MP2) it is comparatively cheap, at worst scaling with N_b^5 with respect to the number of basis functions³ N_b .^[74] On the other hand, it is not variational and has displayed inconsistent convergence behaviour with increasing orders of corrections.^[74,75] The MP2 energy corrections are typically used as initial guesses for what will be referred to as amplitudes in the coupled cluster formalism.

³The formal scaling of the Hartree-Fock method is N_b^4 with respect to the number of basis functions N_b , determined by the calculation of the two-electron four-index integrals.^[73]

Coupled Cluster Theory

Aside from treating it as a perturbation to the Hartree-Fock system, electron correlation may also be grasped by the configuration interaction (CI) ansatz. Herein, the description of the electronic wave function is improved by considering not only the Hartree-Fock wave function but also excited Slater determinants that can be generated from the optimized spin orbitals. A matrix representation of the electronic Hamiltonian is set up in the basis of n -electron Slater determinants and diagonalized to obtain the correlated energies. Thus, the method is variational. The corresponding electronic wave function in intermediate normalization⁴ is given by

$$\begin{aligned} |\Phi^{\text{CI}}\rangle &= (1 + \mathbf{T}) |\Phi_0\rangle \\ &= |\Phi_0\rangle + \sum_{i,a} t_i^a |\Phi_i^a\rangle + \sum_{\substack{i<j \\ a<b}} t_{ij}^{ab} |\Phi_{ij}^{ab}\rangle + \sum_{\substack{i<j<k \\ a<b<c}} t_{ijk}^{abc} |\Phi_{ijk}^{abc}\rangle + \dots \quad , \end{aligned} \quad (2.35)$$

where Φ_0 represents the Hartree-Fock ground state, \mathbf{T} is the cluster operator and Φ_i^a is a singly-excited Slater determinant as defined before - the higher excited determinants $\Phi_{ij\dots l}^{ab\dots d}$ are defined analogously. The amplitudes $(t_i^a, t_{ij}^{ab}, \dots)$ describe the contribution of the respective excited determinant to the wave function. The full cluster operator for a system of n electrons,

$$\mathbf{T} = \mathbf{T}_1 + \mathbf{T}_2 + \dots + \mathbf{T}_n \quad , \quad (2.36)$$

contains the operators \mathbf{T}_i that describe i -tuple excitations, as is illustrated by

$$\mathbf{T}_1 |\Phi_0\rangle = \sum_{i,a} t_i^a |\Phi_i^a\rangle \quad , \quad (2.37a)$$

$$\mathbf{T}_2 |\Phi_0\rangle = \sum_{i>j, a>b} t_{ij}^{ab} |\Phi_{ij}^{ab}\rangle \quad . \quad (2.37b)$$

When all excited determinants up to n -fold excitations are considered, the expansion in Equation (2.35) is termed full configuration interaction wave function. The correlation energy obtained from full CI is exact within a given set of spin orbitals and generally exact in the limit of a complete basis of one-electron functions. Also, the method is size-consistent. However, a full configuration interaction description is only feasible for very small systems. The CI approach becomes more applicable, once the CI expansion is trun-

⁴With this Φ^{CI} is not normalized, but $\langle \Phi_0 | \Phi^{\text{CI}} \rangle = 1$ holds. The CI wave function can be renormalized after determining the expansion coefficients.

cated to include only low-level excitations. This, however, destroys the size-consistency of the ansatz. Hence, methods such as CIS and CISD (including only single- and single- as well as double-excitations, respectively) have a severe drawback.

The coupled cluster scheme offers a different way to approach the full CI wave function. According to it, the correlated wave function can be described by the following expansion

$$|\Phi^{\text{CC}}\rangle = e^{\text{T}} |\Phi_0\rangle = \left(1 + \text{T} + \frac{1}{2}\text{T}^2 + \dots\right) |\Phi_0\rangle \quad , \quad (2.38)$$

with Φ_0 and T as the Hartree-Fock reference wave function and the cluster operator again. The electronic Schrödinger equation with the coupled cluster wave function is

$$e^{-\text{T}} \mathbf{H} e^{\text{T}} |\Phi_0\rangle = \tilde{\mathbf{H}} |\Phi_0\rangle = E_{\text{CC}} |\Phi_0\rangle \quad . \quad (2.39)$$

As the wave function expansion is not linear, a solution in terms of a variational principle is not straightforward. Instead of that the amplitudes are determined by projecting the Schrödinger equation on the respective excited determinant. For instance, in case of the doubly excited determinants the amplitudes are obtained from

$$\langle \Phi_{ij}^{ab} | \tilde{\mathbf{H}} | \Phi_0 \rangle = 0 \quad . \quad (2.40)$$

Once the necessary amplitudes are found, the coupled cluster energy is determined by projection on the Hartree-Fock reference,

$$E_{\text{CC}} = \langle \Phi_0 | e^{-\text{T}} \mathbf{H} e^{\text{T}} | \Phi_0 \rangle = \langle \Phi_0 | \tilde{\mathbf{H}} | \Phi_0 \rangle \quad . \quad (2.41)$$

As is the case for configuration interaction, the cluster operator in the coupled cluster framework has to be restricted to low-level excitation operators to remain computationally tractable. However, in contrast to the truncated CI approach, the coupled cluster method incorporates high-level excitations at any order of truncation. This is due to the exponential of the cluster operator in Equation (2.38), which – aside from the connected T_n excitations – introduces disconnected excitations, meaning products of connected excitation operators. For instance, when the cluster operator T contains connected single and double excitations (T_1 and T_2) the T^2 expression in Equation (2.38) produces disconnected double, triple and quadruple excitations via T_1^2 , T_1T_2 and T_2^2 , respectively. As a consequence of the occurrence of the disconnected excitations, the coupled cluster ap-

proach is size-consistent at any level of truncation of the cluster operator. Moreover, once the T_1 excitation operator is included in T the coupled cluster method should principally cover the same excitation ranks as the full CI method. The difference is that the high-level excitations in the former ansatz are disconnected, whereas they are connected in full CI. Correspondingly, the independent amplitudes in full CI are replaced by products of amplitudes for determinants of lower excitation level in coupled cluster. Thus, the coupled cluster wave function is less flexible than its full CI counterpart.

With respect to applications, coupled cluster schemes are standard approaches in quantum chemistry. Including connected single and double excitations in the cluster operator results in the CCSD method, which in many cases is a decent compromise between accuracy and numerical cost, scaling with N_b^6 with the number of basis functions.^[73] However, by regarding connected triple excitations the accuracy of the coupled cluster method is significantly improved - to the point where even more challenging systems, e. g. with weak dispersive interactions, may be described accurately. The coupled cluster method with full triple excitations, that is CCSDT, scales according to N_b^8 with the number of basis functions.^[73] This prohibitively large scaling is typically avoided with the CCSD(T) method. Herein, selected contributions of the connected triple excitations to the correlation energy are obtained from the converged CCSD amplitudes in a non-iterative procedure inspired by perturbation theory.^[76] In CCSD(T) the scaling of the numerical expense is reduced by one order of magnitude compared to CCSDT, while a significant contribution of the connected triple excitations is grasped. In accord with that, CCSD(T) calculations are often used to determine reference values for other quantum chemical procedures.

Explicit Correlation

The correlation methods introduced up to this point are based on different approaches to incorporate the interdependence of electrons into the wave function. However, all of them share a somewhat unpleasant trait. To be precise, the convergence of the calculated correlation energy to the limit of a complete one-particle basis set is relatively slow. The origin of this behaviour lies in the form of the exact electronic wave function at the coalescence points of two electrons. At such a singular point of the Coulomb potential the true electronic wave function has a cusp, at which its first derivatives are not continuous. These sharp features of the exact wave function and the discontinuity in its first derivatives are not correctly described by conventional basis sets, where the basis functions depend only

on the coordinates of single electrons. In order to approximate the correct behaviour in this region of the electronic interaction, a very large number of conventional basis functions including those with high angular momenta is required.

However, the issue may be approached more efficiently. It was shown by Kato^[77] that at the cusp electronic wave functions are generally well described in terms of interelectron distances $r_{ij} = |\vec{r}_i - \vec{r}_j|$, in particular with respect to their first derivatives. Thus, a natural remedy for the disadvantageous behaviour is the explicit inclusion of the distance between two electrons r_{ij} into the wave function. This is in fact an old idea that was first exploited in the 1920s by Slater^[78,79] as well as Hylleraas^[80] in their respective investigations on two-electron atoms. In current quantum chemistry various extensions of common correlation methods, such as MP2 or CCSD, have been developed to account for the cusp conditions. The resulting schemes are referred to as explicitly correlated methods. With respect to numerical calculations, the main obstacle arising from the inclusion of interelectron distances into the electronic wave function is the increase of many-electron integrals.^[58] This problem may be circumvented by using explicitly correlated Gaussian basis functions, which allow for analytical integral evaluations.^[58] Another commonly employed scheme consists of exploiting resolution-of-identity relations to reduce the multi-electron integrals to products of one- and two-electron integrals. The corresponding branch of methods and approximations is denoted by R12/F12, as in CCSD(T)-F12.^[58,81,82]

For a given correlation scheme and finite basis set, the application of the explicitly correlated method (e. g. MP2-F12) produces correlation energies significantly closer to the complete basis set limit compared to the regular method (MP2). This improvement may be crucial for the accurate description of molecular properties and weakly interacting systems.

2.2.5 Density Functional Theory

A widely used alternative to the wave function-based quantum chemical methods presented above is density functional theory (DFT), which treats the electronic Schrödinger equation by means of the electronic density. The approach is based on the ingenious works of Hohenberg and Kohn.^[83] They showed that the true electronic density of a non-degenerate ground state is linked to a corresponding electron-nuclei interaction potential V_{n-e} in a unique way. Therefore, knowledge of the ground state density allows for the determination of the electronic Hamiltonian as well as the properties associated with it;

in particular, the energy of the electronic ground state. Correspondingly, the ground state energy E_0 may be expressed as a functional of the ground state density ρ_0

$$E_0[\rho_0] = T[\rho_0] + E_{ee}[\rho_0] + E_{ne}[\rho_0] \quad , \quad (2.42)$$

where $T[\rho_0]$, $E_{ee}[\rho_0]$ and $E_{ne}[\rho_0]$ represent contributions of the kinetic energy of the electrons, the electron-electron interaction and the electron-nuclei interaction as functionals of the ground state density, respectively. Moreover, Hohenberg and Kohn presented a variational principle for the ground state energy as the functional of the electronic density, according to which only the true ground state density minimizes the ground state energy. At this point the formalism is intractable, as the functional forms of $T[\rho_0]$ and $E_{ee}[\rho_0]$ remain unidentified. However, the problem of finding suitable functional forms may be reduced by introducing orbitals into the formalism, an idea conceived by Kohn and Sham.^[84]

Kohn-Sham Density Functional Theory

In Kohn-Sham density functional theory (KS-DFT) the electronic density is assumed to be generated by a reference system of non-interacting electrons. Analogously to Equation (2.10) the wave function of such a system can be expressed as a Slater determinant comprising a set of orthonormal Kohn-Sham spin orbitals χ_i^{KS} . Correspondingly, the electron density of the Kohn-Sham system is determined by

$$\rho^{\text{KS}}(\vec{r}) = \sum_i \sum_{\omega} |\chi_i^{\text{KS}}(\vec{r}, \omega)|^2 \quad , \quad (2.43)$$

with the spin variable ω . The total Hamiltonian H^{KS} is given as the sum of one-particle Hamiltonians \hat{h}_i^{KS} ,

$$H^{\text{KS}} = \sum_i \hat{h}_i^{\text{KS}} = \sum_i \left(-\frac{1}{2} \Delta_i + V^{\text{KS}}(\vec{r}_i) \right) \quad , \quad (2.44)$$

with a one-particle potential $V^{\text{KS}}(\vec{r}_i)$. The orbitals are obtained by solving the one-particle Schrödinger equations

$$\left(-\frac{1}{2} \Delta + V^{\text{KS}}(\vec{r}) \right) \chi_i^{\text{KS}} = \epsilon_i^{\text{KS}} \chi_i^{\text{KS}} \quad . \quad (2.45)$$

where ϵ_i^{KS} is the Kohn-Sham orbital energy. With this the central aspect of KS-DFT can be approached. That is the question of how to construct the Kohn-Sham system - meaning $V^{\text{KS}}(\vec{r})$ - in such a way that the resulting density (ρ^{KS}) reproduces the true ground state density as faithfully as possible. With respect to that, the first step is to define the kinetic energy and electron-electron interaction in the Kohn-Sham system, which are

$$T^{\text{KS}}[\rho] = -\frac{1}{2} \sum_i \langle \chi_i^{\text{KS}} | \Delta | \chi_i^{\text{KS}} \rangle \quad , \quad (2.46a)$$

$$E_{\text{ee}}^{\text{KS}}[\rho] = \frac{1}{2} \sum_{i,j} \iint d\vec{x}_1 d\vec{x}_2 |\chi_i^{\text{KS}}|^2 \frac{1}{|\vec{r}_1 - \vec{r}_2|} |\chi_j^{\text{KS}}|^2 \quad . \quad (2.46b)$$

These expressions are inserted into Equation (2.42) to redefine the ground state energy as

$$\begin{aligned} E_0[\rho] &= T^{\text{KS}}[\rho] + E_{\text{ee}}^{\text{KS}}[\rho] + E_{\text{ne}}[\rho] + (T[\rho] - T^{\text{KS}}[\rho]) + (E_{\text{ee}}[\rho] - E_{\text{ee}}^{\text{KS}}[\rho]) \\ &= T^{\text{KS}}[\rho] + E_{\text{ee}}^{\text{KS}}[\rho] + E_{\text{ne}}[\rho] + E_{\text{XC}}[\rho] \quad . \end{aligned} \quad (2.47)$$

$E_{\text{XC}}[\rho]$ is the exchange and correlation functional carrying the portions of the kinetic energy and electron-electron interaction not described by the Kohn-Sham system. Subjecting Equation (2.47) to a minimization of the ground state energy E_0 by varying the KS orbitals (with the orthonormality condition $\langle \chi_i^{\text{KS}} | \chi_j^{\text{KS}} \rangle = \delta_{ij}$) results in effective one-particle problems

$$\left(-\frac{1}{2}\Delta + V_{\text{eff}}(\vec{r}) \right) \chi_i^{\text{KS}} = \epsilon_i^{\text{KS}} \chi_i^{\text{KS}} \quad , \quad (2.48)$$

the Kohn-Sham equations. The effective potential in the KS equations is given by

$$V_{\text{eff}}(\vec{r}_1) = \int \frac{\rho(\vec{r}_2)}{|\vec{r}_1 - \vec{r}_2|} d\vec{r}_2 + \sum_{\alpha} \frac{Z_{\alpha}}{|\vec{r}_1 - \vec{R}_{\alpha}|} + \frac{\partial E_{\text{XC}}}{\partial \rho}(\vec{r}_1) \quad , \quad (2.49)$$

with the first two expressions representing the classical electron-electron and the electron-nuclei interactions, respectively. The last term is the functional derivative of the exchange and correlation functional with respect to the density. Notably, the effective potential in Equation (2.49) and the one-particle potential in Equation (2.45) are the same. Thus, solving the Kohn-Sham problem in the limit of a complete orbital basis produces the true ground state density if the exchange and correlation functional used in the procedure is accurate. With regards to solving the KS equations, it should be noted that solutions are determined in a self-consistent way as the electron density appears in Equation (2.48). Moreover, analogous to the Roothaan-Hall ansatz in HF a finite basis set of atom-centered

functions is commonly used to expand the orbitals in KS-DFT.

The benefits of considering the Kohn-Sham system become apparent upon reconsidering Equation (2.47). Instead of approximating the completely unknown functionals $T[\rho]$ and $E_{\text{ee}}[\rho]$, a sizable portion of the ground state energy is recovered by examining a system of non-interacting electrons in a tractable orbital-based picture. The relatively small residual contributions of the kinetic energy and electron-electron interaction are collected in the exchange and correlation functional E_{XC} , whose form remains unknown. Hence, the problem of functional expressions is shifted to affect only a fraction of the ground state energy. Correspondingly, the aim in KS-DFT is to set up appropriate approximations to the exchange and correlation functional.

Local Density Approximation

A central concept for the design of exchange and correlation functionals is the local density approximation (LDA). Within its framework a system's electronic structure is modeled by a homogeneous electron gas, that is, an electron density on a uniform positive background charge distribution. The total exchange-correlation energy is given by

$$E_{\text{XC}}^{\text{LDA}} = \int \rho(\vec{r}) \epsilon_{\text{XC}}[\rho(\vec{r})] d\vec{r}, \quad (2.50)$$

where $\epsilon_{\text{XC}}[\rho(\vec{r})]$ is the per-particle exchange-correlation energy in the uniformly distributed electron gas. This per-particle energy is taken to be the sum of an exchange and a correlation part. The exchange contribution to ϵ_{XC} ,

$$\epsilon_{\text{X}}[\rho(\vec{r})] = -\frac{3}{4} \left(\frac{3\rho}{\pi} \right)^{\frac{1}{3}}, \quad (2.51)$$

is available from analytic derivation, whereas different expressions for the correlation term were obtained from interpolation of numerical simulations of the homogeneous electron gas.^[85–87] Typically, the LDA performs decently for systems that can be approximated by a homogeneous electron gas to a reasonable extent, for instance a variety of metal solids. However, electron densities of molecules are usually not uniform and thus the scheme does not produce accurate results in these cases.

Generalized Gradient Approximation

In order to move away from a uniform electron gas and improve upon the LDA, gradients of the electronic density may be added to the formalism. The exchange-correlation energy is then described by

$$E_{\text{XC}}^{\text{GGA}}[\rho] = \int f(\rho, \vec{\nabla}\rho) \, d\vec{r} \quad , \quad (2.52)$$

with $f(\rho, \vec{\nabla}\rho)$ containing functionals of the density ρ as well as its gradient $\vec{\nabla}\rho$. This general expression is combined with constraints that produce physically sound behaviour. In particular, it is ensured that correlation effects caused by the Pauli exclusion principle and the electrostatic electron-electron interaction are included in a qualitatively correct way. Exchange-correlation functionals of this type belong to the general gradient approximation (GGA). Often, the GGA functionals are based on the local density approximation and its separate exchange and correlation contributions, but expanded with elaborate mathematical expressions to incorporate the aforementioned constraints. With respect to numerical cost, GGA functionals are comparatively cheap, while often producing results of reasonable, that is at least qualitative, accuracy. Commonly used examples of GGA functionals are the Perdew-Burke-Ernzerhof^[88] (PBE, exchange and correlation), the Perdew-Wang^[87] (PW91, exchange and correlation) and the Lee-Yang-Parr^[89] (LYP, only correlation) functionals.

Hybrid Functionals

Another attempt at increasing the accuracy and reliability of KS-DFT was the introduction of hybrid exchange-correlation functionals. The fundamental idea behind this branch of approximations is to include explicitly calculated contributions of the Hartree-Fock exchange interaction into selected GGA functionals. Typically, optimal performance of the hybrid functionals is obtained if the exchange energy is designed to be a mix of exact HF exchange and GGA functional exchange. The parameters determining the ratio of contributions by exact and approximate exchange are optimized with respect to performance in benchmark calculations on a sizable test set of structures and properties. Employing hybrid instead of GGA functionals leads to significantly longer calculations that may produce more accurate results. Notably though, the improvement over the GGA scheme is not guaranteed. B3LYP and PBE0 are widely used hybrid functionals.^[90,91]

Dispersion Correction – DFT-D

The functional approximations presented up to this point are not able to describe non-covalent dispersive interactions thoroughly. Hence, if a corresponding system - such as a rare gas atom cluster - is to be treated in the DFT framework, additional modifications have to be introduced. In fact, a variety of ways to correct existing functionals to account for dispersion has been designed, for instance the vdW functional family, which includes dispersion self-consistently.^[92,93] A more straightforward approach, however, is Grimme's dispersion correction, DFT-D.^[94] Here a dispersion contribution is added to the self-consistently optimized DFT energy,

$$E_{\text{DFT-D}} = E_{\text{KS-DFT}} + E_{\text{disp}} \quad . \quad (2.53)$$

At the DFT-D2 level, the dispersion correction is determined by two-body interactions,

$$E^{(2)} = - \sum_{\text{A,B}} \sum_{n=6,8,10,\dots} s_n \frac{C_n^{\text{AB}}}{r_{\text{AB}}^n} f_{d,n}(r_{\text{AB}}) \quad . \quad (2.54)$$

It contains pair interactions of atoms A and B at a distance of r_{AB} via multiple central potentials r^{-n} and dispersion coefficients C_n^{AB} . The parameter s_n denotes a scaling factor. The damping function $f_{d,n}$ (with zero-damping) is defined as

$$f_{d,n}(r_{\text{AB}}) = \frac{1}{1 + 6(r_{\text{AB}}/(s_{r,n}R_{\text{AB}}))^{-\alpha_n}} \quad , \quad (2.55)$$

where $s_{r,n}$ is another scaling parameter, R_{AB} is a cut-off radius and α_n is referred to as steepness parameter.^[95] This basic correction is typically extended by considering non-additive contributions of three-body interactions. In the DFT-D3 framework these are added as Axilrod-Teller-Muto interactions,

$$E^{(3)} = \sum_{\text{A,B,C}} \frac{C_9^{\text{ABC}} (3 \cos(\theta_A) \cos(\theta_B) \cos(\theta_C) + 1)}{(r_{\text{AB}}r_{\text{AC}}r_{\text{BC}})^3} f_{d,3}(\bar{r}_{\text{ABC}}) \quad , \quad (2.56)$$

where A, B and C refer to different atoms and the angles θ_i and bond lengths r_{jk} describe the triangle spanned by these atoms.^[95] The argument of the damping function, \bar{r}_{ABC} , is the geometrical mean of the three distances r_{jk} . With the DFT-D4 method further improvements were made by approximating many-body interactions beyond the three-body level and incorporating atomic charge effects into the calculation of the dispersion

coefficients.^[96] For the most part the parameters in the DFT-D approaches are obtained from *ab initio* calculations, only a small number of parameters is set empirically. Also, the evaluation of the dispersion correction is relatively fast, as the correction is not part of the self-consistent optimization of the KS orbitals.

DFT for Periodic Systems

Other than for molecules and clusters, KS-DFT is used to investigate truly extended systems, such as crystal structures or processes at surfaces. This is possible, because these types of systems may credibly be modeled by concatenations of smaller cells containing the important features, i. e. by assuming a periodicity in the system. Likewise the periodicity can be incorporated into the KS-DFT formalism. As a result, the size of the explicitly treated system is reduced to the unit, from which the periodic structure is constructed. Formally, a crystal structure is determined by a lattice and a basis. The former is a grid of points that describes the translational symmetry of the crystal. It is given by

$$\vec{R} = n_1 \vec{a}_1 + n_2 \vec{a}_2 + n_3 \vec{a}_3 \quad , \quad (2.57)$$

with n_1, n_2 and n_3 as integers and \vec{a}_1, \vec{a}_2 and \vec{a}_3 as the lattice vectors. A smallest subunit of the lattice, from which the full grid can be constructed by concatenation in every direction, is denoted a unit cell. The basis defines the atomic positions within a given unit cell. A particular case of a unit cell is the Wigner-Seitz cell, which contains the symmetry of the crystal lattice, but engulfs only the space that is closer to a given reference lattice point than to any other point of \vec{R} . In addition to the lattice in real space another lattice is relevant when examining periodic systems. This is the reciprocal lattice,

$$\vec{G} = m_1 \vec{b}_1 + m_2 \vec{b}_2 + m_3 \vec{b}_3 \quad , \quad (2.58)$$

where m_1, m_2 and m_3 are integers. The reciprocal lattice vectors \vec{b}_i are defined by

$$\vec{b}_1 = 2\pi \frac{\vec{a}_2 \times \vec{a}_3}{|\vec{a}_1 \cdot (\vec{a}_2 \times \vec{a}_3)|} \quad (2.59a)$$

$$\vec{b}_2 = 2\pi \frac{\vec{a}_3 \times \vec{a}_1}{|\vec{a}_1 \cdot (\vec{a}_2 \times \vec{a}_3)|} \quad (2.59b)$$

$$\vec{b}_3 = 2\pi \frac{\vec{a}_1 \times \vec{a}_2}{|\vec{a}_1 \cdot (\vec{a}_2 \times \vec{a}_3)|} \quad , \quad (2.59c)$$

and fulfil the orthogonality relation

$$\vec{a}_i \cdot \vec{b}_j = 2\pi\delta_{ij} \quad (2.60)$$

with the real space lattice vectors. The analogon of the Wigner-Seitz cell in reciprocal space is called the first Brillouin zone.

For one-electron Schrödinger equations with potentials that display the same translational symmetry as the crystal structure,

$$V_{\text{eff}}(\vec{r}) = V_{\text{eff}}(\vec{r} + \vec{R}) \quad , \quad (2.61)$$

the Bloch theorem is valid.^[97] The latter shows that the wave functions solving the one-electron Schrödinger equations can be formulated as

$$\chi_{j,\vec{k}}(\vec{r}) = e^{i\vec{k}\cdot\vec{r}} \cdot u_{j,\vec{k}}(\vec{r}) \quad , \quad (2.62)$$

that is as a product of a plane wave (the wave function for a free electron) and a function $u_{j,\vec{k}}(\vec{r})$ with the periodicity of the crystal. The solutions, meaning the one-electron wave functions as well as the corresponding energies, depend on the crystal momentum \vec{k} , which represents a point in reciprocal space. Furthermore, the different solutions are denoted by the index j . The energy corresponding to a given one-electron wave function changes continuously with \vec{k} , forming a continuous band in reciprocal space. For that reason the index j is referred to as band index. These symmetry considerations are perfectly applicable to KS-DFT and its effective one-particle Schrödinger equations. In this context, the total electronic energy of the examined system is given by

$$E_{\text{tot}} = \sum_{\text{occ. } j} \frac{V}{(2\pi)^3} \int_{1^{\text{st}} \text{ BZ}} \mathrm{d}^3\vec{k} \epsilon_j(\vec{k}) \quad , \quad (2.63)$$

where $\epsilon_j(\vec{k})$ is the energy of band j at crystal momentum \vec{k} and V is the unit cell volume. The energies $\epsilon_j(\vec{k})$ are integrated over the first Brillouin zone, which contains all information with respect to symmetry of the crystal, and summed up for all occupied bands. In numerical calculations the integral over the first Brillouin zone is replaced by a summation over a grid of \vec{k} points. Also, plane-wave instead of atom-centered basis sets are often used to describe the KS orbitals for periodic systems.

At this point various schemes to solve the electronic problem have been introduced. As presented here, their application yields (among other properties) the electronic energy for a given electronic state and nuclear configuration. If nuclear motion is investigated, the electronic problem is typically solved for a sizable set of nuclear configurations. The resulting electronic energies are subsequently used to determine a continuous functional form representing the potential energy surface for the investigated electronic state. In an ensuing treatment of the nuclear Schrödinger equation, the continuous potential function acts as the potential that governs the nuclear motion. Thus, the procedure of potential fitting is at the intersection of the electronic and nuclear problems. Although it is a challenging task with various intricacies, it will not be discussed further. Instead, the focus will be placed on the formulation of the nuclear problem assuming that a suitable representation of the investigated potential energy surface is available.

2.3 The Nuclear Schrödinger Equation

In this section several aspects of working with the time-independent nuclear Schrödinger equation within the Born-Oppenheimer approximation (Equation (2.8)) are described. The solutions of the nuclear problem are states that represent nuclear motion within the given potential energy surface, such as molecular translations, rotations or vibrations. Usually the treatment of the nuclear Schrödinger equation is heavily tailored to the problem at hand. As a consequence there are numerous schemes, not all of which can be presented here. Instead, it is attempted to give a concise description of the cornerstones of obtaining rovibrational states in the context of what is often referred to as *variational schemes*. The section starts off with a general outline of variational calculations of molecular rovibrational states. To this end, the construction of Hamiltonians in a translation-free, body-fixed reference frame, different coordinate systems and approaches to the nuclear wave function are described. This is followed by an account of the normal mode analysis. Finally, the vibrational self-consistent field (VSCF) method is discussed.

2.3.1 Variational Procedures

Concerning the calculation of rovibrational states *variational procedures* typically refers to methods that are direct implementations of the variational principle discussed in Sec-

tion 2.2.2 and Equations (2.13) and (2.14) in particular. However, as it is, the variational principle serves only as a general framework. Accordingly, the coordinate system defining the nuclear Hamiltonian and the basis describing the nuclear wave function have to be suited to the chemical system and property of interest. The general workflow can be summarized with three steps:

Firstly, define a nuclear Hamiltonian by choosing an appropriate coordinate system, determining the kinetic energy operator and a potential energy surface.

Secondly, build a matrix representation of the Hamiltonian with respect to a set of suitable basis functions.

Lastly, obtain the rovibrational states from the Hamiltonian matrix through direct diagonalization or another appropriate procedure.

The possibility of a high degree of specification regarding coordinate systems and basis functions within the variational framework allows for the description of chemical systems with varying rovibrational behaviour in a very accurate way. On the other hand, it also results in a lack of universal applicability for many approaches. Aside from that, the numerical expense of setting up a Hamiltonian matrix for a given set of basis functions increases exponentially with increasing dimensionality. Thus, the approach is restricted to smaller molecules – typically tri- or tetraatomic species – or, for larger systems, a selection of coordinates that are relevant to the investigated process. In the following, a few aspects of calculating rovibrational states with a variational scheme are detailed.

Rovibrational Hamiltonians

Combining Equations (2.2b) and (2.8) the nuclear Schrödinger equation in Cartesian coordinates for a system of N atoms can be phrased as

$$\left(- \sum_{i=1}^N \frac{1}{2M_i} \Delta_i + V \right) \xi(\vec{R}) = E \xi(\vec{R}) \quad , \quad (2.64)$$

where M_i and Δ_i are the mass of atom i and its Laplacian. The Cartesian coordinates listed in \vec{R} are defined with respect to a laboratory-fixed reference frame. V is a poten-

tial energy surface in the Born-Oppenheimer approximation that depends solely on the internal coordinates of the system and is invariant with respect to uniform translations and rotations of the molecule. The problem is $3N$ -dimensional. Of these $3N$ degrees of freedom ($3N - 6$) ($3N - 5$ for linear molecules) can be regarded internal, that is as vibrations. The remaining ones correspond to three uniform translations of the system's center-of-mass and three (for linear species two) uniform rotations, both of which do not affect the internal coordinates.

The first step to calculating bound rovibrational states of a molecule is to remove the translation of the nuclear center-of-mass from the Hamiltonian. This is necessary, as the inclusion of the uniform translations would prevent the nuclear wave function from being square-integrable, thus inhibiting the calculation of a bound spectrum.^[62] Among others, it was shown by Sutcliffe that a linear transformation is sufficient to separate the translation of the center-of-mass from the Cartesian coordinates.^[62] The result is a Hamiltonian that can be decomposed according to

$$\begin{aligned} \mathbf{H}_{\text{nuc}}(\vec{R}) &= \mathbf{H}_{\text{COM}}(\vec{R}_{\text{COM}}) + \mathbf{H}_{\text{TI}}(\vec{R}_{\text{TI}}) \\ &= -\frac{1}{2M_{\text{COM}}}\Delta_{\vec{R}_{\text{COM}}} - \sum_{i=1}^{3N-3} \frac{1}{2M_{\text{TI},i}} \frac{\partial^2}{\partial R_{\text{TI},i}^2} + V(\vec{R}_{\text{TI}}) \quad , \end{aligned} \quad (2.65)$$

where \vec{R}_{COM} and \vec{R}_{TI} represent the center-of-mass and the $(3N - 3)$ translationally invariant (TI) Cartesian coordinates, respectively, and \mathbf{H}_{COM} and \mathbf{H}_{TI} the corresponding Hamiltonians. $M_{\text{TI},i}$ refers to the mass associated with the i th translationally invariant coordinate. The nuclear Hamiltonian \mathbf{H}_{nuc} does not contain any expression that couples \vec{R}_{COM} and \vec{R}_{TI} . As a consequence the overall translations are independent of the rotations and vibrations, which are thus completely described by \mathbf{H}_{TI} . Typically, the first step is followed by the introduction of a body-fixed reference frame, which is attached to the molecule in a predefined and fixed way. For instance, the

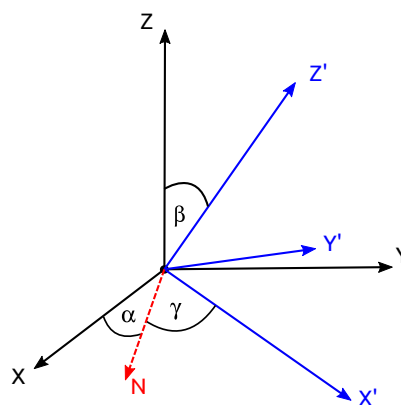


Figure 2.1: Relation between two axes systems. To rotate the black frame into the blue one, the rotations $Z'(\gamma) \circ N(\beta) \circ Z(\alpha)$ have to be applied.

body-fixed axes system can be defined such that its z axis is always oriented parallelly to a certain bond in the investigated molecule. This is referred to as axis embedding. The additional coordinate system is used to define the molecular orientation relative to the original laboratory frame through three Euler angles, as is illustrated in Figure 2.1. Mathematically, the transition from translationally invariant Cartesians to body-fixed coordinates and orientational angles corresponds to an orthogonal transformation defined by the three Euler angles. Among the transformed $(3N - 3)$ Cartesian coordinates only $(3N - 6)$ remain independent. These represent the internal coordinates, invariant with respect to uniform translations and rigid rotations. The transformation is summarized by

$$\mathbf{H}_{\text{TI}}(\vec{R}_{\text{TI}}) \xrightarrow{\hat{U}(\alpha, \beta, \gamma)} \mathbf{H}_{\text{BF}}(\alpha, \beta, \gamma, \vec{R}_{\text{int}}) \quad , \quad (2.66)$$

where \hat{U} is the orthogonal transformation depending on the Euler angles α , β and γ . The transformed Hamiltonian \mathbf{H}_{BF} is defined by a selected body-fixed (BF) frame. It is expressed in terms of a set of internal coordinates \vec{R}_{int} and the Euler angles, which describe the molecular orientation relative to the original laboratory frame. The explicit dependence on the Euler angles can be hidden by exploiting their relations to the angular momentum operators \hat{J} and \hat{J}_i ($i = x, y, z$). Therefore, rovibrational Hamiltonians in a body-fixed reference frame are typically given with respect to the total angular momentum \vec{J} of the system, that is

$$\mathbf{H}_{\text{BF}}(\alpha, \beta, \gamma, \vec{R}_{\text{int}}) \longrightarrow \mathbf{H}_{\text{BF}}^{\vec{J}}(\vec{R}_{\text{int}}) \quad . \quad (2.67)$$

Moreover, the expressions in $\mathbf{H}_{\text{BF}}^{\vec{J}}$ can be assigned to describing either vibrational motion (\mathbf{H}_{vib}) or rotations and the rovibrational coupling ($\mathbf{H}_{\text{rot(vib)}}^{\vec{J}}$), according to

$$\begin{aligned} \mathbf{H}_{\text{BF}}^{\vec{J}}(\vec{R}_{\text{int}}) &= \mathbf{H}_{\text{vib}}(\vec{R}_{\text{int}}) + \mathbf{H}_{\text{rot(vib)}}^{\vec{J}}(\vec{R}_{\text{int}}) \\ &= \mathbf{T}_{\text{vib}}(\vec{R}_{\text{int}}) + V(\vec{R}_{\text{int}}) + \mathbf{T}_{\text{rot(vib)}}^{\vec{J}}(\vec{R}_{\text{int}}) \quad . \end{aligned} \quad (2.68)$$

The vibrational Hamiltonian \mathbf{H}_{vib} contains the internal coordinates but is independent of the angular momentum. It comprises the vibrational kinetic energy operator \mathbf{T}_{vib} as well as the potential energy surface $V(\vec{R}_{\text{int}})$, which is invariant with respect to the system's orientation in (field-free) space. In agreement with that, $\mathbf{H}_{\text{rot(vib)}}^{\vec{J}}$ consists solely of kinetic energy terms – thus, $\mathbf{T}_{\text{rot(vib)}}^{\vec{J}}$. Expectedly, the body-fixed rovibrational Hamiltonian will reduce to \mathbf{H}_{vib} for a molecule with $J = 0$.

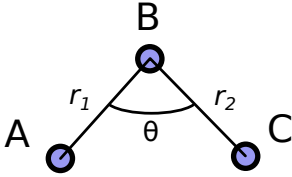
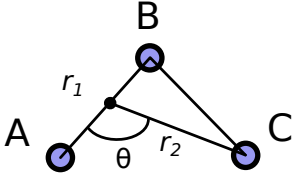
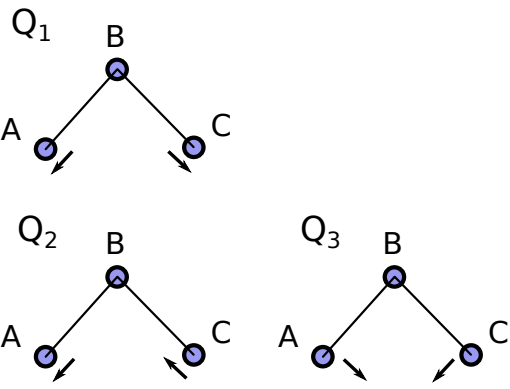
At this point, an appropriate coordinate system to represent the internal coordinates has to be selected. In that regard the strategic objective is to use a set of coordinates that naturally represents the chemical system and the investigated process. For instance, Radau coordinates and hyperspherical coordinates are particularly suited to describe molecules of the AB_2 (such as H_2O) and A_3 (e. g. H_3^+ , O_3^-) type, respectively, as the coordinates represent the molecular symmetry well. Likewise, when molecular scattering is investigated one may benefit from employing Jacobi (scattering) coordinates. The advantage of using suitable representations of the internal degrees of freedom is rooted in the circumstance that this typically decreases coupling among the coordinates. Thus, it introduces separability into the rovibrational problem, greatly facilitating the solution process. Corresponding to that, the description of the internal coordinates in terms of separate Cartesian displacements is inefficient. To illustrate the following descriptions of applicable internal coordinate systems, a listing of definitions and kinetic energy operators for valence, orthogonal Jacobi and normal mode coordinates of a bent triatomic molecule (for instance, H_2O) with $J = 0$ is given in Table 2.1.

Probably, the first type of coordinates that comes to mind for describing the internal degrees of freedom are valence coordinates, i. e. bond lengths and angles. With respect to the potential energy the valence coordinates are fairly decoupled,^[98,99] meaning that the full potential can be expressed rather efficiently in terms of these coordinates. However, the kinetic energy operator includes mixed derivatives, i. e. terms such as $\frac{\partial^2}{\partial q_i \partial q_j}$ (where q_i and q_j are two of the valence coordinates). Correspondingly, there is significant coupling among the coordinates in the kinetic energy as well as a very complicated kinetic energy operator for problems of larger dimensionality.

A different type of coordinates is referred to as orthogonal coordinates, prominent examples being Jacobi, Radau and hyperspherical coordinates.^[64,100,101] As for the valence coordinates, suitably chosen orthogonal coordinates are to a relatively small degree coupled in the potential energy. On the other hand, the kinetic energy operators based on orthogonal coordinates do not feature mixed derivatives or significant coupling. Therefore, the selection of orthogonal coordinates results in rather compact expressions for the rovibrational Hamiltonians.

A third approach to representing the internal motion relies on normal modes of the molecule. These are linear combinations of Cartesian displacements relative to a well-defined equilibrium position. A description of the normal mode analysis is given in the next section. The normal modes are decoupled in the kinetic energy operator and the potential, as long as the term of highest order in the potential is quadratic or lower. For real potentials,

Table 2.1: Illustration of valence, orthogonal Jacobi and normal mode coordinates for a triatomic molecule with a bent equilibrium structure. In the equations m_i denotes the mass of atom i . For the Watson Hamiltonian $I_{\alpha\beta}$ refers to the moment of inertia, $\varepsilon_{\alpha\beta\gamma}$ to the Levi-Civita symbol,^[102] $l_{\beta ik}$ to the Cartesian displacement of atom i along β in mode k and η_{kl}^α to the Coriolis coupling coefficients.

	coordinate system	vibrational kinetic energy operator ^[63,103,104]
valence coord.		$ \begin{aligned} & -\frac{1}{2\mu_1} \frac{\partial^2}{\partial r_1^2} - \frac{1}{2\mu_2} \frac{\partial^2}{\partial r_2^2} \\ & -\frac{1}{2} \left(\frac{1}{\mu_1 r_1^2} + \frac{1}{\mu_2 r_2^2} - \frac{2 \cos \theta}{r_1 r_2} \right) \cdot \left(\frac{\partial^2}{\partial \theta^2} + \cot \theta \cdot \frac{\partial}{\partial \theta} \right) \\ & -\frac{1}{m_B} \frac{\sin \theta}{r_1 r_2} \frac{\partial}{\partial \theta} \left(1 - \frac{1}{r_1} \frac{\partial}{\partial r_2} - \frac{1}{r_2} \frac{\partial}{\partial r_1} \right) \\ & + \frac{\cos \theta}{m_B} \left(\frac{1}{r_1} \frac{\partial}{\partial r_2} + \frac{1}{r_2} \frac{\partial}{\partial r_1} - \frac{\partial^2}{\partial r_1 \partial r_2} - \frac{1}{r_1 r_2} \right) \end{aligned} $
		with the reduced masses
		$\mu_1 = \frac{m_A \cdot m_B}{m_A + m_B} \quad \text{and} \quad \mu_2 = \frac{m_C \cdot m_B}{m_C + m_B}$
orthogonal coord.		$ \begin{aligned} & -\frac{1}{2\mu_1} \frac{\partial^2}{\partial r_1^2} - \frac{1}{2\mu_2} \frac{\partial^2}{\partial r_2^2} \\ & - \left(\frac{1}{2\mu_1 r_1^2} + \frac{1}{2\mu_2 r_2^2} \right) \cdot \left(\frac{\partial^2}{\partial \theta^2} + \cot \theta \cdot \frac{\partial}{\partial \theta} \right) \end{aligned} $
		with the reduced masses
		$\mu_1 = \frac{m_A \cdot m_B}{m_A + m_B} \quad \text{and} \quad \mu_2 = \frac{m_C \cdot m_B \cdot m_A}{m_C + m_B + m_A}$
normal modes (Watson Hamiltonian)		$ -\frac{1}{2} \sum_{i=1}^3 \frac{\partial^2}{\partial Q_i^2} + \frac{1}{2} \sum_{\alpha, \beta} \mu_{\alpha\beta} \hat{\pi}_\alpha \hat{\pi}_\beta - \frac{1}{8} \sum_{\alpha} \mu_{\alpha\alpha} $ <p>with $\alpha, \beta, \gamma \in \{x, y, z\}$ and</p> $\hat{\pi}_\alpha = \sum_{k,l=1}^3 \eta_{kl}^\alpha Q_k \left(-i \frac{\partial}{\partial Q_l} \right), \quad \mu_{\alpha\beta} = (\mathbf{I}^{-1})_{\alpha\beta},$ $I'_{\alpha\beta} = I_{\alpha\beta} - \sum_{k=1}^3 \sum_{l=1}^3 \sum_{m=1}^3 \eta_{km}^\alpha \eta_{lm}^\beta Q_k Q_l,$ $\eta_{kl}^\alpha = \sum_{\beta\gamma} \varepsilon_{\alpha\beta\gamma} \sum_{i=1}^N l_{\beta ik} l_{\gamma il}$

which typically contain higher-order terms beyond the quadratic one, normal modes are useful if a unique and well-pronounced potential minimum and thus equilibrium configuration exists and processes are examined that correspond to only small displacements from this minimum structure. For large-amplitude motion of the nuclei or the calculation of high-energy states, the normal modes are strongly coupled in the potential energy and consequently are not an efficient way to describe the internal coordinates. The normal mode representation of the internal coordinates is used in the commonly applied Watson Hamiltonian.^[105] Within that approach the body-fixed axes system is embedded into a particular reference frame, the Eckart frame, which minimizes the coupling between vibrations and rotations close to a predefined reference configuration.^[106] Notably, the general form of the Watson Hamiltonian remains the same irrespective of the dimensionality of the problem. Thus, its application to arbitrary chemical systems is more straightforward than for Hamiltonians based on other coordinate systems.

To conclude this part, it should be emphasized again that the general outline given here served only to introduce a few of the basic but important considerations that factor into the preparation of the time-independent nuclear Hamiltonian. These are details that to some degree relate to this thesis. Generally though, the exhaustive field of describing the time-independent nuclear Schrödinger equation hosts many more schemes and details about constructing nuclear Hamiltonians efficiently and thoroughly.

Nuclear Wave Functions

In order to exploit the variational principle in actual calculations, a matrix representation of the rovibrational Hamiltonian has to be set up. For this the nuclear wave function is expanded into a set of basis functions. Similarly to the Hamiltonian, this basis set should be suited to the problem. The nuclear wave function $\xi(\vec{R})$ in Equations (2.8) and (2.64) depends on all $3N$ nuclear degrees of freedom. First, the separability of the center-of-mass translation from the nuclear coordinates in the Hamiltonian (Equation (2.65)) allows for a product decomposition of the wave function,

$$\xi(\vec{R}) = \xi_{\text{COM}}(\vec{R}_{\text{COM}}) \cdot \xi_{\text{rv}}(\vec{R}_{\text{TI}}) \quad . \quad (2.69)$$

The wave functions ξ_{COM} describing the overall translations are plane waves. For the calculation of rovibrational states they are irrelevant and thus will be disregarded from

here on out. Instead the focus is placed on the rovibrational wave functions of the translationally invariant coordinates $\xi_{\text{rv}}(\vec{R}_{\text{TI}})$. With the introduction of a body-fixed frame into the Hamiltonian, the rovibrational problem can be parametrized by the internal coordinates as well as three Euler angles and the associated angular momentum operator \vec{J} (see Equations (2.66) and (2.67)). Consequently, $\xi_{\text{rv}}(\vec{R}_{\text{TI}})$ becomes $\xi_{\text{rv}}^{\vec{J}}(\alpha, \beta, \gamma, \vec{R}_{\text{int}})$. Furthermore, dividing the body-fixed rovibrational Hamiltonian into a vibrational part and a rotational-rovibrational coupling part (see Equation (2.68)) suggests a product ansatz for the rovibrational wave function as well. Usually, the latter is expanded according to

$$\xi_{\text{rv}}^{\vec{J}}(\alpha, \beta, \gamma, \vec{R}_{\text{int}}) = \sum_{k=-J}^J \psi^k(\vec{R}_{\text{int}}) |JMk\rangle \quad . \quad (2.70)$$

Herein, $\psi^k(\vec{R}_{\text{int}})$ represents the vibrational states of the system that are coupled to the rotational part via a parametric dependence on k , the projection of the total angular momentum J on the body-fixed z axis. The rotational portion of the wave function is described in a basis of symmetric-top wave functions $|JMk\rangle$, where J is the total angular momentum, while M and k are its projections on the z axis in the laboratory frame (Z in Figure 2.1) and the body-fixed frame (Z' in Figure 2.1), respectively. The functions are given by

$$|JMk\rangle = \sqrt{\frac{2J+1}{8\pi^2}} D_{Mk}^{J*}(\alpha, \beta, \gamma) = \sqrt{\frac{2J+1}{8\pi^2}} e^{iM\alpha} d_{Mk}^J(\cos\beta) e^{ik\gamma} \quad , \quad (2.71)$$

where $d_{Mk}^J(x)$ is

$$d_{Mk}^J(x) = \frac{(-1)^u}{2^M} \sqrt{\frac{(J+M)!(J-M)!}{(J+k)!(J-k)!}} (1-x)^{\frac{u}{2}} (1+x)^{\frac{v}{2}} P_{J-M}^{(u,v)}(x) \quad , \quad (2.72)$$

with the Jacobi polynomials $P_a^{(b,c)}(x)$ and $u = M - k$ and $v = M + k$.^[107] These rotation functions fulfil several eigenvalue equations involving the angular momentum operator \hat{J} . In particular, they obey (among others)

$$\hat{J}^2 |JMk\rangle = J(J+1) |JMk\rangle \quad , \quad (2.73a)$$

$$\hat{J}_z |JMk\rangle = M |JMk\rangle \quad , \quad (2.73b)$$

$$\hat{J}_z^{\text{BF}} |JMk\rangle = k |JMk\rangle \quad , \quad (2.73c)$$

where BF indicates a projection onto the body-fixed axes system.^[108] When solving the rovibrational problems, these relations can obviously be exploited, making the symmetric-top functions highly appropriate basis functions.

In view of the vibrational part $\psi^k(\vec{R}_{\text{int}})$ of the nuclear wave function, more basis functions have to be selected. A common approach is the expansion of the vibrational wave functions into a direct-product basis of one-dimensional basis functions,

$$\psi^k(\vec{R}_{\text{int}}) = \sum_{j_1=1}^{B_{j_1}} \cdots \sum_{j_{N_i}=1}^{B_{j_{N_i}}} c_{j_1 \dots j_{N_i}} \left(\prod_{l=1}^{N_i} \phi_{j_l}^{(l)}(R_{\text{int},l}) \right), \quad (2.74)$$

where N_i is the number of internal coordinates and $\phi_{j_l}^{(l)}(R_{\text{int},l})$ is one of B_{j_l} one-dimensional basis functions of a type denoted by (l) representing the internal coordinate $R_{\text{int},l}$. The contribution of a given product of basis functions to the vibrational wave function is described by the expansion coefficient $c_{j_1 \dots j_{N_i}}$. Depending on the choice of basis functions different types of representations for the vibrational Hamiltonian matrix are obtained. If a basis set can be found such that the matrix elements can be determined analytically, the matrix representation is called a variational basis representation (VBR).^[65] In the VBR, the errors to the vibrational states are only due to the truncation of the basis set that is unavoidable in numerical calculations. Unfortunately, a full analytic evaluation of the Hamiltonian matrix is possible only for selected model potentials. Thus, a VBR is typically not available for systems described by fully coupled potential energy surfaces. Then, representations that rely on accurate numerical quadrature methods have to be employed, such as the finite basis (FBR) or discrete variable representations (DVR) of the internal coordinates.

The one-dimensional basis functions of a coordinate in the FBR are typically described by sets of orthonormal functions, for which an expression for the corresponding part of the kinetic energy operator can be derived analytically. Ideally, these basis functions are chosen such that accurate quadrature schemes, for example Gauss quadrature, are readily applicable to them. This is because the elements of the potential matrix are usually unknown in these bases and have to be evaluated by numerical quadrature over the different internal coordinates. In accord with that, common choices for the basis functions are the solutions of one-dimensional problems like the harmonic oscillator and the Morse potential or general orthogonal polynomials, such as Hermite polynomials (for radial coordinates) or Legendre polynomials (for angular coordinates), for which accurate (Gauss) quadrature schemes are known.^[64]

On the other hand, the discrete variable representation is a direct-product, but grid-based representation of the Hamiltonian. The DVR for a single coordinate is related to the corresponding FBR based on orthogonal polynomials through a unitary transformation. This transformation can be obtained from setting up the coordinate matrix in the FBR and diagonalizing it. To be precise, the transformation that diagonalizes the coordinate matrix in the FBR is the same transformation that facilitates a transition from the FBR to the DVR. The eigenvalues of the FBR coordinate matrix are the grid points defining the DVR. In agreement with that, each of the actual one-dimensional DVR basis functions is to a high degree localized at one of the grid points while vanishing at the remaining ones. Moreover, it can be shown that the DVR grid points, that is the eigenvalues of the FBR coordinate matrix, are the nodes of a Gauss quadrature over the original FBR functions; the quadrature weights may be found in the eigenvectors. In the DVR, the matrix representations of functions of the regular coordinate operator are approximated to be diagonal. Matrix elements are calculated by inserting DVR grid points as an argument into the corresponding function. Consequently, the potential matrix is effectively diagonal with non-vanishing elements corresponding to the potential at the DVR grid points. To set up the kinetic energy matrix in the DVR, usually the corresponding FBR matrix is constructed and subsequently transformed to the DVR. Also, analytical expressions for the kinetic energy in the DVR are known for several types of orthogonal polynomials.^[109] In view of the connection to the FBR, typical DVR schemes are the Legendre, Hermite and Jacobi DVRs, but also the sinc and sine DVRs, each of them being suited to describe particular types of motion.^[109,110] Aside from these, there are various schemes to reduce the number of basis functions and improve the numerical performance. Often, these consist of contracting primitive basis functions to obtain optimized ones. This can be achieved by first solving nuclear problems in reduced dimensions to access the improved basis functions. In case of contracting basis functions in one dimension this is referred to as potential optimized DVR.^[111]

With respect to the direct-product wave function of Equation (2.74) full DVR representations are widely used. This is partly due to the clear approach to optimizing the DVR basis sets (through contraction and truncation) and the straightforward way of calculating expectation values on the grid. Furthermore, in comparison to the standard FBR bases, which are not localized in position space, the localized DVR functions are suited to treat a wider range of nuclear motion, including large amplitude motion, more efficiently.^[64] However, depending on the problem also mixed DVR-FBR representations of (ro)vibrational wave functions are used.^[104,112]

Once a matrix representation of the (ro)vibrational Hamiltonian is constructed, the system's (ro)vibrational states and the energies are approximated by the corresponding eigenvectors and eigenvalues, respectively. Thus, an eigenvalue problem has to be solved. If the Hamiltonian matrices are small enough, usually when triatomic molecules are investigated, a direct diagonalization may be feasible. However, for larger molecules, direct diagonalizations are definitely intractable. In these cases, iterative eigensolvers may be used, which do not require storing the full Hamiltonian matrix in memory.^[113–116]

2.3.2 Normal Mode Analysis

Due to its importance for the description of molecular vibrations and its common application in quantum chemical investigations, the normal mode analysis is further explained in this section. The method allows for the estimation of approximate fundamental vibrational transitions of a chemical system at a stationary point on its potential energy surface. The central idea is to approach the nuclear problem in the harmonic approximation. This is illustrated by considering a Taylor expansion of the potential energy surface around the minimum configuration,

$$\begin{aligned}
 V(\vec{R}_0 + \Delta\vec{R}) &= V(\vec{R}_0) + \sum_i \left(\frac{\partial V}{\partial R_i} \right)_0 \Delta R_i \\
 &+ \frac{1}{2} \sum_{i,j} \left(\frac{\partial^2 V}{\partial R_i \partial R_j} \right)_0 \Delta R_i \Delta R_j + \dots \quad ,
 \end{aligned}
 \tag{2.75}$$

with the minimum configuration \vec{R}_0 and displacement vector $\Delta\vec{R}$ comprising the Cartesian displacements ΔR_i . The index $()_0$ indicates that displacements with respect to a stationary point on the PES are considered. For the normal mode analysis the series expansion is truncated after the second derivatives and $V(\vec{R}_0)$ is set to zero. Also, the first derivatives of the potential with respect to the coordinates vanish at a stationary point. Thus, the potential is reduced to

$$V(\vec{R}_0 + \Delta\vec{R}) = \frac{1}{2} \sum_{i,j} \left(\frac{\partial^2 V}{\partial R_i \partial R_j} \right)_0 \Delta R_i \Delta R_j \quad .
 \tag{2.76}$$

This is the potential of a system of coupled harmonic oscillators. The problem can be decoupled by switching to mass-weighted Cartesian coordinates,

$$q_i = \sqrt{m_i} \cdot \Delta R_i \quad , \quad (2.77)$$

where m_i is the mass of the atom displaced by ΔR_i . The resulting potential expression is

$$V(\vec{q}) = \frac{1}{2} \sum_{i,j} \left(\frac{\partial^2 V}{\partial q_i \partial q_j} \right)_0 q_i q_j = \frac{1}{2} \sum_{i,j} D_{ij} q_i q_j \quad , \quad (2.78)$$

with the mass-weighted Hessian matrix D carrying the force constants for displacements along the mass-weighted Cartesian coordinates. The decoupled normal modes and their frequencies are obtained from diagonalizing D . The resulting eigenvectors correspond to the normal modes and the eigenvalues λ_i are related to the modes' frequencies ω_i by

$$\omega_i = \sqrt{\lambda_i} \quad . \quad (2.79)$$

The relation

$$E_{n_i}^i = \omega_i \left(n_i + \frac{1}{2} \right) \quad , \quad (2.80)$$

with n_i being a natural number or zero, describes the energies of the decoupled harmonic oscillators' states. An approximation of the true vibrational ground state energy at 0 K is given by the sum of the harmonic oscillator ground state energies, the vibrational zero-point energy

$$E_{\text{VZPE}} = \frac{1}{2} \sum_{i=1}^{3N-6} \omega_i \quad . \quad (2.81)$$

The normal mode analysis is used to validate the outcome of structure relaxations and approximate the fundamental vibrational properties of the investigated system. However, it may also be the first step to a more sophisticated treatment of the rovibrational problem, as was indicated in the preceding section and will be laid out further in the upcoming one.

2.3.3 Vibrational Self-Consistent Field Method

At different points in the description of the nuclear problem, it was emphasized that the approach to obtaining solutions is usually strongly adapted to the chemical system. However, among the discussed coordinate systems and Hamiltonians, the Watson Hamiltonian

based on a normal mode description of the vibrational motion stood out in the sense that its general shape was not changed by the number of dimensions of the problem. Obviously, this is a very desirable property concerning the general applicability of corresponding methods. A further step towards a black-box scheme to describe nuclear motions is given by the vibrational self-consistent field (VSCF) framework – at least for molecules that are well-described in the normal mode coordinate system. The VSCF approach is to some degree related to the variational procedures described before, as it is based on the Watson Hamiltonian and exploits the variational principle.^[66] However, instead of calculating the fully coupled vibrational states by diagonalizing a Hamiltonian matrix, approximations of the states are obtained self-consistently. In fact, VSCF is rather comparable to the Roothaan-Hall-Hartree-Fock (RHHF) method: The vibrational wave functions are expanded into products of single-mode functions (denoted modals, corresponding to orbitals in HF); the modals are expressed in terms of more tractable basis functions (analogous to using Gaussian basis functions for the LCAO functions in the RHHF scheme); the variational principle is used to derive effective one-particle problems such that each modal moves in an averaged potential generated by the other modals (like an electron feels a mean-field potential generated by the other electrons in HF theory).

The full Watson Hamiltonian for M vibrational modes is given by

$$\begin{aligned} H_{\text{Watson}} = & -\frac{1}{2} \sum_{i=1}^M \frac{\partial^2}{\partial Q_i^2} + \frac{1}{2} \sum_{\alpha, \beta} (\hat{J}_\alpha - \hat{\pi}_\alpha) \mu_{\alpha\beta} (\hat{J}_\beta - \hat{\pi}_\beta) \\ & - \frac{1}{8} \sum_{\alpha} \mu_{\alpha\alpha} + V(Q_1, \dots, Q_M) \quad , \end{aligned} \quad (2.82)$$

where Q_i is a normal mode coordinate and $\alpha, \beta \in \{x, y, z\}$.^[105] The operators \hat{J}_α and $\hat{\pi}_\alpha$ represent the total and vibrational angular momentum and $\mu_{\alpha\beta}$ is related to the moment of inertia. Definitions of $\hat{\pi}_\alpha$ and $\mu_{\alpha\beta}$ are given in Table 2.1. The potential V is defined in terms of the normal modes as well. In the VSCF scheme initially molecules with vanishing total angular momentum ($J = 0$) are considered. Thus, the kinetic energy expression is reduced to the one listed in Table 2.1. The wave function $\Psi_{\text{vib}}^{\vec{n}}(Q_1, \dots, Q_M)$ for a vibrational state denoted by the vector \vec{n} is expanded as

$$\Psi_{\text{vib}}^{\vec{n}}(Q_1, \dots, Q_M) = \prod_{i=1}^M \phi_i^{(n_i)}(Q_i) \quad , \quad (2.83)$$

with the one-mode wave function (modal) $\phi_i^{(n_i)}(Q_i)$ describing only normal mode i and the (state) vector $\vec{n} = (n_1, \dots, n_M)$ containing the quantum numbers n_i for the different modals. Unlike for electrons, a straightforward Hartree product ansatz is sufficient; the vibrational wave function does not have to be antisymmetrized, because the normal modes are distinguishable. The VSCF energy for a given vibrational state defined by the state vector \vec{n} is variationally minimized by optimizing the modals under the constraint that they remain orthonormal, $\langle \phi_i^{(n_i)} | \phi_j^{(n_j)} \rangle = \delta_{ij}$. Analogously to Equation (2.18) in HF theory, this yields a set of single-modal equations for the state \vec{n} ,

$$\hat{h}_i^{\vec{n}}(Q_i) \phi_i^{(n_i)}(Q_i) = \epsilon_i \phi_i^{(n_i)}(Q_i) \quad . \quad (2.84)$$

The modal energies are represented by ϵ_i and the effective one-mode Hamiltonian $\hat{h}_i^{\vec{n}}$ is described as

$$\begin{aligned} \hat{h}_i^{\vec{n}}(Q_i) = & -\frac{1}{2} \frac{\partial^2}{\partial Q_i^2} \\ & + \left\langle \prod_{l \neq i}^M \phi_l^{(n_l)} \left| V + \frac{1}{2} \sum_{\alpha, \beta} \hat{\pi}_\alpha \mu_{\alpha\beta} \hat{\pi}_\beta - \frac{1}{8} \sum_{\alpha} \mu_{\alpha\alpha} \left| \prod_{k \neq i}^M \phi_k^{(n_k)} \right. \right. \right\rangle . \end{aligned} \quad (2.85)$$

The second term in Equation (2.85) is an effective potential for the investigated modal that depends on the remaining modals. Thus, the equations have to be solved self-consistently, as was the case in the Hartree-Fock method. After the optimal modals are determined the VSCF wave function of the vibrational state \vec{n} can be assembled. The VSCF energy of the state \vec{n} is then calculated via

$$E^{\vec{n}} = \langle \Psi_{\text{vib}}^{\vec{n}} | H_{\text{VSCF}}^{\vec{n}} | \Psi_{\text{vib}}^{\vec{n}} \rangle = \langle \Psi_{\text{vib}}^{\vec{n}} | \sum_{i=1}^M \hat{h}_i^{\vec{n}} | \Psi_{\text{vib}}^{\vec{n}} \rangle \quad , \quad (2.86)$$

where the effective one-modal Hamiltonians are parametrized by the optimized set of modals. In analogy to the Roothaan-Hall scheme for HF theory, the modals in VSCF are expanded into sets of primitive basis functions. Typically, these are harmonic oscillator functions or distributed Gaussians.^[67,117] The expansions allow for a matrix formulation of the effective one-modal eigenvalue problems, facilitating its numerical solution. As VSCF is a mean-field theory, often additional measures are necessary to end up with accurate vibrational states. To this end, several methods have been developed to improve the VSCF results. These correspond to correlation methods in electronic structure calculations and follow analogous routes to improve the wave function – prominent examples

are vibrational configuration interaction (VCI), perturbation theory (VPT2) and coupled cluster (VCC).^[118-120] If properties of rotationally excited species are of interest, product combinations of the wave functions from VSCF-based procedures and symmetric-top eigenstates can be used to approach the full Watson Hamiltonian of Equation (2.82).^[118]

Chapter 3

Summary

This chapter comprises an overview of the results that were obtained in this work and described in the two publications and the submitted manuscript listed in the next chapter. The important insights are highlighted and their relevance to quantum chemical investigations of matrix isolation experiments in general is explained. Overall, the objective of this work was to model the fundamental vibrational properties of small molecules entrapped in rare gas matrices in a highly accurate way. This is important, as a precise reproduction of experimental data with theoretical modeling bridges the gap between a matrix isolation experiment and the vast range of information available from theory. To this end, a general workflow had to be developed and applied to relevant test systems in order to validate the methods and expand the understanding of the investigated matrix effects.

3.1 Carbon Dioxide in Argon - Preparation Phase

Paper A is concerned with adequately describing the interplay of guest-host and host-host interactions for molecules in extended rare gas structures. In particular, we are interested in determining the extent of the rare gas environments necessary for cluster models to behave like periodic arrangements of larger cells. With respect to the general objective of this thesis, that is establishing a generally applicable procedure to model vibrational motion of molecules in rare gas matrices, the work published in **Paper A** is a preparatory step. The test system we selected for this groundwork study is a single carbon dioxide molecule in argon. There are mostly two reasons for this choice. Firstly, the CO₂

3.1. CARBON DIOXIDE IN ARGON - PREPARATION PHASE

molecule has long been known to display a matrix effect in argon. To be precise, in the corresponding infra-red spectra multiple signals are observed for both, the fundamental vibrational bending and antisymmetric stretching excitations.^[18,37,121–123] For the bending excitations the signal group comprises a high-energy doublet and a low-energy single peak separated by 1 cm^{-1} to 2 cm^{-1} . On the other hand, in the region of the antisymmetric stretching mode two single peaks with a distance of 6 cm^{-1} are observed. These findings are currently interpreted as site effects caused by isolated CO_2 molecules in different environments. This perspective is supported by several experimental matrix isolation studies with increased dilution of the guest species and very low temperatures.^[18,37,123] Obviously, the observed signal shifts and splittings are of interest for this thesis. The second reason for selecting the carbon dioxide molecule in argon as a test system is that the molecule's electronic ground state should be rather well-described by standard density functional theory methods. As a consequence CO_2 in argon may be considered a rather accessible benchmark system. Corresponding to that, several theoretical investigations attempted to model the effect of argon environments on the antisymmetric stretching vibration of CO_2 . In particular, there are the DFT studies by Jose *et al.*^[124] and the works of Severson^[125] as well as Wang and Xie,^[126] respectively, using diffusion Monte Carlo and path integral Monte Carlo simulations. These studies were successful at reproducing the peak shifts relative to free CO_2 (and in case of Wang and Xie the occurrence of two signals), despite being based on relatively small CO_2 -argon clusters of up to only 25 rare gas atoms. However, with these manageable cluster sizes the question of how the outer shells of Ar atoms affect the immediate surroundings of the guest and thus indirectly the molecular properties remained open. Therefore, we were further encouraged to use CO_2 in argon for approaching this issue in a systematic study. The general outline for this consisted of examining the convergence of structural and vibrational properties of CO_2 -argon clusters with an increasing number of rare gas atoms and comparing the results to reference values calculated for larger matrix models employing periodic boundary conditions.

To this end, we investigate CO_2 molecules in three different argon fcc environments in **Paper A**. The three types of surroundings correspond to two single-vacancy and one double-vacancy sites. The reference models for the environments are periodic bulk structures based on a cubic fcc cell containing 108 argon atoms. This approach has been employed by Hochlaf and coworkers^[127,128] in preceding studies on the effect of unit cell sizes on the properties of N_2 and CO in argon. Regarding the cluster modeling, four structures containing one to four shells of argon atoms around the carbon dioxide are probed

for each environment. In all three investigated types of surroundings the inclusion of four neighboring shells amounts to treating 54 argon atoms. All modeling structures are shown in Figure 3.1. The structures of each periodic reference cell and cluster are optimized and the fundamental vibrational excitations of the carbon dioxide are approximated through normal mode analyses. The electronic structure of the various systems is described within the framework of dispersion-corrected density functional theory with the GGA functional PBE and the hybrid PBE0 method.

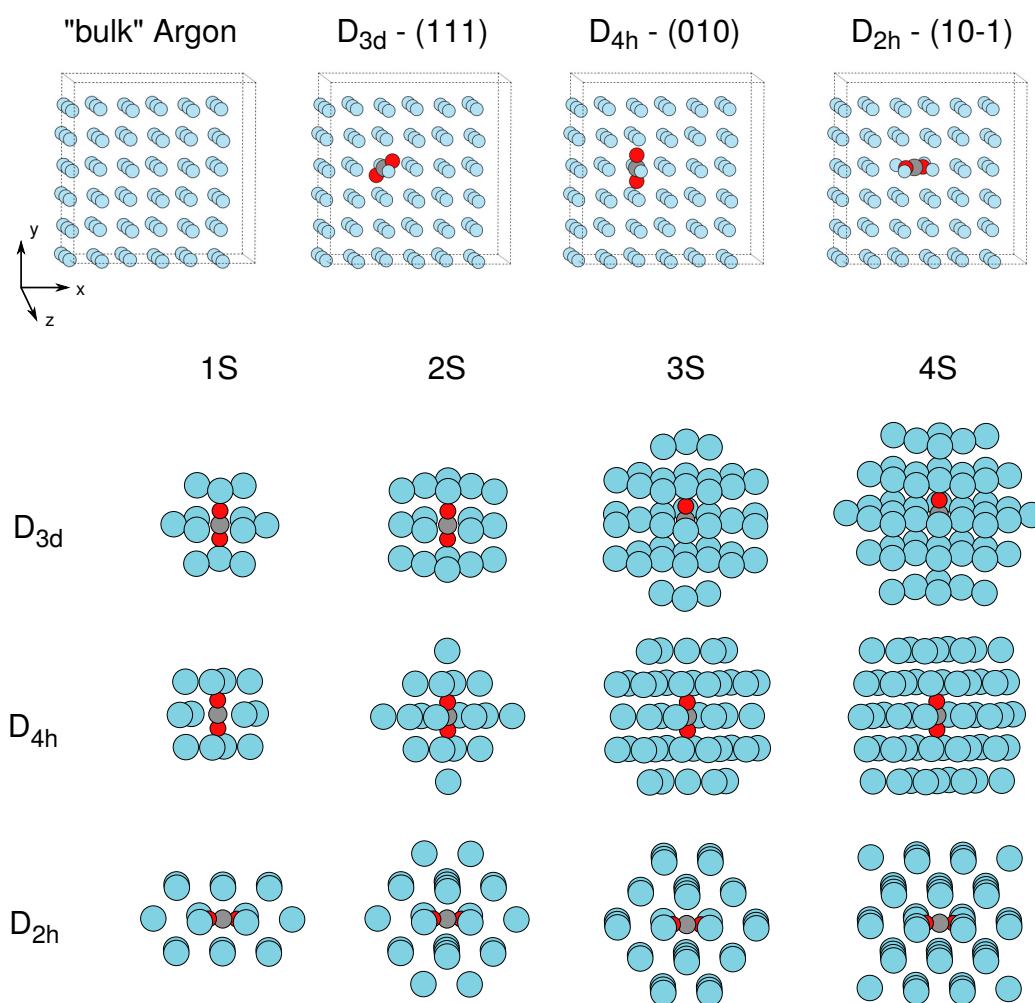


Figure 3.1: CO_2 -argon structures. Top: Periodic models. Lower rows: Clusters. The labels D_{3d} , D_{4h} and D_{2h} refer to the local symmetry of the CO_2 -argon environment and (111), (010) and (10-1) indicate the respective direction of the molecular axis in the cell. XS denotes the number of argon atom shells around CO_2 . Figure taken from **Paper A**.

3.1. CARBON DIOXIDE IN ARGON - PREPARATION PHASE

Through analysis of the calculations on the bulk models using periodic boundary conditions several insights are gained. Concerning the optimized structures of the guest-host environments, change matrix plots show that the carbon dioxide molecule effects sizable changes mostly in its immediate vicinity. Thus, the guest and its distorted surroundings can be considered a local impurity in the matrix system. Moreover, additional information on the cavity structures is obtained. The optimizations of the single-vacancy structures produce cavities that are elongated along the molecular axis and narrowed equatorial to it compared to the pure argon structure. For the double-vacancy environment the majority of direct argon atom neighbors approaches the CO₂ molecule during the optimization, indicating that increased interactions with the guest stabilize the rather spacious vacancy site. Expectedly, the atomic displacements in the first shell are more pronounced and affect the outer shells more strongly for the single-vacancy environments. The attractive guest-host interactions show that the double-vacancy structural motif is slightly more stable than the two single-vacancy structures, which feature more or less equally strong interactions. Finally, the harmonic vibrational analyses produce normal mode frequencies that, while shifted relative to the measured signals, are in quantitative agreement with the experimentally observed matrix effects. With regards to the fundamental antisymmetric stretching excitation, two signals split by roughly 6 cm⁻¹ appear in matrix isolation infra-red spectra in argon. Our calculations indicate that the high-energy part may be attributed to carbon dioxide in a single-vacancy site, while the low-energy component is rooted in the double-vacancy environment. Likewise, for the fundamental bending excitations multiple signals are observed in matrix isolation experiments. The characteristic pattern consists of a single signal accompanied by a slightly blue-shifted doublet. This behaviour is also found in our study, where the CO₂ entrapped in the double-vacancy site displays bending modes split by 1 cm⁻¹ at slightly blue-shifted energies compared to the single-vacancy situations. Our assignment of the signals in the antisymmetric stretching and bending regions to single- and double-vacancy environments matches the ones of Dahoo *et al.*^[18] as well as Vigasin and collaborators.^[123] In view of these results, the periodic bulk models can be considered a valid reference for describing the matrix effects of carbon dioxide in argon.

After establishing the appropriate reference systems, the CO₂-argon cluster models are examined. The results on the clusters speak for an indirect, but notable influence of the outer shells on several properties of the guest-host system. Structural features, such as atomic displacements caused by the guest, are affected most strongly. Especially the constitution of the double-vacancy environment is significantly improved by considering four

neighboring shells of argon atoms around the carbon dioxide molecule. This is revealed by the host atom displacements relative to the periodic reference as well as the cavity volume. Moreover, sizable changes to the guest-host interaction energies are observed upon including more shells of argon atoms. With respect to frequency shifts and splittings, the qualitative features of the carbon dioxide normal modes observed in our periodic bulk models are found in the clusters as well. The effect of the additional argon atoms on the normal mode frequencies of the entrapped CO₂ remains relatively small with deviations in the range of 3 cm⁻¹ among the cluster structures of a given environment. However, it is notable that the expected trends regarding frequency shifts relative to the free molecule are typically reinforced upon including the fourth shell of argon atoms. For instance, for the carbon dioxide in the single-vacancy sites the blue-shift of the antisymmetric stretching excitation is consistently strongest for the largest cluster, while in the double-vacancy environment the corresponding red-shift is most pronounced. This is relatively consistent over all investigated quantum chemical methods and basis sets and clearly indicates an indirect influence of the outer shells of rare gas atoms on the vibrational frequencies of the guest molecule.

The central conclusion from **Paper A** with respect to the overarching objective of this thesis is that including a large number of host atoms is paramount to accurately model the vibrational and structural properties of extended guest-matrix systems through clusters. An analogous insight for the unit cell size in modeling procedures based on periodic structures was obtained by Hochlaf and collaborators^[127,128] in their studies of CO and N₂ in argon. The effect of the outer shells of rare gas atoms on the vibrational properties of the guest molecule is indirect and thus rather small. Nevertheless, it may still amount to a few cm⁻¹ in the fundamental excitations, which can be a sizable fraction of overall small effects. Hence, this should not be neglected in an attempt to quantitatively reproduce experimental findings. More important though is the influence on the structural constitution of the immediate rare gas surroundings. The outer rare gas atoms provide the framework for a balanced description of guest-host and host-host interactions and are thus crucial to appropriately describing the structures of the guest-host systems as a whole. In accord with that, the cluster approaches selected by Jose *et al.*, Severson as well as Wang and Xie are probably insufficient for credibly modeling carbon dioxide in extended argon matrices. Aside from providing these insights on structural modeling, our results back up the site effect hypothesis for carbon dioxide in argon.

3.2 Trifluoride in Neon - Establishing the Model

Based on the knowledge obtained from the work described in **Paper A**, the broader aim of the thesis was approached; that is, designing a systematically improvable workflow to investigate guest molecule-rare gas matrix systems with *ab initio* methods in a highly accurate way. The focal points of the scheme are the determination of optimized guest-host structures and the evaluation of the molecular vibrational properties in the presence of the rare gas atoms. In **Paper B** and **Paper C** the resulting procedure is described and applied to the trifluoride anion F_3^- entrapped in neon and argon, respectively. This compound is examined for several reasons. Firstly, it exemplifies the role of matrix isolation in the investigation of highly unstable species, having been detected only through matrix isolation spectroscopy^[129–132] and mass spectrometry.^[133] In correspondence to that, theoretical investigations are crucial for a thorough characterization of the anion. Furthermore, the trifluoride serves as a strong benchmark system for our procedure. It displays a sizable matrix effect, i. e. a red-shift of about 15 cm^{-1} for the fundamental antisymmetric stretching excitation when going from neon matrices to heavier rare gases.^[132] The trifluoride is bound rather weakly and features significant multireference character, constituting an intricate electronic structure.^[134–136] In accord with that, several studies established that the key to accurately treating the anion is the application of high-level quantum chemical correlation methods.^[134–146] Additionally, preceding calculations revealed sizable vibrational anharmonicity in the free trifluoride.^[131] A modeling workflow able to accurately describe this complicated system may be readily transferred to other systems. Finally, to the best of our knowledge there is no previous study dealing with the trifluoride in extended rare gas environments via quantum chemical methods. A corresponding investigation will thus produce new insights into the origin of the matrix effect as well as the structural and vibrational properties of the trifluoride-rare gas systems.

The modeling procedure described in **Paper B** can be organized in three general steps, which are taken to assess the properties of compound systems of a small (di- to pentatomic) molecule M and N rare gas (Rg) atoms:

1. determination of an accurate potential energy surface for $M\text{-Rg}_N$ systems
2. structure optimizations of the $M\text{-Rg}_N$ structures
3. vibrational analyses of the optimized $M\text{-Rg}_N$ structures.

The first fundamental design decision concerns the description of the system's electronic structure, that is the potential energy surface, which is used in the ensuing structure optimizations and vibrational analyses. For this, we select a tool frequently applied when describing larger compound systems with accurate quantum chemical methods: A truncated many-body expansion (MBE) of the compound system's potential energy surface (PES). Accordingly, the latter is estimated as the sum over contributions by selected subsystems within the complete guest-host structure. In the context of matrix-isolated species, this has been applied to HRgX compounds (Rg: Ar, Kr, Xe; X: F, Cl, Br, I) by Bihary *et al.*^[147] and Niimi and collaborators,^[148,149] and to Na atoms in various rare gas matrices by McCaffrey and coworkers,^[150] just to name a few. The fragmentation-based approach offers several advantages over a single calculation of the whole system with an affordable quantum chemical method. First, the most relevant contributions to the MBE-PES can typically be determined more accurately than the complete system. This is particularly important for the appropriate description of the electronic structure and properties of challenging guest molecules with, for instance, multireference character. Once its components are assembled, the MBE-PES can be used to describe corresponding systems of arbitrary sizes without additional electronic structure calculations. Moreover, the decomposition facilitates an interpretation of the effect of the rare gas atoms on the guest molecule through the terms in the MBE. Thus, changes in the molecular properties can be attributed to two-body M-Rg or three-body M-Rg-Rg interactions, for example. Finally, the truncated MBE is systematically improvable, as impactful errors to the PES introduced by the truncation are easily remedied by adding previously neglected terms.

For trifluoride in neon, the MBE-PES is truncated after the two-body terms, containing contributions by free F_3^- and Ne atoms as well as F_3^- -Ne and Ne-Ne pair interactions. Discrete representations of the components of the MBE-PES are set up with the CCSD(T)-F12b method and appropriate basis sets of valence triple-zeta quality. Initial test calculations on the free trifluoride using this coupled cluster approach revealed T1 diagnostics beyond 0.02. As expected from the studies of Heard *et al.*,^[134] Wright and Lee^[135] as well as Czernek and Živný,^[136] this speaks for a significant multireference character of the anion. However, the good agreement of the calculated vibrational excitation energies for free F_3^- with infra-red spectra of F_3^- in neon suggest that CCSD(T)-F12b is able to describe the region around the global potential minimum in an appropriate way, despite not fully grasping the multireference character. Importantly, coupled cluster schemes involving connected triple excitations are also suited to treat non-covalent interactions.^[151,152]

For the internal F_3^- potential as well as the F_3^- -Ne and the Ne-Ne interaction potentials about 11000, 47000 and 215 configurations were sampled, respectively. From these data sets continuous forms of the PES are generated via fitting procedures. For the continuous expressions of the internal trifluoride potential and the F_3^- -Ne interaction we use permutationally invariant polynomials (PIP) as implemented in the monomial symmetrization approach by Bowman and coworkers.^[153] Unlike more physically motivated functional forms based on, for example, Morse or Lennard-Jones potentials, by default the polynomials do not describe the asymptotic limits of the respective potential contributions correctly. They are, however, more flexible and consequently able to represent the *ab initio* data points more accurately if the fitting data set is large enough. In view of the required very precise description of F_3^- and the F_3^- -Ne interaction close to the equilibrium configuration, we considered the accuracy of the potential in that region more important than obtaining a globally valid representation. The final continuous representations of the F_3^- and F_3^- -Ne potentials are characterized by root mean square deviations well below 10 cm^{-1} in the relevant regions and accurately reproduce potential scans for selected configurations. For the Ne-Ne interaction the precedingly published Ne-Ne potential function by Vogel *et al.*^[154] was refitted to our calculated CCSD(T)-F12b data.

The second stage of the modeling workflow consists of identifying guest-host environments, which credibly represent matrix structures. We attempt to model the latter based on extended cluster structures, instead of bulk models with periodic boundary conditions. This choice is mainly motivated by the more straightforward applicability of the cluster approach to charged molecules. As was worked out in **Paper A**, the most important factor when using cluster structures to model extended systems is to make them large enough to adequately represent the extended environments. Accordingly, the basic model is a cubic fcc cell of 500 rare gas atoms containing the guest molecule at the center, which is shown in Figure 3.2. The rare gas atoms are divided into a movable section comprising several layers of host atoms around the guest (dark blue in Fig. 3.2) and the rare gas atoms beyond that (grey in Fig. 3.2), which are frozen and represent a crystal framework affecting the movable core. The guest-host environment is thus portrayed as a local impurity in an otherwise ordered crystal structure. The scheme has been introduced as dynamical cell rigid walls (DCRW) boundary conditions and used in studies of molecular iodine and HRgX (X: Cl, I) compounds in rare gas matrices.^[147,155] Although not being truly extended in the sense of periodic, the model is an improvement over simple approaches employing small clusters for the description of matrix environments.

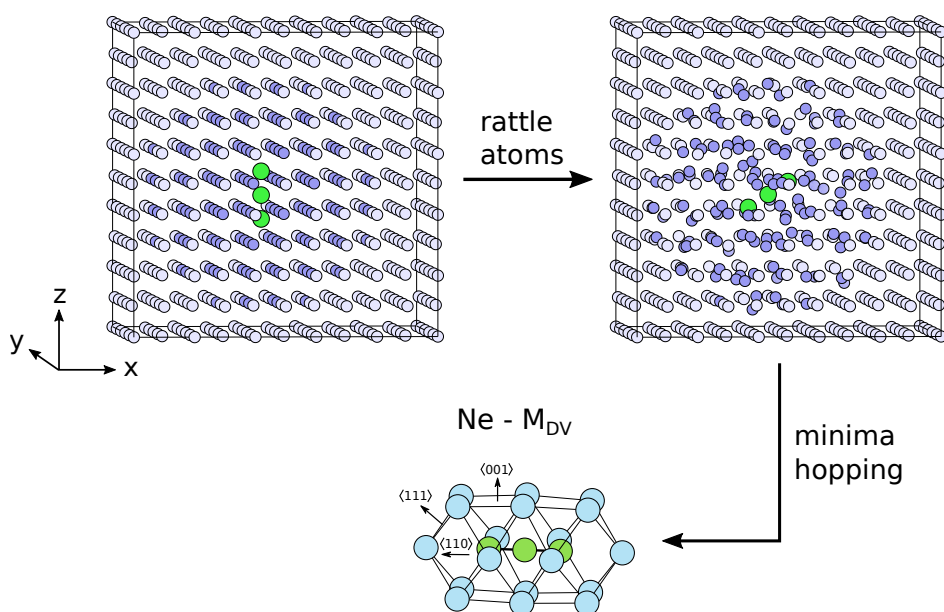


Figure 3.2: Trifluoride-neon models. Top: Complete trifluoride-neon clusters. Movable Ne atoms: blue. Fixed Ne atoms: grey. Before initiating the minima hopping runs, the movable section is rattled. Lower row: Structural motif identified for neon. M_{DV} refers to the position of F_3^- in a double-vacancy cavity. The upper part is taken from **Paper B**, while the bottom image is included in **Paper E1**.

Optimized guest-host environments are obtained with minima hopping (MH).^[156] This global optimization technique has been shown to be rather efficient at sampling flat potential energy surfaces compared to other schemes, such as the basin hopping algorithm employed in a study by Hochlaf and coworkers^[157] on NO^+ ions in argon clusters. MH optimizations are run for three trifluoride-neon models, containing a differing number of vacancy sites in the structure. In one model all neon atoms are kept. For the other two, the formation of a single- and a double-vacancy cavity is facilitated by removing one and two rare gas atoms from the trifluoride's surroundings, respectively. Despite the different constitutions of the models, the guest-host environments in the minima found by the MH runs can be assigned to the same structural motif (N_{hex} in **Paper B**, $Ne-M_{DV}$ in Figure 3.2). Accordingly, the trifluoride is situated in a double-vacancy site and oriented normal to hexagonal planes in the structure. This is the same double-vacancy environment as the one described in **Paper A** for CO_2 in argon. In the F_3^- -Ne models with less than two vacancy sites, one or more neon atoms are displaced into interstitial space to form the double-vacancy cavity. In these cases, the immediate rare gas environment is more disordered. The trifluoride seems to dominate the cavity formation, emphasizing the weakness

of the Ne-Ne pair potential, which is characterized by a well-depth of about 30 cm^{-1} . Similarly to CO_2 in argon the structural changes in the neon environment caused by the trifluoride seem to be rather localized, once again pointing towards the interpretation of the guest molecule as a local impurity in the matrix framework. The trifluoride structure is not drastically affected by the presence of the neon atoms, experiencing a small bond and angle compression.

In the final step of our procedure we evaluate the vibrational properties of the entrapped molecule based on the guest-host environments optimized in the second step. To principally allow for results of almost quantitative accuracy, we deemed it important to account for the molecular vibrational anharmonicity and intermode coupling as well as the effect of the rare gas atoms on the molecular motion. To this end, we determine the vibrational states of the molecule with a variational procedure as described in Section 2.3 of Chapter 2, that is by solving a vibrational (nuclear) Schrödinger equation. Obviously, not all degrees of freedom can be included in such a scheme. Therefore we consider the rare gas atoms frozen in the vibrational analyses. As a consequence, the effect of the environment on the molecular vibrations enters the procedure only statically through the potential. Moreover, the degrees of freedom of the guest species are separated into two groups. The ones essential to the investigated properties are included explicitly in the nuclear Hamiltonian, while the rest is treated adiabatically, i. e. they are implicitly included through an effective potential. In the latter the implicitly treated coordinates are optimized for a given configuration of the explicitly regarded degrees of freedom. As an example, for our triatomic test species we consider the three internal coordinates explicitly in the Hamiltonian, but optimize the molecular orientation in the environment and the motion of the molecular center-of-mass for each configuration of the internal degrees of freedom. Through that a part of the coupling between the explicitly and the implicitly treated coordinates is recovered.

To obtain the fundamental vibrational states of the trifluoride, we solve the Schrödinger equation defined by a three-dimensional Hamiltonian in orthogonal Jacobi coordinates with an effective potential for a number of optimized trifluoride-neon environments. The presence of the host typically effects a slight compression of the fundamental vibrational states. Moreover, certain environments seem to produce stronger intermode coupling compared to the free molecule. This is indicated by the occurrence of non-vanishing densities in the nodal regions and slightly tilted densities in the lowest antisymmetric stretching and bending states. The fundamental stretching excitations are blue-shifted in

a consistent way compared to the gas phase reference; the symmetric stretching mode by around 6 cm^{-1} , the antisymmetric stretching mode by roughly 3 cm^{-1} . For the latter mode, the calculations typically yield excitation energies within 524 cm^{-1} and 526 cm^{-1} , which match the experimentally observed one,^[132] 525 cm^{-1} . Concerning the bending vibrations, the lowest observed excitation in our calculations displays a transition energy that is twice as large as expected for the fundamental one. To accurately resolve the degenerate fundamental bending excitations of a (quasi-)linear molecule not only the bending angle has to be described, but also the rotation about the molecular axis. Since we include the latter only implicitly through the effective potential, we impose isotropy upon rotation about the molecular axis on the nuclear wave function. As a result, we cannot describe the nodal structure associated with the fundamental bending excitations. However, the first bending overtone has a totally symmetric component, which can be resolved by our model. The lowest calculated bending excitations should therefore correspond to the first bending overtones. These are blue-shifted as well, although the magnitude of the shifts varies more strongly than for the stretching modes. This may point to an increased sensitivity of the bending mode to the rare gas environment. The accurate reproduction of the experimentally observed fundamental excitation energies validates our modeling approach.

All in all, we consider the workflow established in **Paper B** a relatively integral representative of models used to describe matrix isolation spectroscopy. Concerning the constitution of the potential energy surface, earlier attempts to investigate matrix effects were restricted to guest-host interactions based on true diatomics-in-molecules potentials.^[147,158,159] With these, the interaction regards only two atoms at once, that is a matrix atom and an atom that is part of the guest molecule. For instance, in the studies of HRgX species (Rg: Ar, Kr, Xe; X: F, Cl) in rare gas environments by Bihary *et al.*^[147] the interactions of HRgX molecules with rare gas atoms are described in terms of isolated H-Rg, Rg-Rg and X-Rg pairs. In our interaction potentials the complete guest molecule with all its internal degrees of freedom is treated, providing a rather accurate description of guest-host interactions that goes beyond the two-atom picture. For the identification of optimized rare gas environments we do not rely on starting structures with predefined molecular orientations along high-symmetry directions in the cell. This would be a common approach, which has been employed by us in **Paper A**, but also in other investigations of matrix isolated species, such as the works of Niimi *et al.*^[148,149] and Bihary and collaborators.^[147] Instead of that, we opt for a less biased procedure and use an opti-

mization scheme, which produces relaxed structures from a disordered arrangement of the guest and host atoms embedded in a crystalline framework of matrix atoms. With respect to the vibrational properties of the guest, we aim for very accurate and reliable results. Therefore, we include the molecular vibrational anharmonicity and intermode coupling, while other studies restrict themselves to normal mode analyses.^[127,128,157] Unlike in the path integral Monte Carlo studies by Wang and Xie^[126] we do not target a specific predetermined vibrational transition, but calculate all the transitions available for the given choice of explicitly treated coordinates and the accessible region of the potential energy surface. Moreover, the external molecular degrees of freedom are treated implicitly and static effects by the environment are included.

3.3 Trifluoride in Argon - Extending the Model

In **Paper C** the investigation of the trifluoride anion in rare gas matrices is continued. For this we apply the modeling workflow described in **Paper B** to the trifluoride in argon environments with analogous structural models and computational procedures.

To study the trifluoride-argon models, we initially used a many-body expanded PES combining the internal trifluoride potential introduced in **Paper B** with two-body F_3^- -Ar and Ar-Ar interaction terms. However, in the course of the investigation it became apparent that an important contribution to the PES was not regarded. Therefore, we extended the initial potential energy surface by including three-body F_3^- -Ar₂ interactions. The new MBE-PES is used only to refine the stability analyses of the guest-host models and the anharmonic vibrational analyses of the entrapped trifluoride anions. Corresponding to that, in **Paper C** we present highly accurate F_3^- -Ar, Ar-Ar and F_3^- -Ar₂ interaction potentials. The F_3^- -Ar potential is determined by fitting PIP functions to a database of about 60000 CCSD(T)-F12b/aug-cc-pVTZ-F12 interaction energies, while the Ar-Ar interaction is described by refitting the Ar-Ar potential function of Patkowski and Szalewicz^[160] to 226 *ab initio* points. To obtain a F_3^- -Ar₂ potential, PIP functions are fitted to the three-body interaction energies of about 73000 F_3^- -Ar₂ configurations collected with CCSD(T)-F12b/aug-cc-pVDZ-F12 calculations. The quality of the continuous potential functions is ascertained through examining mean errors and *ab initio* potential scans. Judging from the increased magnitudes of the F_3^- -Ar and Ar-Ar interaction potentials compared to their neon counterparts, a stronger influence of the Ar atoms in the guest-host systems

is expected. For example, the well-depths of the Ne-Ne and Ar-Ar potentials amount to roughly 30 cm^{-1} and 95 cm^{-1} , respectively. The individual F_3^- -Ar₂ interactions are mostly repulsive and much weaker than the attractive F_3^- -Ar interactions.

The MH optimizations of the three basic trifluoride-argon models yield three structural motifs, one typical of each vacancy situation. The corresponding surroundings of the trifluoride are shown in Figure 3.3. Aside from the double-vacancy environment (Ar-M_{DV}) observed for F_3^- in neon as well, there is an interstitial (Ar-M_{IN}) and a single-vacancy motif (Ar-M_{SV}). While the occurrence of different environments is in part due to the

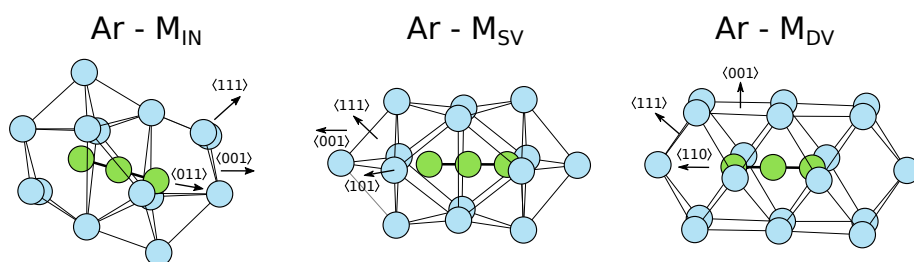


Figure 3.3: Structural motifs identified for the argon models. M_{IN}, M_{SV} and M_{DV} refer to F_3^- in an interstitial, a single-vacancy and a double-vacancy cavity, respectively. The images are used in **Paper E1**.

increased spacing in the argon crystal framework, it also points to the stronger Ar-Ar interaction potential, which does not allow the trifluoride to displace host atoms as strongly as in neon. The effect of the argon environment on the trifluoride structure is relatively small. However, there is a distinct difference between the double-vacancy motif and the remaining environments. For the former one of the F-F bonds in the trifluoride is elongated, whereas the other motifs display solely compressed bonds. This shows that the F_3^- -Ar interaction is able to affect the molecular properties in qualitatively different ways. The stabilities of the different argon environments are estimated from the total interaction energies in the optimized structures. At the level of two-body interactions, that is a PES including only F_3^- -Ar and Ar-Ar interactions, the single- and double-vacancy motifs are more stable than the interstitial environment. This discrepancy is further cemented after adding three-body F_3^- -Ar₂ interactions and the harmonic vibrational zero-point energies for the movable section of the cells. Moreover, the relative stabilities of the more favorable motifs are inverted when the three-body interactions and zero-point energies are considered. This illustrates the well-known importance of relatively small effects in the determination of thermodynamically favored structures for extended argon systems.^[161,162]

The anharmonic vibrational analyses presented in **Paper C** show that the effect of the three environments on the trifluoride vibrations matches their influence on the molecular geometries. In particular, relative to the free trifluoride the interstitial and single-vacancy motifs display blue-shifts to both stretching modes, whereas the double-vacancy environment produces red-shifted corresponding excitations. The latter motif (Ar-M_{DV}) is the sole environment that yields vibrational excitation energies approaching the measured quantities. When only the two-body interactions are included in the PES, the corresponding theoretical ($387 \pm 1 \text{ cm}^{-1}$) and experimental^[144] (389 cm^{-1}) values typically agree very well for the symmetric stretching mode. However, the agreement is only qualitative for the fundamental antisymmetric stretching excitation - calc.: around $517 \pm 1 \text{ cm}^{-1}$, exp.^[132]: 510.6 cm^{-1} . With respect to the quantitative reproduction of the experimental reference by our workflow, this means that at this point a significant factor seems to be neglected in the model for trifluoride-argon. This missing contribution is identified as the F_3^- - Ar_2 three-body interaction, whose addition to the MBE-PES notably affects the vibrational excitation energies yielded by our procedure. The changes of the latter obey specific trends, irrespective of the structural motif. The symmetric stretching mode is affected rather weakly and if at all slightly blue-shifted, whereas the antisymmetric stretching excitations are significantly red-shifted. Notably, for the doubly-vacancy environment the latter excitation energies are reduced to about $508 \pm 1 \text{ cm}^{-1}$, while their symmetric stretching counterparts are left mostly unchanged. Thus, the differences between the experimentally observed excitation energies and those computed for the double-vacancy motif are further reduced by regarding the F_3^- - Ar_2 terms. This improvement is another indicator of the relevance of non-additive three-body interactions for polarizable species in argon environments.

The results of the vibrational analyses in **Paper C** clearly suggest that the double-vacancy environment is the dominant host structure for the trifluoride in actual matrix isolation experiments. According to our estimate of the structural stability, it is also the environment most strongly stabilized by guest-host and host-host interactions as well as vibrational zero-point effects. The energetical distance of the double-vacancy environment to the second-most stable single-vacancy motif amounts to roughly 4 kJ mol^{-1} , i. e. is very small. However, if the matrix is allowed to form slowly enough the more stable minimum may be preferred. Likewise, conversions between the two motifs are unlikely once an environment is formed, due to the low temperatures in the matrix isolation experiment. In addition to that, while testing various influences on the cavity stability we have en-

countered another indication for a preferred formation of the double-vacancy site. This is further described in **Paper E1**. To be precise, we ran constant-temperature molecular dynamics simulations with consecutively increasing temperatures between 4 K and 60 K for cells with zero, one or two vacancies. In the simulations all constraints on the atoms were lifted with the objective to study how fast the different environments would disband. Generally, at 30 K any long-ranged order would be destroyed within 20 ps simulation time. When comparing the different structures and temperatures, it became apparent that for the double-vacancy environment a particular trifluoride-argon aggregate displayed relatively high stability against the increasing temperatures. Accordingly, this structural feature may assemble rather early in a condensation process, i. e. at relatively high temperatures, and ensuingly promote the formation of the double-vacancy environment. It is important to stress that this kinetic perspective should by no means be considered a proof, but more a clue that demands further examination. Despite these preceding arguments for the preference of the double-vacancy motif, the single-vacancy environment should be formed as well, at least to a small extent. This is in line with the infra-red experiments of Redeker *et al.*,^[132] where a blue-shifted, broad and weak shoulder to the antisymmetric stretching peak has been observed. Although our calculations predict a stronger blue-shift, this feature may originate from the F_3^- in the single-vacancy site.

3.4 Conclusion and Outlook

The central aim of the present work was to compose a modeling procedure for very accurate investigations of the vibrational properties of small molecules in cryogenic rare gas environments. Judging from the results in **Paper B** and **Paper C**, we are confident that our modeling workflow is appropriate for this objective. In accord with that, it should be applicable in an analogous way to other molecules. To this end, several aspects may have to be adapted to the investigated systems. In the first step of the modeling scheme we applied calculations at the CCSD(T)-F12 level with a basis set of triple zeta quality. If applicable, this is typically a good choice, when aiming for accurate results. However, principally other electronic structure methods can be employed in the workflow as well. Likewise, different functional forms may be used in the fitting of the potential functions.^[163–166] For the second step, other global optimization techniques are available.^[167–169] In comparison to that, the final step of the modeling workflow, the vibrational analysis of the entrapped molecule, requires more attention when transferring to other systems.

Already for tetra- or pentaatomic guests a full description of all internal degrees of freedom in the variational calculation becomes significantly more difficult. To reduce the dimensionality of the problem, a selection of indispensable internal coordinates may be treated explicitly, while the remaining coordinates are either included implicitly via the effective potential or frozen. This should be applicable if the investigated properties are well described by a manageable subset of the internal degrees of freedom. Moreover, an explicit treatment of a larger number of internal coordinates can be facilitated by further contracting the basis functions, for instance with the methods of Bacić and Light or Handy and collaborators.^[170,171] However, there are also situations, where an explicit inclusion of uniform molecular rotations or translations is necessary for fully reproducing the experimental data. This is illustrated by water molecules in neon and argon matrices, for which rovibrational transitions can be observed.^[36,172,173] Additionally, a thorough description of molecular rotations would allow the calculation of the fundamental bending excitations in (quasi-)linear molecules. This is desirable, as our results indicate that those excitations can be very sensitive to the environment, possibly serving as identifiers for structural motifs. A guideline to explicitly treating translations and rotations of entrapped molecules has been provided by the full nine-dimensional calculation of vibration-rotation-translation (VRT) quantum states of water in a frozen fullerene C₆₀ unit by Felker and Bacić.^[174] In principle, a corresponding expansion of our vibrational procedure facilitates the accurate description of all types of molecular motion in the environments. Thus, depending on the examined system, a nuclear problem in reduced dimensions with an effective potential could be assembled modularly and solved. Yet, practically this remains a challenging task, as coordinates and basis functions have to be selected carefully and the numerical cost of solving the problems becomes prohibitive rapidly. The latter aspect is especially true for the calculation of rovibrational states of the entrapped molecules, where aside from the problem of dimensionality the huge density of (VRT) states is an obstacle.

Beyond that, the vibrational procedure can be extended to include the coupling between the environmental and molecular motion. This dynamic contribution to the matrix effects is currently not regarded in our vibrational analyses, where the matrix atoms are frozen. Possible routes to include the motion of host atoms have been described in the studies of Bihary *et al.*,^[147,155] Wang and Xie^[126] as well as Niimi and coworkers.^[148] The former two rely on VSCF and path integral Monte Carlo schemes, respectively, and would thus require abandoning our current approach. The third route demands repeated variational calculations in the course of a classical Monte Carlo simulation, which seems compatible

with our method. However, due to the large number of calculations necessary, it may be practical only for one- or two-dimensional nuclear problems. The resulting neglect of further coordinates in the variational procedures may introduce inaccuracies comparable in magnitude to the dynamic part of the matrix effect. Thus, it is not clear that this modification of our workflow is sensible. Alternatively, the dynamic matrix effect may be assessed from complementary classical molecular dynamics simulations based upon the MBE-PES. To this end, power spectra can be retrieved from the classical trajectories of the free molecule and the guest-host system and compared to corresponding static quantum chemical calculations.

Overall, the studies presented in **Paper A**, **Paper B** and **Paper C** illustrate the use of theoretical (quantum chemical) methods when investigating chemical or physical experiments. In general, theoretical studies may not only yield the same information as experiments, but also provide insights beyond the measured properties. Regarding vibrational matrix isolation spectroscopy, this means that, aside from reproducing the observed signals, theoretical studies may uncover the relations between the observations and structural features of the matrix systems unavailable from experiments. For instance, our modeling workflow (**Paper B**, **Paper C**) accurately reproduces the experimentally measured excitation energies in case of matrix-isolated trifluoride anions. This allows for linking the observed signals to certain guest-host environments. Moreover, due to choosing a truncated many-body expansion to model the systems' potential energy surfaces, the influence of the rare gas atoms on the molecular properties can be attributed to concrete interaction types. This generates a more thorough understanding of the way different rare gas matrices interact with guest molecules.

Chapter 4

Publications

Paper A

"A Validation of Cluster Modeling in the Description of Matrix Isolation Spectroscopy"

F. Bader,* T. Lindic and B. Paulus

J. Comput. Chem. **41**, 751–758 (2020)

DOI: 10.1002/jcc.26123

URL: <https://doi.org/10.1002/jcc.26123>

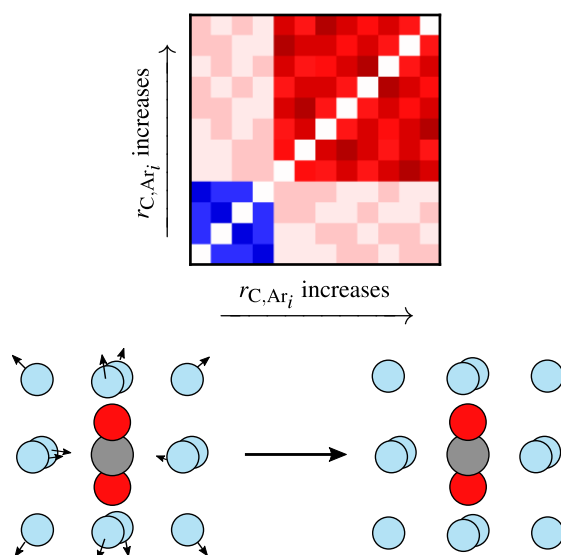


Figure 4.1: Graphical Abstract of **Paper A** (© 2019 Wiley Periodicals, Inc.)

Author contributions:

The project was planned by B. Paulus and myself. T. Lindic and I collected the electronic structure data. The results were analyzed collaboratively by the authors. I drafted the manuscript and T. Lindic and B. Paulus helped revising it.

The pages 67 to 83 contain the printed article, which is protected by copyright.

Paper B

"A pair potential modeling study of F_3^- in neon matrices"

F. Bader,* J. C. Tremblay and B. Paulus

Phys. Chem. Chem. Phys. **23**, 886–899 (2021)

DOI: 10.1039/d0cp05031h

URL: <https://doi.org/10.1039/D0CP05031H>

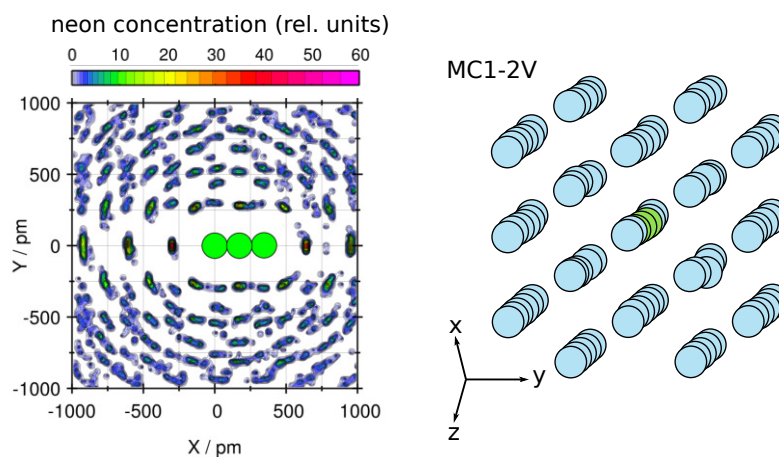


Figure 4.2: Graphical Abstract of **Paper B** (© PCCP Owner Societies 2021)

Author contributions:

The project was conceived by myself. The methodology was worked out by myself and J. C. Tremblay. I performed all calculations. Some of the used computational programs were implemented by myself and J. C. Tremblay. The results were analyzed by J. C. Tremblay, B. Paulus and myself. I authored the manuscript, supported by J. C. Tremblay and B. Paulus.

The pages 85 to 98 contain the printed article, which is protected by copyright.

Paper C

"Theoretical modeling of molecules in weakly interacting environments: Trifluoride anions in argon"

F. Bader,* J. C. Tremblay and B. Paulus

manuscript submitted to Physical Chemistry Chemical Physics on May 26, 2021

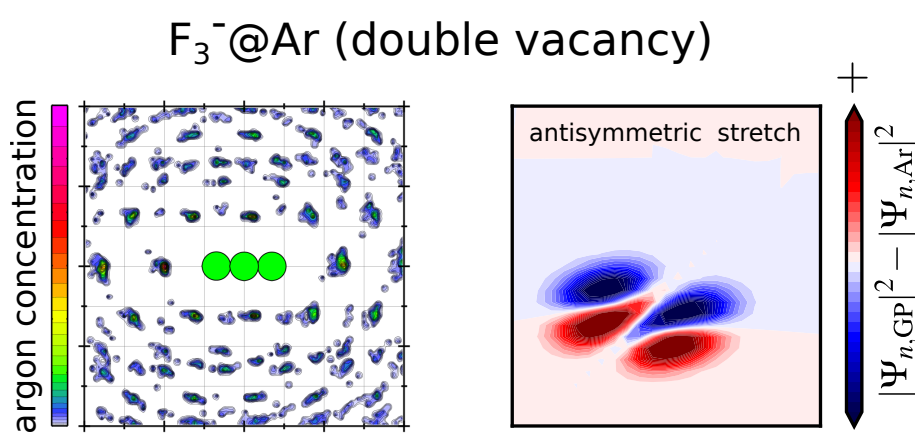


Figure 4.3: Graphical Abstract of **Paper C**

Author contributions:

The idea to examine the system was mine. The investigation was planned by myself and J. C. Tremblay, with contributions by B. Paulus. All calculations were run by myself. J. C. Tremblay, B. Paulus and I analyzed and interpreted the results. The manuscript was drafted by myself, with revisions from J. C. Tremblay and B. Paulus.

Cite this: DOI: 00.0000/xxxxxxxxxx

Theoretical modeling of molecules in weakly interacting environments: Trifluoride anions in argon

Frederik Bader,^{*a} Jean Christophe Tremblay^b and Beate Paulus^a

Received Date

Accepted Date

DOI: 00.0000/xxxxxxxxxx

The properties of molecules can be affected by the presence of a host environment. Even in inert rare gas matrices such effects are observable, as for instance in matrix isolation spectroscopy. In this work we study the trifluoride anion in cryogenic argon environments. To investigate the structure and vibrational properties of the guest-host systems, a potential energy surface of compound F_3^- -argon structures is determined from *ab initio* calculations with the CCSD(T)-F12b approach. Argon environments are probed with minima hopping optimizations of extended trifluoride-argon clusters. The vibrations of F_3^- within the optimized environments are examined with anharmonic vibrational analyses. Among the three identified structural surroundings for the trifluoride, two are characterized by relatively favorable guest-host and host-host interactions as well as vibrational zero-point energies. A striking dependence of the trifluoride properties on the particular argon environment reveals the delicate influence of the host atoms on the guest molecule. Very good agreement with measured data suggests that in experiment F_3^- occupies a double-vacancy site.

1 Introduction

In matrix isolation spectroscopy molecules are entrapped in a frozen unreactive material, that is a matrix, and examined spectroscopically. While inside the host structure, the guest molecules are shielded from intermolecular interactions that may trigger further reactions. Likewise, the interactions between the guest molecules and the matrix are weak because of the inert character of commonly used host materials, such as rare gases or molecular nitrogen. As a consequence, the matrix isolation technique can be used to investigate highly reactive species and weakly interacting systems that would not be stable in other media. Despite their general weakness, the guest-host interactions influence the spectroscopic behaviour of the guest molecules by affecting sensitive properties, for example vibrational excitation energies. The resulting changes observable in the experimental data are denoted matrix effects. With respect to vibrational spectroscopy, the guest-host interactions typically express themselves as peak shifts and splittings in the molecular spectra. The matrix effects are often not particularly large. Nonetheless, their investigation through experimental as well as computational schemes is a worthwhile endeavour. That is because unravelling the origin of the effects yields insights into the specific way a given matrix material interacts with a given guest species. In particular, appropriate theoret-

ical analyses may help to assign the bands in more complicated spectra or link the observed signals to certain structural environments, thus providing information typically not directly available from experiment.

The trifluoride anion F_3^- is a compound that nicely illustrates the importance of matrix isolation. Unlike the triatomic monoanions of the heavier halogens, the trifluoride has at this point been generated exclusively in rare gas or nitrogen matrices and mass spectrometry experiments.^{1–8} Aside from providing a proof of existence, the infra-red (IR) vibrational spectra of F_3^- in varying rare gas environments reveal information about the interaction of the molecule with its surroundings through a matrix effect. Namely, in comparison to neon matrices the fundamental antisymmetric stretching excitation is red-shifted by about 15 cm^{-1} in argon and krypton.^{4,5} In principle, this observation could be explained qualitatively in terms of stronger interactions between the trifluoride and the more polarizable rare gas atoms. A more thorough understanding of the observed signals may be obtained through a theoretical study. The first step in this direction has been taken by Riedel and coworkers, who probed the interaction of the trifluoride and a single neon or argon atom with high-level *ab initio* calculations.⁴ However, in order to represent the situation in a matrix isolation experiment properly a more complete modeling approach is necessary.

To be precise, a quantum chemical model of the trifluoride anion in the presence of rare gas matrix atoms has to comprise two important features. First and foremost, the electronic structure of the guest species has to be described accurately. Various the-

^a Institut für Chemie und Biochemie, Freie Universität Berlin, D-14195, Berlin, Germany. E-mail: f.bader@fu-berlin.de

^b Laboratoire de Physique et Chimie Théoriques, CNRS-Université de Lorraine, UMR 7019, ICPM, 1Bd Arago, 57070 Metz, France.

oretical investigations on the free trifluoride anion identified the necessity of highly accurate quantum chemical correlation methods for an adequate description of the molecule.^{4,5,9-20} Regarding fundamental vibrational excitations, coupled cluster schemes including triple excitations have been shown to produce results of good accuracy.^{4,5,20} Aside from that, several shells of rare gas atoms around the trifluoride have to be included to correctly model the interplay between guest-host and host-host interactions. Concerning the extent of the guest-host system an obvious, tested approach would be the use of density functional theory (DFT) methods.²¹⁻²³ However, this is not applicable due to the delicate electronic structure of the trifluoride. Alternatives to a DFT description of the complete system are wave function embedding methods or a many-body expansion (MBE) of the potential energy surface.^{24,25} With the former an accurate correlation method can be used to describe the trifluoride, while a computationally cheaper scheme, such as DFT, is used for the host atoms. Then, the guest-host interaction is determined by embedding the correlated wave function in a potential generated by the host atoms as described by the lower-level method. In the MBE approach the full system is separated into subsystems. Likewise, the full potential energy surface is decomposed into energy contributions by the fragments and all interactions among them. By truncating the MBE the potential energy surface of the full system can be approximated in terms of the isolated subsystems and interactions between only a small number of fragments, for instance two- and three-body terms. The latter are typically small enough to be treated with an accurate quantum chemical method.

In a preceding investigation of F_3^- in neon we have presented a modeling procedure to determine the fundamental vibrational properties of triatomic molecules in rare gas environments.²⁶ The scheme is based on a many-body expansion of the potential energy surface for $F_3^-X_N$ systems of arbitrary size and yields optimized structural environments for the trifluoride as well as fundamental anharmonic vibrational states of the molecule in the presence of matrix atoms. Here, we transfer and expand this procedure to the trifluoride anion entrapped in argon environments. For this more terms in the many-body expanded potential energy surface are necessary, as shown by the comparison to matrix isolation experiments.

2 Computational Details

In this work we investigate the trifluoride anion in solid argon. To this end, the potential energy surface of $F_3^-Ar_N$ systems is described by a many-body expansion of the potential energy,

$$\begin{aligned}
 E_{\text{tot}} = & E_{F_3^-}(\vec{R}_{F_3^-}) + N \cdot E_{Ar} + \sum_{i,j>i}^N E_{Ar_i-Ar_j}(\vec{R}_{Ar_i}, \vec{R}_{Ar_j}) \\
 & + \sum_{i=1}^N E_{F_3^-Ar_i}(\vec{R}_{F_3^-}, \vec{R}_{Ar_i}) \\
 & + \sum_{i,j>i}^N E_{F_3^-Ar_i-Ar_j}(\vec{R}_{F_3^-}, \vec{R}_{Ar_i}, \vec{R}_{Ar_j}) + \dots,
 \end{aligned} \quad (1)$$

where $E_{F_3^-}$ and E_{Ar} are the internal trifluoride potential and the energy of a single Ar atom, while $E_{F_3^-Ar_i}$, $E_{Ar_i-Ar_j}$ and $E_{F_3^-Ar_i-Ar_j}$ refer to the respective two- and three-body interactions. For our study we use two truncated forms of the potential energy surface, denoted PES-2B and PES-3B. The former contains only terms up to two-body interactions in the many-body expansion (free F_3^- , free Ar atoms, F_3^-Ar and Ar-Ar interactions), while the latter additionally features three-body $F_3^-Ar_2$ interactions. In a first step, continuous representations of the constituents of the many-body expanded potential energy surface have to be determined. We describe the free trifluoride anion with the corresponding potential function presented in our previous study.²⁶ The remaining components of the truncated PES are obtained from fitting different potential functions to CCSD(T)-F12b energies.

2.1 *ab initio* data sets

The electronic structure data for the F_3^-Ar interaction potential was collected with the same computational setting as in the previous work to maintain comparability between the different rare gas systems. Therefore, the CCSD(T)-F12b method was combined with a cc-pVTZ-F12 basis set and appropriate augmentation functions as well as auxiliary basis sets for density fitting and singles corrections.²⁷⁻³² The calculated interaction energies were counterpoise-corrected to account for the basis set superposition error (BSSE).³³ This is backed by test calculations exhibiting BSSEs of 45 cm^{-1} for the strongly attractive region of the F_3^-Ar interaction, even though the triple-zeta F12 basis set should approach the basis set limit. All calculations were performed with the Molpro software package.^{34,35}

The *ab initio* data set for the F_3^-Ar interaction potential consisted of 60085 configurations. The internal trifluoride coordinates were restricted to bond lengths between 1.45 \AA and 2.15 \AA as well as F-F-F angles between 140° and 180° . The argon atom was moved within the fraction of a sphere of 10 \AA around the central F atom that was irreducible upon permuting F atoms. Data points in this configuration space were collected with a combination of grid-based and stochastic sampling. With the former strategy a set of roughly 14000 *ab initio* energies was obtained. The remaining configurations were sampled stochastically. Details on the grid-based sampling procedure are described in the supplementary information.

For the $F_3^-Ar_2$ interaction potential the investigated configuration space was restricted analogously to the F_3^-Ar interactions. The fitting data set comprised the energies of 72970 configurations, which were obtained from Molpro calculations with the CCSD(T)-F12b method, an aug-cc-pVDZ-F12 basis set and corresponding auxiliary basis sets.^{27-32,34,35} The configuration space was sampled with various schemes. The largest portion, that is about 54000 configurations, was stochastically sampled. Close to 19000 of these structures were focussed on the interaction regime with relatively short trifluoride-argon distances. Furthermore, *ab initio* molecular dynamics at the MP2/6-31G* level as implemented in Gaussian 16 with varying initial structures and conditions were used to gather 9654 further configurations.³⁶ A set of 8838 geometries was collected by sampling along the triflu-

oride normal modes in the presence of two Ar atoms. Lastly, 2307 F_3^- -Ar₂ arrangements were cut out of selected optimized minima from the minima hopping (MH) runs with the PES truncated at the two-body interaction level. The final fitting data set was obtained by deleting F_3^- -Ar₂ configurations with energies outside of -30 cm^{-1} and 120 cm^{-1} from this set of structures.

To describe the Ar-Ar interaction potential a data set of 226 configurations was determined, sampling distances between 2 \AA and 24.5 \AA .

2.2 Potential functions and fitting

The continuous interaction potential functions are permutationally invariant polynomials (PIP) determined with the monomial symmetrization approach (MSA) of Bowman and coworkers.³⁷ For the F_3^- -Ar potential the maximal polynomial order was set to $N = 7$, which results in 348 coefficients to optimize. The Morse parameter a_0 inherent to the MSA procedure was set to 4.0 Bohr. Also, an energy weighting was used to improve the fit in regions of attractive interactions. These are the same settings as for the F_3^- -Ne potential of our previous work. Moreover, we have supplemented the potential function with a smooth damping function that tunes out the interaction between 9 \AA and 10 \AA ,

$$f(r_{F_c-Ar}) = \begin{cases} 1 & r_{F_c-Ar} < r_{c1} \\ \frac{1}{2} \cdot \left(1 + \cos\left(\pi \cdot \frac{r_{F_c-Ar} - r_{c1}}{r_{c2} - r_{c1}}\right)\right) & r_{c1} \leq r_{F_c-Ar} \leq r_{c2} \\ 0 & r_{F_c-Ar} > r_{c2} \end{cases} \quad (2)$$

with r_{F_c-Ar} being the distance between the central F atom and the argon atom. The cutoff parameters r_{c1} and r_{c2} were set to 9 \AA and 10 \AA , respectively.

To describe the F_3^- -Ar₂ interaction potential PIP functions of maximum order $N = 5$ (364 coefficients) and $a_0 = 2.7 \text{ Bohr}$ were used. The inclusion of F_3^- -Ar₂ interactions is restricted to the argon atoms in the first two shells of neighboring atoms by using a damping function. The latter has the same functional form as for the F_3^- -Ar interactions (Equation (2)), with the argument r_{F_c-Ar} corresponding to the larger of the two F_c -Ar distances and the cut-off parameters r_{c1} and r_{c2} being 6 \AA and 7 \AA .

Lastly, the potential function for the Ar-Ar interaction is taken from the work of Patkowski and Szalewicz and refitted to the calculated Ar-Ar interaction energies.³⁸ The functional form is

$$V(R) = (A + B \cdot R + C \cdot R^{-1} + D \cdot R^2 + E \cdot R^3) \cdot e^{-\alpha \cdot R} - \sum_{j=3}^8 f_{2j}(R; b) \cdot \frac{C_{2j}}{R^{2j}}, \quad (3)$$

with the parameters A , B , C , D and C_6 being optimized during the fitting procedure. The other parameters are taken from reference³⁸ and not reoptimized. The functions $f_{2j}(R; b)$, with

$$f_{2j}(R; b) = 1 - e^{-b \cdot R} \cdot \sum_{k=0}^{2j} \frac{(b \cdot R)^k}{k!}, \quad (4)$$

are damping functions introduced by Tang and Toennies.³⁹

2.3 Structure optimizations

With the resulting PES-2B argon environments for the trifluoride are determined via minima hopping (MH) optimizations.⁴⁰ The basic model for the argon environments is a cubic fcc $5 \times 5 \times 5$ super cell of 500 Ar atoms with a lattice constant of 5.35 \AA . The latter is larger than the experimental value of 5.30 \AA , but leads to Ar-Ar distances in the cell that are close to the equilibrium distance in the employed argon pair potential.⁴¹ The trifluoride is placed at the center-of-mass of this cell. Two additional initial structures for modeling vacancy sites are obtained by removing one and two argon atoms from the vicinity of the molecule, respectively. For the minima hopping optimizations several structural manipulations are applied to the initial cells. These are described in the supplementary information together with further computational details of the MH optimizations and the structural analyses. When assessing the stability of the minima identified during the MH runs, the guest-host and host-host interaction energies are examined with PES-3B. Also, normal mode analyses are performed with PES-2B for the (movable) core section of the cubic cells to estimate the vibrational zero-point energies of the systems. For the minima that contain vacancy sites a correction based on the per-atom binding energy in a pure argon fcc structure is introduced to the host-host interaction energy. Likewise, in the corresponding normal mode analyses the core section of the cubic cells is slightly expanded. These measures are taken to simplify comparing the models with a differing number of Ar atoms. Details are given in the supplementary material.

2.4 Anharmonic vibrational analyses

In the final step, the structures obtained in the MH runs are used to calculate fundamental vibrational properties of the F_3^- anion in the presence of the argon atoms. This is achieved by solving a three-dimensional nuclear Schrödinger equation in an effective potential. The Hamiltonian in Jacobi coordinates and atomic units is

$$\hat{H}(r, R, \vartheta) = -\frac{1}{2m_A} \frac{\partial^2}{\partial r^2} - \frac{1}{2m_B} \frac{\partial^2}{\partial R^2} - \left(\frac{1}{2m_A r^2} + \frac{1}{2m_B R^2} \right) \cdot \left(\frac{\partial^2}{\partial \vartheta^2} + \cot \vartheta \cdot \frac{\partial}{\partial \vartheta} \right) + \min_{\vec{R}_M, \alpha, \beta, \gamma} V_{\text{tot}}(r, R, \vartheta, \vec{R}_M, \alpha, \beta, \gamma; \vec{R}_{Ar_N}), \quad (5)$$

where r , R and ϑ are the scattering coordinates and angle, respectively. The coordinate r is the distance between a terminal and the central F atom, while R corresponds to the distance of the center-of-mass of these atoms to the remaining F atom. The trifluoride center-of-mass coordinates are denoted \vec{R}_M and the Euler angles α , β and γ define the orientation of the trifluoride in the environment. \vec{R}_{Ar_N} refers to the frozen argon atom coordinates. The masses m_A and m_B are defined as

$$m_A = \frac{m_F \cdot m_F}{m_F + m_F} \quad m_B = \frac{m_F \cdot (m_F + m_F)}{m_F + m_F + m_F}, \quad (6)$$

where $m_F = 18.998403$ u is the mass of a fluorine atom. The nuclear problem is solved by setting up a corresponding matrix representation and extracting the eigenstates with a coupled two-term Lanczos eigensolver using full reorthogonalization.^{42–46} The basis functions are direct products of potential optimized (r and R , 25 functions each) and regular Legendre functions (ϑ , 205 basis functions) in a discrete variable representation (DVR),

$$|\Psi_n\rangle = \sum_{i,j,k} C_{ijk}^{(n)} |\psi_i^r\rangle |\psi_j^R\rangle |\psi_k^\vartheta\rangle, \quad (7)$$

where $|\psi_m^l\rangle$ denotes a DVR basis function of coordinate l .^{47–49} The Powell algorithm is used to optimize the center-of-mass coordinates and the molecular orientation for each (r , R , ϑ) configuration.⁵⁰ The regions of configuration space, which are not regarded in the fitting procedures, are neglected by introducing a potential cut-off. The vibrational analyses are performed with PES-2B and PES-3B.

3 Results and discussion

3.1 Interaction potentials

The F_3^- -Ar potential obtained from fitting PIP functions to the corresponding *ab initio* data set describes interaction energies in the range of -900 cm^{-1} to 2100 cm^{-1} . Further properties of the fitted potential are shown in the left column of Figure 1. The top panel shows the distribution of F_3^- -Ar interaction energies in the relevant range, between -800 cm^{-1} and 800 cm^{-1} , as well as the cumulative root mean square (rms) error. The fitting data set is focussed on capturing the attractive interaction between the compounds. Accordingly, for negative interaction energies the rms error is 3.5 cm^{-1} , while it amounts to roughly 8.5 cm^{-1} over the whole data set.

In the second panel of the left column of Figure 1 the mean errors of the fit in energy windows of 25 cm^{-1} are shown. In case of the F_3^- -Ar interaction the fit does not seem to behave systematically over the whole range of investigated interaction energies. For strongly attractive interaction energies below -800 cm^{-1} the mean errors are positive, pointing towards an overestimation by the fit. Beyond that and up to energies of about -500 cm^{-1} the fit tends to lie below the *ab initio* points, whereas it overshoots the data points slightly in the range of -500 cm^{-1} and -250 cm^{-1} . Between -250 cm^{-1} and 200 cm^{-1} the mean errors approach zero, indicating that roughly equal amounts of data points are over- and underestimated. For the more repulsive interactions the mean errors become larger and trend towards negative values. Generally, this kind of oscillatory behaviour should be treated with caution. However, as the mean errors in the attractive range of interaction energies are below 1 cm^{-1} , any systematic behaviour is not strongly pronounced in the relevant region. Hence, we think that in our case this is not an indictment of the fit. The final three panels in the left column of Figure 1 depict potential scans along different coordinates that were not included in the fitting data set. They show that the fit is able to reproduce the energies in the region of attractive interactions very accurately.

The right column of Figure 1 contains information on the F_3^- -Ar₂ interaction potential. The data distribution in the top panel

reveals that the three-body interaction between the trifluoride and two argon atoms is very weak. The energy range of the fitting data set was truncated to lie between -30 cm^{-1} and 120 cm^{-1} . However, the majority of data points features energies between 0 cm^{-1} and 50 cm^{-1} , speaking for a slightly repulsive contribution to the compound potential energy surface. The cumulative rms error is in the range of 2 cm^{-1} for attractive configurations, but drops to 1 cm^{-1} as soon as the large number of weakly repulsive interactions are taken into account. The overall rms error is 1.1 cm^{-1} .

The mean errors within energy windows of 5 cm^{-1} shown in the second panel in the right column of Figure 1 are close to zero in the well-sampled region between -10 cm^{-1} and 70 cm^{-1} . This indicates that the fit neither over- nor underestimates the CCSD(T)-F12 data points within that energy range in a systematic way. Also, the selected potential scans in the final three panels illustrate the qualitative agreement between the *ab initio* energies and the fit. While the bond length scan speaks for a very accurate description of the discrete data, the fit is slightly too repulsive for most of the angles in the ϑ_{FFF} scan. Moreover, the final panel shows that the fitted potential may become too repulsive for small $r_{\text{F-Ar}}$ distances. Yet, the deviations are small enough to consider the fit accurate.

The comparison of the fitted Ar-Ar interaction potential to the *ab initio* points indicates a very accurate fit. The rms error is 0.2 cm^{-1} . The equilibrium distance is 3.784 Å and the depth of the potential well is 96.297 cm^{-1} . These values are close to their counterparts given by Patkowski and Szalewicz, namely 3.762 Å and 99.351 cm^{-1} .³⁸ The final parameter set for the Ar-Ar interaction potential is listed in Table 1.

Table 1 Optimized parameters for the Ar-Ar interaction potential in atomic units. * Parameters taken from Szalewicz and Patkowski, not reoptimized during fitting procedure.^{38,51,52}

A / E_h	581.172	$C_6 / E_h a_0^6$	60.112
$B / E_h a_0^{-1}$	-117.887	$C_8 / E_h a_0^8$	1491.114*
$C / E_h a_0$	-530.076	$C_{10} / E_h a_0^{10}$	50240.000*
$D / E_h a_0^{-2}$	9.262	$C_{12} / E_h a_0^{12}$	1898195.000*
$E / E_h a_0^{-3}$	-0.266*	$C_{14} / E_h a_0^{14}$	86445426.000*
α / a_0^{-1}	1.553*	$C_{16} / E_h a_0^{16}$	4619452502.000*
b / a_0^1	2.393*		

3.2 Argon environments

During the first segment of the MH runs the cells with rattled Ar atoms were equilibrated such that the fcc crystal structure is for the most part recovered. For each vacancy situation the minima identified during this equilibration period (roughly 200) were disregarded in the further analysis. The remaining minima can be clustered with respect to the orientation of the mostly linear trifluoride in the intact Ar fcc structure. In this way ten sets of structurally comparable minima were obtained: five for the 0V setup (denoted MCX-0V with X ranging from 1 to 5), two for the 1V systems (MCX-1V) and three for cells with two vacancies (MCX-2V). The examination of the argon environments for the structures in the MCX-YV clusters revealed that each vacancy situation featured a different structural motif.

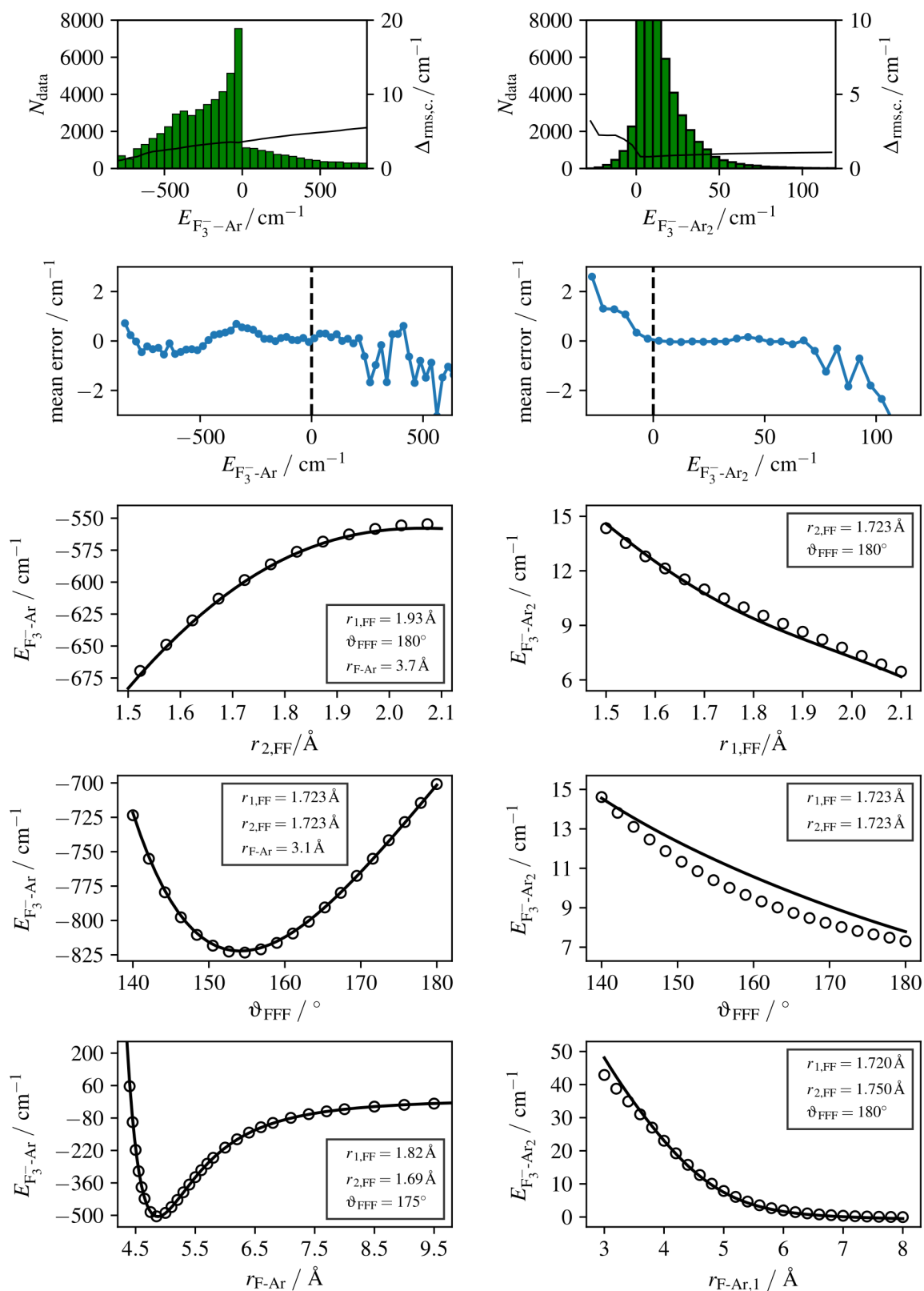


Fig. 1 Interaction potentials for F_3^- -Ar (left panels) and F_3^- -Ar₂ (right panels). Top: Distribution of data points and cumulative rms error. Second row: mean errors in energy windows of 25 cm^{-1} (left) and 5 cm^{-1} (right), respectively. Last three rows: Illustrative potential scans along various coordinates. Markers: *ab initio* data points. Lines: Potential fits. Additional information on the scans is provided in the supplementary material.

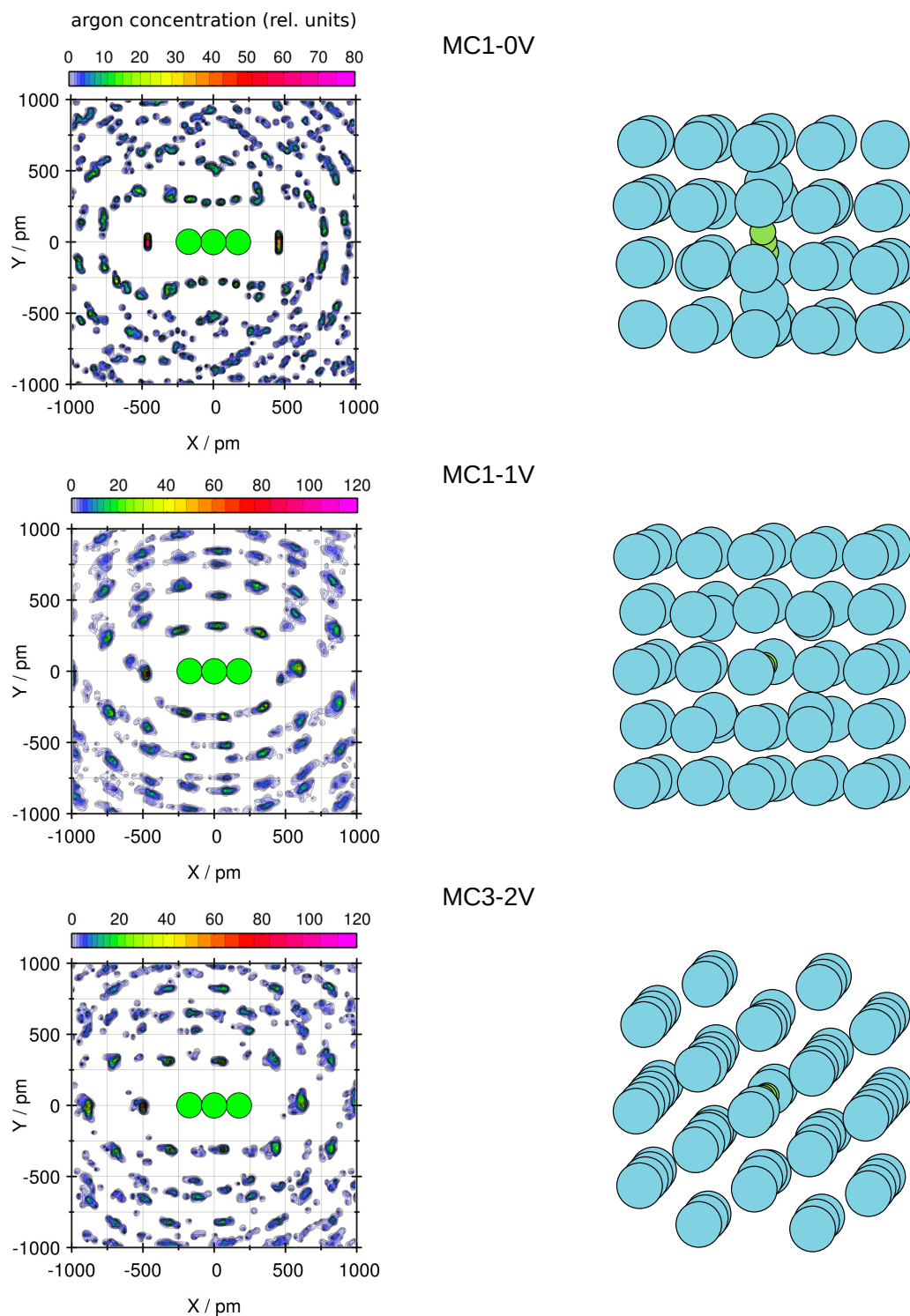


Fig. 2 Plane projection plots for the MC1-0V, MC1-1V and MC3-2V clusters alongside extracts from the corresponding most stable minima. The former plots show the average density of argon atoms around F_3^- in the minima of the MCX-YV clusters relative to a uniform distribution of argon atoms.

For the 0V structures the trifluoride anion is typically centered in a cavity in interstitial place. It has pushed aside mainly two argon atoms to accommodate itself in the tight confines. These Ar atoms are located at opposite sides and ends of the molecule. Moreover, the trifluoride is not aligned with a high-symmetry axis of the

crystal framework. This is illustrated by a snapshot of the typical 0V cell shown on the right in the first row of Figure 2. On the left a representative plane projection plot is shown for the minima of the MC1-0V cluster. In the plot the cavity is rather tight and somewhat concave, confirming that the environment is very nar-

row. Correspondingly, the trifluoride motion should be hindered. Likewise, a sharp pattern for the distribution of argon atoms in the plane projection is clearly discernible, indicating that this is indeed the dominant environment. In the following the structural motif of the 0V minima is denoted M_{IN} or interstitial motif.

In the MCX-1V clusters the cavity occupied by the trifluoride corresponds to the single-vacancy site incorporated into the cell. Within the cavity the trifluoride bonding axis is to a large degree aligned with a direction perpendicular to quadratic planes in the cell (see second row in Figure 2). This structural motif will be referred to as M_{SV} or single-vacancy motif. In the plane projection plots the cavity appears larger than for the 0V case and of convex shape. Moreover, the trifluoride is not centered in the cavity. The distribution functions show that the distances from the central F atom to the two closest Ar atoms along the molecular axis are roughly 4.8 Å and 5.9 Å, respectively. Correspondingly, a stronger trifluoride-argon interaction for one of the terminal F atoms seems to be preferred over a weaker interaction for both terminal F atoms. Thus, the cavity generated by a single vacancy already seems to be too long for the F_3^- in the sense that not all interactions with the Ar atoms in the first neighboring shell are as attractive as possible.

Regarding the 2V structures, two situations occur. For the MC1-2V minima the MH runs produced structures with two single-vacancy cavities. One of them is empty, while the other hosts the trifluoride anion. For these structures the argon environment around the guest molecule corresponds to the one observed for the 1V cells. The second case concerns the MC2-2V and MC3-2V minima. Here, the MH runs yielded a single cavity that comprises both vacancy sites in the cell. The cavity and the trifluoride in it are oriented along a direction normal to hexagonal planes of argon atoms, as shown in the final row of Figure 2. According to that, the motif is called double-vacancy motif and M_{DV} . The plane projection plot for the minima of the MC3-2V cluster expectedly shows that the cavity for this environment is wider than for the 0V and 1V structures. It is elongated too, with distances of around 5.0 Å and 6.2 Å between the central F atom and the two closest Ar atoms along the molecular axis. As was the case for the M_{SV} motif, the trifluoride within the M_{DV} environment is not located at the center of the cavity, but slightly shifted towards one end.

The effect of the different environments on the internal trifluoride coordinates is illustrated in Figure 3. For all three vacancy situations the optimized trifluoride structures are almost linear, with intramolecular angles above 177°. The trifluoride bond lengths of the minima in the M_{IN} and M_{SV} environments are reduced by below 0.01 Å compared to the free trifluoride. The similar behaviour of the two motifs is peculiar, as the structural surroundings are very different from each other. In particular, the M_{SV} cavity should be significantly less strained than the interstitial M_{IN} motif. Compared to that, the trifluoride structures for the M_{DV} clusters behave differently. Here, one of the bond lengths is close to the value for the free molecule, while the other is slightly elongated within the range of 5 mÅ to 7 mÅ. Probably, the reason for the notable geometry distortion of F_3^- in the argon M_{DV} environment, meaning the elongation of only one bond, is found in the F_3^- -Ar interactions with the immediate argon surroundings. A

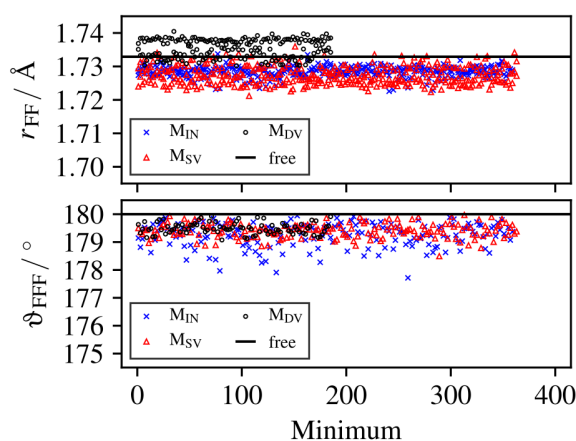


Fig. 3 Trifluoride bond lengths and intramolecular angle for the minima found in the MH runs. Only every other minimum is shown.

closer look at these interactions uncovers that typically the elongated bond involves the terminal F atom, which in the M_{DV} plane projection plots is closer to the nearest Ar atom along the molecular axis. Thus, the distortion seems to be motivated by maximizing the attractive interaction involving the corresponding terminal F and axial Ar atoms, while the molecule is anchored by the interactions of the central F atom with its equatorial Ar neighbors.

At this point loose predictions of the argon atoms' effect on the vibrational behaviour of the trifluoride can be established. Judging from our observations in the preceding study on neon systems, the compression of the internal coordinates for the molecules in the $M_{IN/SV}$ environments should correspond to an increased rigidity of the molecule, a hardening of the potential around the equilibrium structure and blue-shifts to the fundamental vibrational excitations. Given the stronger F_3^- -Ar interaction, stronger signal shifts are expected. With respect to the minima of the M_{DV} motif, the bond elongation may indicate a weakening of the potential around the minimum with respect to changes of the bond lengths. This should correspond to a red-shift of the stretching vibrations. However, as only one bond is directly affected, it is not clear how this will actually factor into the calculation of the vibrational states.

In Table 2 the averaged cohesive energies and harmonic zero-point energies for the minima of the different MCX-YV clusters are listed. With respect to the total cohesive energies, the M_{SV} and M_{DV} structures are most stable. The motifs are separated by only about 10 meV and thus their stability should be considered equal. In comparison, the minima of the interstitial motif are less stabilized by roughly 150 meV to 160 meV. The exception to this is the MC1-2V cluster. The corresponding minima feature cohesive energies between the values of the M_{IN} and M_{SV} structures, despite the trifluoride molecules being embedded in the M_{SV} environment. From the contributions of the F_3^- -Ar, F_3^- -Ar₂ and Ar-Ar interactions, it is apparent that this is due to the presence of an additional empty single-vacancy site in the movable section of the cells and the resulting loss of optimized Ar-Ar interactions. Therefore, this cluster is disregarded in the remaining stability analysis.

Table 2 Averaged total cohesive energies and contributions by the guest-host and host-host interactions as well as harmonic zero-point energies (ZPE) (in eV) of the minima in the MCX-YV clusters. ZPEs are obtained from normal mode analyses including all movable atoms for the ten most stable structures of each MCX-YV cluster.

cluster	$E_{F_3^- - Ar}$	$E_{F_3^- - Ar_2}$	E_{Ar-Ar}	E_{coh}	E_{ZPE}	E_{tot}
MC1-0V (M_{IN})	-1.23	0.27	-35.04	-36.00	0.96	-35.04
MC2-0V (M_{IN})	-1.24	0.26	-35.04	-36.02	0.96	-35.06
MC3-0V (M_{IN})	-1.23	0.27	-35.05	-36.01	0.96	-35.05
MC4-0V (M_{IN})	-1.23	0.27	-35.05	-36.01	0.96	-35.05
MC5-0V (M_{IN})	-1.23	0.27	-35.05	-36.01	0.96	-35.05
MC1-1V (M_{SV})	-1.29	0.27	-35.14	-36.16	0.93	-35.23
MC2-1V (M_{SV})	-1.29	0.27	-35.14	-36.16	0.93	-35.23
MC1-2V (M_{DV})	-1.29	0.27	-35.06	-36.08	0.93	-35.15
MC2-2V (M_{DV})	-1.30	0.23	-35.10	-36.17	0.90	-35.27
MC3-2V (M_{DV})	-1.30	0.23	-35.10	-36.17	0.90	-35.27

Concerning the interplay of guest-host and host-host interactions, the interstitial motif is least balanced. The attractive contributions, that is the two-body interactions, are rather small, while the repulsive ones stemming from the three-body $F_3^- - Ar_2$ term are relatively large. For the other two structural environments, the attractive $F_3^- - Ar$ interactions are very similar and more stabilizing than for the M_{IN} motif. However, the remaining contributions to the cohesive energy behave differently for the former two motifs. In case of M_{SV} the Ar-Ar interaction is more attractive compared to M_{IN} and M_{DV} , whereas the repulsive $F_3^- - Ar_2$ interactions are on par with the M_{IN} structures. On the other hand, in the double-vacancy motif the missing contributions by the optimized Ar-Ar interactions are compensated by a reduced repulsive three-body interaction, befitting the more spacious cavity.

The harmonic zero-point energies typically decrease with increasing number of vacancy sites in the cell, indicating a concurrent reduction of spatial strain in the structures. As for all vacancy situations the same number of degrees of freedom was included in the harmonic analyses, the changes of zero-point energies should be a result of the particular environments. Again, the MC1-2V minima behave similar to the 1V structures, as they correspond to M_{SV} environments. When the zero-point energies are added to the cohesive energies the trends regarding the stability of the environments are mostly reinforced, that is the single- and double-vacancy motifs become even more stable than the interstitial motif. Also, relative to M_{SV} the stability of M_{DV} is further increased, with the latter motif now being about 40 meV more stable than the former. Nonetheless, they are still similarly stable.

3.3 Vibrational properties of F_3^- in argon

The fundamental anharmonic vibrational properties of the trifluoride anion in the ten most stable minima of each MCX-YV cluster were examined. Vibrational states were assigned through excitation energies as well as nodal structure. The states are denoted by the triples (n_s, n_a, n_ϑ) , containing the quanta in the symmetric (n_s), antisymmetric (n_a) and bending (n_ϑ) modes. The discussion of the vibrational analyses is initially focussed on the calculations based on PES-2B. Only in the latter portion of the discussion these results are compared to those of the PES-3B calculations.

To start off with the effect of the argon environment on the

vibrational states, representative nuclear densities and difference densities for the fundamental vibrational states are shown in Figure 4. The upper two rows display the nuclear densities after integration along r and R (first row) and ϑ (second row) for the most stable MC1-0V minimum. They illustrate that the fundamental vibrational states are not changed qualitatively by the interactions with the argon atoms. The densities along ϑ reveal that the trifluoride is slightly bent even in the vibrational ground state (first column on the left). Moreover, the fundamental bending excitation can be identified via the node in the ϑ -density in the right-most column. The fundamental n_s (second column) and n_a (third column) excitations for the quasi-linear trifluoride are characterized by nodes along the $(r+R)$ - and the $(r-R)$ -direction, respectively.

The differences between the nuclear densities of the free trifluoride and the entrapped molecule may help to uncover more delicate effects of the argon on the vibrational states. To this end, the final three rows of Figure 4 show difference density plots for the densities integrated along ϑ and the most stable minima of the MC1-0V, MC2-1V and MC2-2V clusters, representing the M_{IN} , M_{SV} and M_{DV} motifs. The difference densities for the trifluorides in the former two structural environments are very similar to each other. Based on the slightly shortened trifluoride bond lengths in the M_{IN} and M_{SV} surroundings, the fundamental vibrational trifluoride states are expected to appear compressed as well. This seems to be the case, as the corresponding nuclear densities in the presence of argon atoms are centered at smaller r and R values. On the other hand, the vibrational states of the trifluoride in the argon M_{DV} environment behave differently. Here, the difference densities (final row of Figure 4) show that the states are expanded towards larger distances r and R . Moreover, the expansion typically seems to be aligned more strongly with either r or R (R in Figure 4). This agrees well with the observation that in the argon M_{DV} motif one of the trifluoride bonds is elongated.

In Table 3 averages of the fundamental vibrational excitation energies are shown for the different potential energy surfaces (PES-2B, PES-3B) and MCX-YV clusters alongside theoretical and experimental reference values. At this point the reader shall be reminded that the current constitution of our model for the calculation of the vibrational states does not allow for a description of the fundamental bending excitation. Instead, the excitation energy corresponding to the first bending overtone is determined. A full account of this is given in our previous work.²⁶

Firstly, a general trend regarding the calculated fundamental excitation energies can be extracted from the values in Table 3. That is a sizable difference in the sensitivity of the bending and the stretching modes with respect to the environment. Whereas the averages of the stretching excitation energies are rather consistent within a given argon environment, the bending excitations are characterized by strongly varying transition energies. In accordance with that, the empirical standard deviations of the calculated averages differ as well. For the stretching excitations, they usually range around 1 cm^{-1} , allowing the qualitative analysis of the excitation energies for individual minima through the averages of the corresponding MCX-YV cluster. Contrasting to that, the bending excitation energies are scattered for the minima of each MCX-YV cluster, typically featuring averages with standard

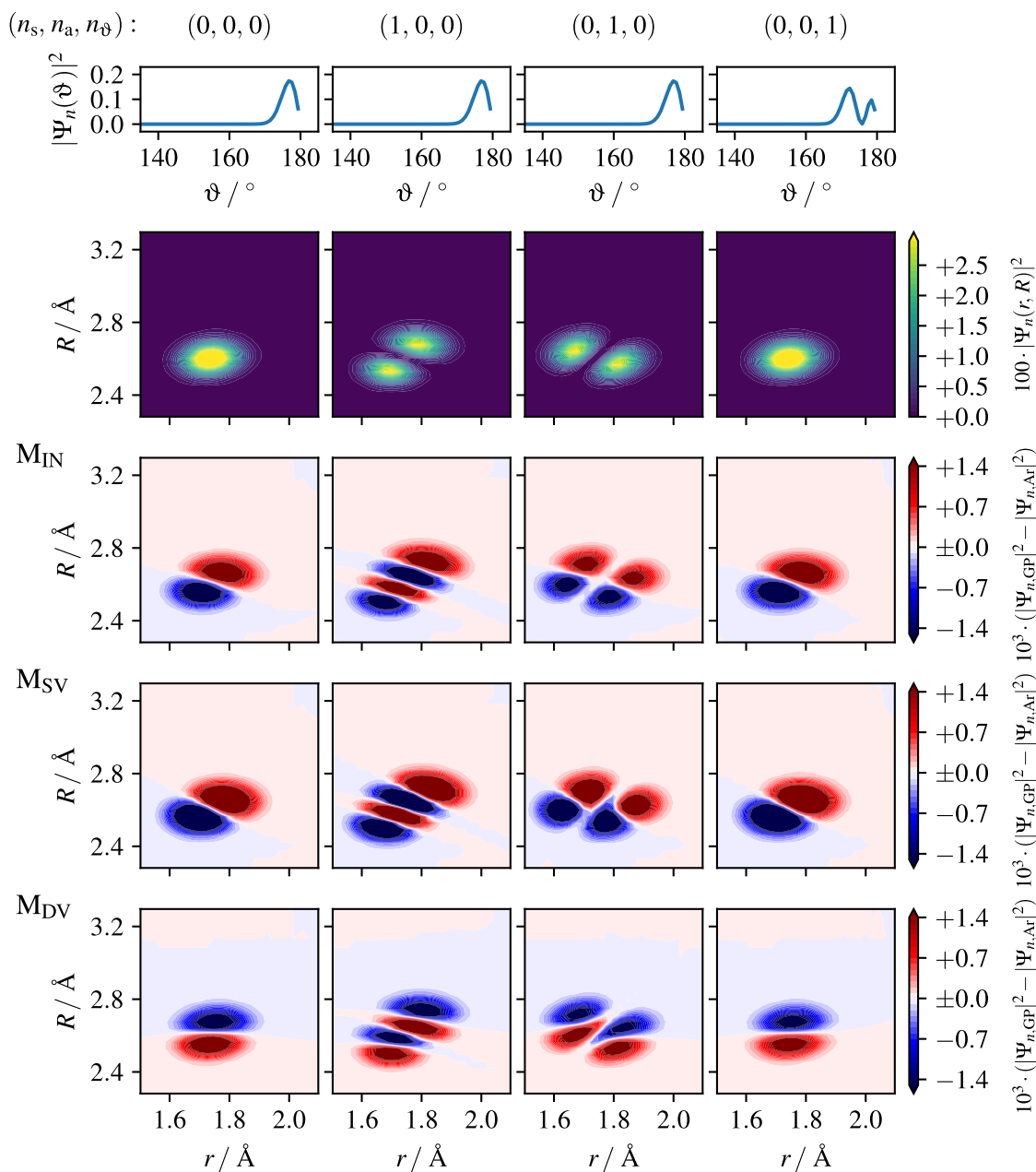


Fig. 4 Nuclear densities of fundamental vibrational states for F_3^- in argon. Vibrational analyses based on PES-2B. Top two rows: Nuclear densities integrated along r and R (first row) and ϑ (second row) for the most stable structure of the MC1-0V cluster. Final three rows: Difference densities along r and R for the most stable minima of the MC1-0V (M_{IN}), MC2-1V (M_{SV}) and MC2-2V (M_{DV}) clusters, calculated with respect to the densities of free F_3^- .

deviations of 10 cm^{-1} or more. On the one hand, this qualitative difference between the stretching and bending modes indicates a greater effect of the environments on the latter. On the other, the stronger fluctuations of the bending energies should partly be a result of the adiabatic treatment of the Euler angles defining the molecular orientation.

With respect to the fundamental vibrational transitions of the trifluoride in the M_{IN} environments, blue-shifts to the excitational energies of all three modes relative to the free molecule are observed. For the symmetric stretching mode the increase of the

average excitation energy amounts to approximately 10 cm^{-1} to 12 cm^{-1} . Likewise, the antisymmetric stretching mode is typically blue-shifted by 6 cm^{-1} to 8 cm^{-1} . The energy associated with the first bending excitation increases by 25 cm^{-1} to almost 80 cm^{-1} compared to the free molecule. In view of the structural surroundings the blue-shifts compared to the free molecule are in agreement with the expectations. The trifluoride is located in a very narrow cavity with relatively strained Ar-Ar interactions and matching guest-host interactions on the repulsive side of the most attractive F_3^- -Ar distance. Thus, any further bond elonga-

Table 3 Averaged fundamental vibrational excitation energies (in cm^{-1}) of the ten most stable minima in each MCX-YV cluster. 2B and 3B refer to calculations with PES-2B and PES-3B, respectively. Values for the free F_3^- molecule are taken from Table 3 of our previous work.²⁶ Experimental values are taken from the works of Riedel *et al.* and Andrews and coworkers.^{4,5,53}

	$\bar{\nu}_s$		$\bar{\nu}_a$		$\bar{\nu}_\theta$	
	2B	3B	2B	3B	2B	3B
free F_3^-						
exp.	389	389	510.6	510.6	-	-
MC1-0V (M_{IN})	406	407	530	522	549	554
MC2-0V (M_{IN})	404	405	528	519	543	547
MC3-0V (M_{IN})	405	406	529	520	540	544
MC4-0V (M_{IN})	404	406	529	520	528	533
MC5-0V (M_{IN})	405	406	529	520	580	586
MC1-1V (M_{SV})	408	410	530	521	593	595
MC2-1V (M_{SV})	407	410	529	520	541	543
MC1-2V (M_{SV})	408	410	529	521	605	607
MC2-2V (M_{DV})	387	387	517	508	528	525
MC3-2V (M_{DV})	388	387	517	507	528	531

tion or bending should yield more unfavorable trifluoride-argon interactions, essentially leading to a hardening of the trifluoride potential around the equilibrium structure and a blue-shift of the vibrational excitations.

The fundamental excitation energies of the trifluoride in the M_{SV} environments are very similar to the M_{IN} structures. Aside from the general tendencies, the actual averaged excitation energies and standard deviations match as well. Although the similarity of the excitation energies for the M_{IN} and M_{SV} minima is in line with the analyses of the internal F_3^- coordinates and the nuclear densities, it is somewhat unexpected upon considering the varying structural constitution of the two environments and the sensitivity of vibrational excitations. Unlike M_{IN} the M_{SV} motif features a proper vacancy site, such that the environment is not strongly distorted by accommodating the trifluoride. Accordingly, the host-host as well as guest-host interactions should be relatively unstrained, which is confirmed by the cohesive energies listed in Table 2. Therefore, the origin of the blue-shift to the stretching excitation energies cannot be the same as for the M_{IN} environment. Rather than being hindered by unfavorable F_3^- -Ar interactions, it seems that the trifluoride in the M_{SV} motif is fixated by strongly attractive interactions with the host atoms. The increased rigidity of the trifluoride may be rationalized in terms of particularly strong interactions for the equilibrium configuration that decrease significantly upon displacement of the molecule. With regards to the potential landscape around the minimum configuration, this corresponds to an effective potential hardening, which would explain the calculated blue-shifts.

The situation is different for the M_{DV} structures. Here, both stretching modes are characterized by red-shifted averaged fundamental excitation energies compared to the free trifluoride. The symmetric one is shifted by 6 cm^{-1} to 7 cm^{-1} and the antisymmetric one by about 5 cm^{-1} . While the stretching vibrations for the trifluoride in the M_{DV} environment appear different from the other structural motifs, the excitation energies of the first bending overtone do not. With blue-shifts of roughly 25 cm^{-1} compared to the free molecule, the fundamental excitations are

similar to those of the other environments. However, it is notable that among the typical averages for the ν_θ excitation both M_{DV} values range at the low end. This may speak for an increased flexibility of the trifluoride with respect to bending motions in the M_{DV} cavity. The red-shifts of the fundamental stretching excitations are in accord with the constitution of the cavity and the internal trifluoride coordinates. As the former is wider than in the M_{SV} environment, spatial strain in the form of narrow distances between guest and host atoms should not factor into the effect of the argon atoms on the vibrational trifluoride properties. Compared to the M_{SV} minima the contributions of the F_3^- -Ar interactions to the total cohesive energies are slightly larger for the M_{DV} motif. Yet, a corresponding decrease of flexibility for the trifluoride does not occur. Instead, the specific arrangement of argon atoms around the trifluoride seems to cause a softening of the potential along one of the bond stretching directions. Accordingly, the equilibrium configuration features one elongated trifluoride bond and vibrational excitations through stretching modes are facilitated.

With measured excitation energies of 389 cm^{-1} and 510.6 cm^{-1} for ν_s and ν_a , respectively, the experimental investigation of matrix-isolated trifluoride in argon reveals a red-shift of the fundamental stretching modes compared to the neon systems (exp.⁵: 525 cm^{-1} , calc.²⁶: 399 cm^{-1} , 525 cm^{-1}) as well as the theoretical values for the free trifluoride (see Table 3). At the PES-2B level, the M_{IN} and M_{SV} environments produce stretching excitations that are blue-shifted relative to the free trifluoride and the neon reference values. In contrast to that, the M_{DV} environment captures the correct trend. Correspondingly, both stretching modes are red-shifted compared to the free molecule and the one entrapped in neon. However, while the calculated fundamental excitation energies of the symmetric stretching mode (387 cm^{-1}) are rather close to the experimental reference value, the red-shift of the antisymmetric stretching excitation to about 517 cm^{-1} is not quite pronounced enough. This may be due to the M_{DV} environment not being the exact structural environment observed in experiment, but it could also be a result of including only two-body interactions in the potential energy surface.

In order to determine the effect of the F_3^- -Ar₂ interactions on the vibrational trifluoride properties, the vibrational analyses of the ten most stable structures of each MCX-YV cluster are repeated with PES-3B. The inspection of the resulting nuclear densities showed that typically the vibrational states are not changed qualitatively by including the three-body interactions (see Figure 2 in the supplementary material for an example). On the contrary, the excitation energies are affected notably. This is obvious from the fundamental excitation energies (3B) listed in Table 3. Strikingly, the addition of the three-body interaction term influences the stretching excitations in different ways. Across the three structural environments the symmetric stretching mode is slightly blue-shifted, whereas the antisymmetric stretching excitations experience a sizable red-shift between 8 cm^{-1} and 10 cm^{-1} . The calculated bending excitation is consistently blue-shifted by 2 cm^{-1} to 6 cm^{-1} . Also, the standard deviations associated with the averages remain comparable to those obtained for PES-2B. Through

inclusion of the F_3^- -Ar₂ interactions the agreement between the experimentally observed signals and the excitation energies calculated for M_{DV} is further improved.

Judging from the anharmonic vibrational analyses solely the M_{DV} environment seems to affect the trifluoride in a way that fully agrees with the experimental observations. This is in line with the stability analysis showing that the double-vacancy motif is the most stable one if zero-point effects and F_3^- -Ar₂ interactions are accounted for. However, given the comparable stability of the M_{SV} environment, the reason for the M_{DV} motif's dominance in experiment is not quite identified. Corresponding to that, Redeker *et al.* observed a blue-shifted shoulder to the antisymmetric stretching signal in their infra-red spectra of F_3^- in argon.⁵ This speaks for a different trapping site in the argon matrix, such as the M_{SV} environment. However, our vibrational analyses do not necessarily confirm this hypothesis, as the calculated blue-shift relative to M_{DV} is too large. From a theoretical perspective different aspects may contribute to the preference of M_{DV}. Concerning the stability of the different environments, Ar₃-three- or F_3^- -Ar₃-four-body interactions may further favor the larger cavity. Also, the trifluoride motion should be least impaired in the M_{DV} cavity, effecting entropic stabilization. Alternatively, kinetic factors may support a favored double-vacancy site formation.

4 Conclusion

To conclude, we have studied trifluoride anions in argon environments with respect to the structures of the rare gas surroundings and the vibrational properties of the entrapped F_3^- . Two potential energy surfaces were used to examine different trifluoride-argon models. The results were analyzed and compared to matrix isolation experiments.

Using minima hopping optimizations, we extracted three underlying structural environments in the trifluoride-argon systems, whose occurrence is linked to the number of vacancy sites in the cell. The interstitial motif M_{IN} is dominant in cells without vacancy sites, M_{SV} prevails in single-vacancy cells and the M_{DV} environments appear only in structures with two vacancies. The M_{DV} and M_{SV} motifs were found to be the most stable environments. Moreover, we observed somewhat unexpected effects of the argon surroundings on the internal trifluoride coordinates that speak for a significant influence of the guest-host interaction on the vibrational properties. The final step of the investigation consisted of the vibrational analyses of the structures obtained in the minima hopping runs. In the examination of the fundamental vibrational states and excitation energies we observed that the M_{IN/SV} structures and the double-vacancy motif display qualitatively different properties. Notably, among the different environments only M_{DV} produces stretching excitations in qualitative agreement with the experimental observations. We showed that the agreement with experiment can be made almost quantitative by accounting for F_3^- -Ar₂ interactions in the model potential energy surface. This emphasizes the importance of non-additive three-body interactions in a highly accurate description of weakly interacting systems. In order to predict corresponding matrix effects in future applications, we aim to expand our model to calculating full rovibrational states of the guest molecule.

Upon request to the authors PES-2B and PES-3B are available.

Acknowledgements

The authors acknowledge the Zentraleinrichtung für Datenverarbeitung (ZEDAT) of the Freie Universität Berlin for supplying computational resources.⁵⁴

Conflicts of interest

There are no conflicts of interest to declare.

Funding

The authors acknowledge funding by the Deutsche Forschungsgemeinschaft (DFG) under project PA 1360/12–1. F. Bader gratefully acknowledges the Elsa-Neumann scholarship of Berlin.

Notes and references

- 1 B. S. Ault and L. Andrews, *J. Am. Chem. Soc.*, 1976, **98**, 1591–1593.
- 2 B. S. Ault and L. Andrews, *Inorg. Chem.*, 1977, **16**, 2024–2028.
- 3 A. A. Tuinman, A. A. Gakh, R. J. Hinde and R. N. Compton, *J. Am. Chem. Soc.*, 1999, **121**, 8397–8398.
- 4 S. Riedel, T. Köchner, X. Wang and L. Andrews, *Inorg. Chem.*, 2010, **49**, 7156–7164.
- 5 F. A. Redeker, H. Beckers and S. Riedel, *RSC Adv.*, 2015, **5**, 106568–106573.
- 6 P. H. Svensson and L. Kloo, *Chem. Rev.*, 2003, **103**, 1649–1684.
- 7 T. Schlama, K. Gabriel, V. Gouverneur and C. Mioskowski, *Angew. Chem. Int. Ed. Engl.*, 1997, **36**, 2342–2344.
- 8 X. Chen, M. A. Rickard, J. W. Hull Jr., C. Zheng, A. Leugers and P. Simoncic, *Inorg. Chem.*, 2010, **49**, 8684–8689.
- 9 P. A. Cahill, C. E. Dykstra and J. C. Martin, *J. Am. Chem. Soc.*, 1985, **107**, 6359–6362.
- 10 G. L. Heard, C. J. Marsden and G. E. Scuseria, *J. Phys. Chem.*, 1992, **96**, 4359–4366.
- 11 T. G. Wright and E. P. F. Lee, *Mol. Phys.*, 1993, **79**, 995–1009.
- 12 C. S. Ewig and J. R. Van Wazer, *J. Am. Chem. Soc.*, 1990, **112**, 109–114.
- 13 N. O. J. Malcolm and J. J. W. McDouall, *J. Phys. Chem.*, 1996, **100**, 10131–10134.
- 14 F. Mota and J. J. Novoa, *J. Chem. Phys.*, 1996, **105**, 8777–8784.
- 15 D. J. Tozer and P. Carlos, *Mol. Phys.*, 1997, **90**, 515–524.
- 16 A. Artau, K. E. Nizzi, B. T. Hill, L. S. Sunderlin and P. G. Wentholt, *J. Am. Chem. Soc.*, 2000, **122**, 10667–10670.
- 17 B. Braïda and P. C. Hiberty, *J. Phys. Chem. A*, 2008, **112**, 13045–13052.
- 18 J. Czernek and O. Živný, *J. Chem. Phys.*, 2008, **129**, 194305.
- 19 Z. Sun and H. F. Schaefer III, *Phys. Chem. Chem. Phys.*, 2018, **20**, 18986–18994.
- 20 D. Wang, D. Wang, L. Fu, J. Wang, G. Shi, Y. Li and X. Huang, *RSC Adv.*, 2019, **9**, 1929–1932.
- 21 K. Mahjoubi, D. M. Benoit, N.-E. Jaidane, M. M. Al-Mogren

- and M. Hochlaf, *Phys. Chem. Chem. Phys.*, 2015, **17**, 17159–17168.
- 22 Y. Makina, K. Mahjoubi, D. M. Benoit, N.-E. Jaidane, M. M. Al-Mogren and M. Hochlaf, *J. Phys. Chem. A*, 2017, **121**, 4093–4102.
 - 23 F. Bader, T. Lindic and B. Paulus, *J. Comput. Chem.*, 2020, **41**, 751–758.
 - 24 S. J. Lee, M. Welborn, F. R. Manby and T. F. Miller III, *Acc. Chem. Res.*, 2019, **52**, 1359–1368.
 - 25 J. Murrell, S. Carter, S. Farantos, P. Huxley and A. Varandas, *Molecular Potential Energy Functions*, John Wiley & Sons, Chichester, New York, 1984.
 - 26 F. Bader, J. C. Tremblay and B. Paulus, *Phys. Chem. Chem. Phys.*, 2021, **23**, 886–899.
 - 27 T. B. Adler, G. Knizia and H.-J. Werner, *J. Chem. Phys.*, 2007, **127**, 221106.
 - 28 K. A. Peterson, T. B. Adler and H.-J. Werner, *J. Chem. Phys.*, 2008, **128**, 084102.
 - 29 H.-J. Werner, G. Knizia and F. R. Manby, *Mol. Phys.*, 2011, **109**, 407–417.
 - 30 N. Sylvetsky, M. K. Kesharwani and J. M. L. Martin, *J. Chem. Phys.*, 2017, **147**, 134106.
 - 31 S. Kritikou and J. G. Hill, *J. Chem. Theory Comput.*, 2015, **11**, 5269–5276.
 - 32 R. A. Shaw and J. G. Hill, *J. Chem. Theory Comput.*, 2017, **13**, 1691–1698.
 - 33 S. F. Boys and F. Bernardi, *Mol. Phys.*, 1970, **19**, 553–566.
 - 34 H.-J. Werner, P. J. Knowles, G. Knizia, F. R. Manby, M. Schütz, P. Celani, W. Györffy, D. Kats, T. Korona, R. Lindh, A. Mitrushenkov, G. Rauhut, K. R. Shamasundar, T. B. Adler, R. D. Amos, A. Bernhardsson, A. Berning, D. L. Cooper, M. J. O. Deegan, A. J. Dobbyn, F. Eckert, E. Goll, C. Hampel, A. Hesselmann, G. Hetzer, T. Hrenar, G. Jansen, C. Köppl, Y. Liu, A. W. Lloyd, R. A. Mata, A. J. May, S. J. McNicholas, W. Meyer, M. E. Mura, A. Nicklass, D. P. O’Neill, P. Palmieri, D. Peng, K. Pflüger, R. Pitzer, M. Reiher, T. Shiozaki, H. Stoll, A. J. Stone, R. Tarroni, T. Thorsteinsson and M. Wang, *MOL-PRO, version 2015.1, a package of ab initio programs*, 2015.
 - 35 H.-J. Werner, P. J. Knowles, G. Knizia, F. R. Manby and M. Schütz, *WIREs Comput. Mol. Sci.*, 2012, **2**, 242–253.
 - 36 M. J. Frisch, G. W. Trucks, H. B. Schlegel, G. E. Scuseria, M. A. Robb, J. R. Cheeseman, G. Scalmani, V. Barone, G. A. Petersson, H. Nakatsuji, X. Li, M. Caricato, A. V. Marenich, J. Bloino, B. G. Janesko, R. Gomperts, B. Mennucci, H. P. Hratchian, J. V. Ortiz, A. F. Izmaylov, J. L. Sonnenberg, D. Williams-Young, F. Ding, F. Lipparini, F. Egidi, J. Goings, B. Peng, A. Petrone, T. Henderson, D. Ranasinghe, V. G. Zakrzewski, J. Gao, N. Rega, G. Zheng, W. Liang, M. Hada, M. Ehara, K. Toyota, R. Fukuda, J. Hasegawa, M. Ishida, T. Nakajima, Y. Honda, O. Kitao, H. Nakai, T. Vreven, K. Throssell, J. A. Montgomery, Jr., J. E. Peralta, F. Ogliaro, M. J. Bearpark, J. J. Heyd, E. N. Brothers, K. N. Kudin, V. N. Staroverov, T. A. Keith, R. Kobayashi, J. Normand, K. Raghavachari, A. P. Rendell, J. C. Burant, S. S. Iyengar, J. Tomasi, M. Cossi, J. M. Millam, M. Klene, C. Adamo, R. Cammi, J. W. Ochterski, R. L. Martin, K. Morokuma, O. Farkas, J. B. Foresman and D. J. Fox, *Gaussian 16 Revision C.01*, 2016, Gaussian Inc. Wallingford CT.
 - 37 Z. Xie and J. M. Bowman, *J. Chem. Theory Comput.*, 2010, **6**, 26–34.
 - 38 K. Patkowski and K. Szalewicz, *J. Chem. Phys.*, 2010, **133**, 094304.
 - 39 K. Tang and J. P. Toennies, *J. Chem. Phys.*, 1984, **80**, 3726–3741.
 - 40 S. Goedecker, *J. Chem. Phys.*, 2004, **120**, 9911–9917.
 - 41 D. N. Batchelder, D. L. Losee and R. O. Simmons, *Phys. Rev.*, 1967, **162**, 767.
 - 42 R. Freund, *Linear Algebra for Large Scale and Real-Time Applications*, Springer, Dordrecht, 1993, pp. 137–163.
 - 43 R. W. Freund, M. H. Gutknecht and N. M. Nachtigal, *SIAM J. Sci. Comput.*, 1993, **14**, 137–158.
 - 44 H. O. Karlsson and S. Holmgren, *J. Chem. Phys.*, 2002, **117**, 9116–9123.
 - 45 J. C. Tremblay and T. Carrington Jr., *J. Chem. Phys.*, 2006, **125**, 094311.
 - 46 J. C. Tremblay, S. Beyvers and P. Saalfrank, *J. Chem. Phys.*, 2008, **128**, 194709.
 - 47 D. T. Colbert and W. H. Miller, *J. Chem. Phys.*, 1992, **96**, 1982–1991.
 - 48 J. Echave and D. C. Clary, *Chem. Phys. Lett.*, 1992, **190**, 225–230.
 - 49 V. Szalay, *J. Chem. Phys.*, 1993, **99**, 1978–1984.
 - 50 W. H. Press, S. A. Teukolsky, B. P. Flannery and W. T. Vetterling, *Numerical Recipes in Fortran 77: The Art of Scientific Computing*, Cambridge University Press, Cambridge CB2 1RP, 1992.
 - 51 K. Patkowski, G. Murdachaew, C.-M. Fou and K. Szalewicz, *Mol. Phys.*, 2005, **103**, 2031–2045.
 - 52 C. Hättig and B. A. Hess, *J. Phys. Chem.*, 1996, **100**, 6243–6248.
 - 53 L. Andrews and X. Wang, *Phys. Chem. Chem. Phys.*, 2018, **20**, 23378–23385.
 - 54 L. Bennett, B. Melchers and B. Proppe, *Curta: A General-purpose High-performance Computer at ZEDAT, Freie Universität Berlin*, 2020.

**Supplementary Material: "Theoretical modeling
of molecules in weakly interacting environments:
Trifluoride anions in argon"**

Frederik Bader,^{*,†} Jean Christophe Tremblay,[‡] and Beate Paulus[†]

†Institut für Chemie und Biochemie, Freie Universität Berlin, D-14195, Berlin, Germany

*‡Laboratoire de Physique et Chimie Théoriques, CNRS-Université de Lorraine, UMR 7019,
ICPM, 1Bd Arago, 57070 Metz, France*

E-mail: f.bader@fu-berlin.de

Grid-based sampling for the F_3^- -Ar potential

A part of the *ab initio* data set for the F_3^- -Ar interaction potential was collected with grid-based sampling. This was done by incrementally changing the following six coordinates: the trifluoride bond lengths, the F-F-F angle, the distance between the central F atom and the Ar atom ($r_{\text{F-Ar}}$) and the two angles used to define the orientation of the argon around the trifluoride (θ , ϕ). These are depicted in Figure 1.

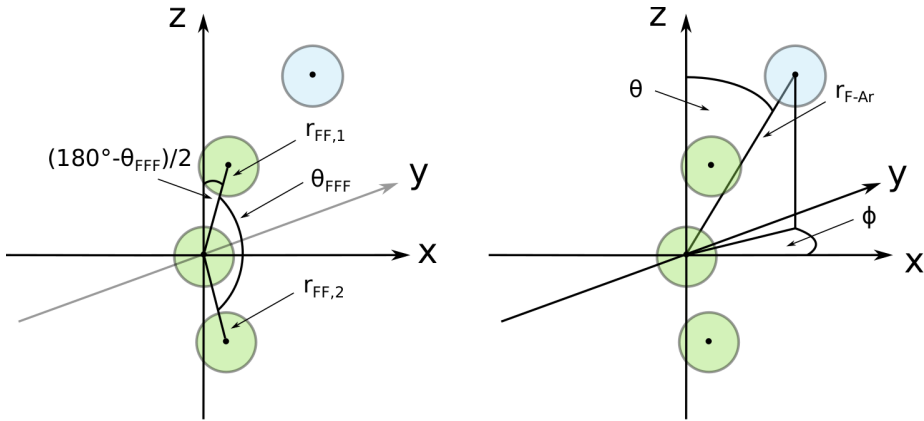


Figure 1: Coordinates included in the grid-based sampling.

For non-linear trifluoride configurations the grid-based sampling was employed to supply additional data in the region of strongest attractive interaction. Thus, the distance $r_{\text{F-Ar}}$ was varied between 4.0 \AA and 5.5 \AA with a step of 0.5 \AA . The F-F bond lengths were incremented between 1.69 \AA and 1.77 \AA in steps of 0.02 \AA , laying a focus on the bond length region close to equilibrium, while the intramolecular angle was set to 150° , 160° and 170° . The remaining two (orientational) angles were changed from 0° to 90° and 0° and 180° in steps of 30° and 60° , respectively. For linear trifluoride configurations the bond lengths were sampled with an irregular grid between 1.5 \AA and 2.0 \AA . The distance between the central F atom and the Ar atom was varied between 3.0 \AA and 10.0 \AA in steps of 0.5 \AA and the polar angle θ was set to the values 0° , 5° , 15° , 25° , 35° , \dots , 85° , 90° . The azimuthal angle ϕ is a redundant coordinate for the linear trifluoride and was thus not sampled. In total, the grid-based strategies comprised about 14000 data points.

Test scans for the F_3^- -Ar and F_3^- -Ar₂ potentials

The six test scans presented in Fig.1 of the main text are obtained with the coordinate configurations listed in Table 1. The coordinate systems are defined as shown in Figure 1 above.

Table 1: Coordinate configurations for the potential scans shown in Fig. 1 of the main text. The row "panel" refers to the panel in Fig. 1 of the main text.

panel	F_3^- -Ar			F_3^- -Ar ₂		
	3	4	5	3	4	5
$r_{FF,1}$	1.930	1.723	1.820	scan	1.723	1.720
$r_{FF,2}$	scan	1.723	1.690	1.723	1.723	1.750
θ_{FFF}	180.0	scan	175.0	180.0	scan	180.0
r_{F-Ar}	3.700	3.100	scan	3.523	3.100	scan
θ	63.0	90.0	1.0	124.6	90.0	60.0
ϕ	134	0	0	313.6	90.0	0.0
$r_{F-Ar,2}$	-	-	-	4.853	5.105	3.600
θ_2	-	-	-	136.2	54.0	120.0
ϕ_2	-	-	-	67.2	83.1	0.0

Structural modeling and minima hopping runs

To model the matrix environment a trifluoride anion was placed at the center-of-mass of a cubic fcc $5 \times 5 \times 5$ super cell of 500 argon atoms. Then, the argon atoms were split in two groups: the 104 atoms closest to the guest and the remaining ones. The positions of the atoms in the latter group were fixed to retain a fcc crystal structure environment. Likewise, the trifluoride was treated as a linear rigid rotor. Depending on how many vacancy sites were examined zero, one or two argon atoms were removed from the trifluoride's vicinity. Then, the positions of the movable (inner) argon atoms and the orientation of the trifluoride as well as its center-of-mass position were rattled and loosely equilibrated with a local LBFGS relaxation. At this point, five minima hopping (MH) optimizations sharing a list of minima were started. In total, 1000 local minima were examined. The initial temperature was set

to 200 K. The molecular dynamics part of the MH runs was run with a time step of 1 fs and terminated as soon as the trajectory was found to be in a minimum for the second time. The local relaxation step was performed with the LBFGS method and a stopping force criterion of $0.05 \text{ eV}/\text{\AA}$. The temperature and energy adjustment parameters were set to $\beta_1 = 1.1$, $\beta_2 = 1.1$, $\beta_3 = 1.0/1.1$, $\alpha_1 = 0.98$ and $\alpha_2 = 1.0/0.98$. The initial energy acceptance criterion was $E_0 = 0.5 \text{ eV}$. After the MH optimizations the constraints on the trifluoride were lifted and the structures yielded by the MH runs locally reoptimized with the LBFGS method and a force criterion of $0.01 \text{ eV}/\text{\AA}$. This part of the modeling procedure was carried out with the Atomic Simulation Environment.¹

The plane projection plots were generated with the trajectory analysis tool TRAVIS.²

Cohesive and vibrational zero-point energies

The cohesive energies were calculated by summing up the energies of the individual guest-host and host-host interactions. To account for the fact that the three trifluoride-argon models contain a differing number of argon atoms, the energy contribution of the Ar-Ar pairs was corrected in case of the MCX-1V and MCX-2V structures. In order to do this, for each removed rare gas atom the average binding energy of an argon atom in an argon bulk fcc crystal is added to the host-host energy contribution. The average binding energy is estimated from the pure $5\times 5\times 5$ fcc argon supercell by taking half of the interaction energy of a central argon atom with all other 499 rare gas atoms in the cell. The correction is 90 meV for each removed Ar atom.

The scheme is motivated by the circumstance that in matrix isolation the environment forms around the guest molecule. Thus, the rare gas atoms displaced by the trifluoride should become part of the argon bulk structure, instead of being fully removed from the frozen matrix.

The zero-point energies are obtained from harmonic normal mode analyses based on PES-2B. Only the degrees of freedom in the movable part of the structures are included, while the outer rare gas atoms remain frozen. However, for the single- and double-vacancy models the movable section is expanded by one and two argon atoms, respectively, to maintain comparability of the zero-point energies to the cell without vacancies.

Vibrational states of entrapped F_3^- based on PES-3B

Analogous to Fig. 4 in the main text, Figure 2 illustrates the nuclear densities for the fundamental vibrational states of the entrapped F_3^- described by PES-3B.

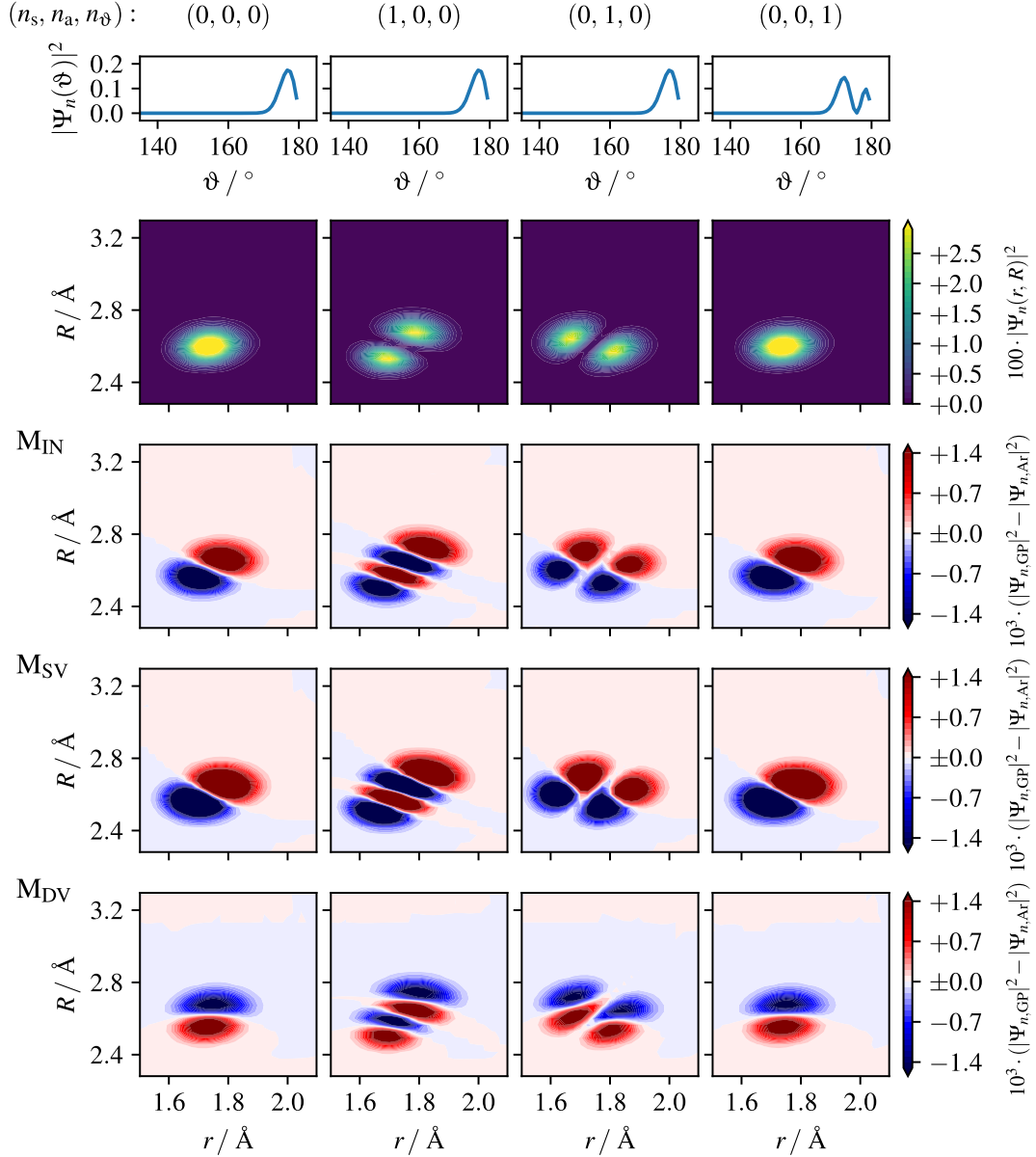


Figure 2: Nuclear densities of vibrational states of F_3^- in argon, obtained with PES-3B. Top two rows: Densities integrated along r and R (first row) and ϑ (second row) for the most stable structure of the MC1-0V cluster. Final three rows: Difference densities along r and R for the most stable minima of the MC1-0V (M_{IN}), MC2-1V (M_{SV}) and MC2-2V (M_{DV}) clusters, calculated with respect to the nuclear densities of free F_3^- .

References

- (1) Larsen, A. H.; Mortensen, J. J.; Blomqvist, J.; Castelli, I. E.; Christensen, R.; Dulak, M.; Friis, J.; Groves, M. N.; Hammer, B.; Hargus, C. et al. The atomic simulation environment – a Python library for working with atoms. *J. Phys. Condens. Matter* **2017**, *29*, 273002.
- (2) Brehm, M.; Thomas, M.; Gehrke, S.; Kirchner, B. TRAVIS – A free analyzer for trajectories from molecular simulation. *J. Chem. Phys.* **2020**, *152*, 164105.

Bibliography

- [1] K. Müller-Dethlefs and P. Hobza, *Chem. Rev.*, 2000, **100**, 143–168.
- [2] K. A. Dill, *Biochemistry*, 1990, **29**, 7133–7155.
- [3] K. E. Riley and P. Hobza, *Wiley Interdiscip. Rev. Comput. Mol. Sci.*, 2011, **1**, 3–17.
- [4] V. Balzani, A. Credi, F. M. Raymo and J. F. Stoddart, *Angew. Chem. Int. Ed.*, 2000, **39**, 3348–3391.
- [5] R. R. Knowles and E. N. Jacobsen, *Proc. Natl. Acad. Sci. U.S.A.*, 2010, **107**, 20678–20685.
- [6] H. J. Davis and R. J. Phipps, *Chem. Sci.*, 2017, **8**, 864–877.
- [7] F. D. Toste, M. S. Sigman and S. J. Miller, *Acc. Chem. Res.*, 2017, **50**, 609–615.
- [8] K. Leopold, G. T. Fraser, S. Novick and W. Klemperer, *Chem. Rev.*, 1994, **94**, 1807–1827.
- [9] L. Roncaratti, L. Belpassi, D. Cappelletti, F. Pirani and F. Tarantelli, *J. Phys. Chem. A*, 2009, **113**, 15223–15232.
- [10] A. El Kerdawy, J. S. Murray, P. Politzer, P. Bleiziffer, A. Hesselmann, A. Görling and T. Clark, *J. Chem. Theory Comput.*, 2013, **9**, 2264–2275.
- [11] V. E. Bondybey, A. M. Smith and J. Agreiter, *Chem. Rev.*, 1996, **96**, 2113–2134.
- [12] C. Limberg, R. Köppe and H. Schnöckel, *Angew. Chem. Int. Ed.*, 1998, **37**, 496–499.
- [13] G. Wang and M. Zhou, *Int. Rev. Phys. Chem.*, 2008, **27**, 1–25.
- [14] E. Whittle, D. A. Dows and G. C. Pimentel, *J. Chem. Phys.*, 1954, **22**, 1943–1943.

- [15] I. Dunkin, *Chem. Soc. Rev.*, 1980, **9**, 1–23.
- [16] H. Schnöckel and S. Schunck, *Chemie in unserer Zeit*, 1987, **21**, 73–81.
- [17] S. Süzer and L. Andrews, *J. Chem. Phys.*, 1987, **87**, 5131–5140.
- [18] P. Dahoo, I. Berrodier, V. Raducu, J. Teffo, H. Chabbi, A. Lakhlifi and L. Abouaf-Marguin, *Eur. Phys. J. D*, 1999, **5**, 71–81.
- [19] B. I. Swanson and L. H. Jones, *J. Chem. Phys.*, 1981, **74**, 3205–3215.
- [20] S. Coussan, Y. Bouteiller, J. Perchard and W. Zheng, *J. Phys. Chem. A*, 1998, **102**, 5789–5793.
- [21] M. Pettersson, J. Lundell and M. Räsänen, *J. Chem. Phys.*, 1995, **102**, 6423–6431.
- [22] L. Khriachtchev, M. Pettersson, N. Runeberg, J. Lundell and M. Räsänen, *Nature*, 2000, **406**, 874–876.
- [23] M. Lorenz, M. Räsänen and V. E. Bondybey, *J. Phys. Chem. A*, 2000, **104**, 3770–3774.
- [24] H. Tanskanen, L. Khriachtchev, J. Lundell and M. Räsänen, *J. Chem. Phys.*, 2006, **125**, 074501.
- [25] M. Tsuge, A. Lignell, M. Räsänen and L. Khriachtchev, *J. Chem. Phys.*, 2013, **139**, 204303.
- [26] C. Zhu, K. Niimi, T. Taketsugu, M. Tsuge, A. Nakayama and L. Khriachtchev, *J. Chem. Phys.*, 2015, **142**, 054305.
- [27] E. M. Maçôas, L. Khriachtchev, M. Pettersson, R. Fausto and M. Räsänen, *Phys. Chem. Chem. Phys.*, 2005, **7**, 743–749.
- [28] S. Nishino and M. Nakata, *J. Phys. Chem. A*, 2007, **111**, 7041–7047.
- [29] Y. Zhao, J. Su, Y. Gong, J. Li and M. Zhou, *J. Phys. Chem. A*, 2008, **112**, 8606–8611.
- [30] F. A. Redeker, H. Beckers and S. Riedel, *Chem. Eur. J.*, 2020, **26**, 1763.
- [31] L. Andrews, *J. Am. Chem. Soc.*, 1976, **98**, 2147–2152.

BIBLIOGRAPHY

- [32] L. F. Pinelo, R. W. Kugel and B. S. Ault, *J. Phys. Chem. A*, 2015, **119**, 10272–10278.
- [33] P. H. Kasai, *J. Am. Chem. Soc.*, 1982, **104**, 1165–1172.
- [34] T. Yamada, K. Komaguchi, M. Shiotani, N. P. Benetis and A. R. Sørnes, *J. Phys. Chem. A*, 1999, **103**, 4823–4829.
- [35] M. E. Jacox, *Chem. Soc. Rev.*, 2002, **31**, 108–115.
- [36] D. F. Dinu, M. Podewitz, H. Grothe, K. R. Liedl and T. Loerting, *J. Phys. Chem. A*, 2019, **123**, 8234–8242.
- [37] D. F. Dinu, M. Podewitz, H. Grothe, T. Loerting and K. R. Liedl, *Phys. Chem. Chem. Phys.*, 2020, **22**, 17932–17947.
- [38] M. Ertelt, D. A. Hrovat, W. T. Borden and W. Sander, *Chem. Eur. J.*, 2014, **20**, 4713–4720.
- [39] I. Reva, C. M. Nunes, M. Biczysko and R. Fausto, *J. Phys. Chem. A*, 2015, **119**, 2614–2627.
- [40] A. Gutiérrez-Quintanilla, M. Chevalier, R. Platakyte, J. Ceponkus and C. Crépin, *Phys. Chem. Chem. Phys.*, 2020, **22**, 6115–6121.
- [41] D. F. Dinu, M. Podewitz, H. Grothe, T. Loerting and K. R. Liedl, *Theor. Chem. Acc.*, 2020, **139**, 1–15.
- [42] F. Redeker, H. Beckers and S. Riedel, *Chem. Commun.*, 2017, **53**, 12958–12961.
- [43] L. Li, T. Stüker, S. Kieninger, D. Andrae, T. Schlöder, Y. Gong, L. Andrews, H. Beckers and S. Riedel, *Nat. Commun.*, 2018, **9**, 1–6.
- [44] H. Stoll, *Phys. Rev. B*, 1992, **46**, 6700.
- [45] H. Stoll, *Chem. Phys. Lett.*, 1992, **191**, 548–552.
- [46] N. J. Mayhall and K. Raghavachari, *J. Chem. Theory Comput.*, 2011, **7**, 1336–1343.
- [47] R. M. Richard and J. M. Herbert, *J. Chem. Phys.*, 2012, **137**, 064113.
- [48] S. J. Lee, M. Welborn, F. R. Manby and T. F. Miller III, *Acc. Chem. Res.*, 2019, **52**, 1359–1368.

- [49] A. Strom, A. Gutiérrez-Quintanilla, M. Chevalier, J. Ceponkus, C. Crépin and D. T. Anderson, *J. Phys. Chem. A*, 2020, **124**, 4471–4483.
- [50] A. Ibrahim, L. Wang, T. Halverson, R. J. Le Roy and P.-N. Roy, *J. Chem. Phys.*, 2019, **151**, 244501.
- [51] Y. Kwon, P. Huang, M. V. Patel, D. Blume and K. B. Whaley, *J. Chem. Phys.*, 2000, **113**, 6469–6501.
- [52] C. Callegari, K. K. Lehmann, R. Schmied and G. Scoles, *J. Chem. Phys.*, 2001, **115**, 10090–10110.
- [53] F. Briec, C. Schran, F. Uhl, H. Forbert and D. Marx, *J. Chem. Phys.*, 2020, **152**, 210901.
- [54] A. Szabo and N. S. Ostlund, *Modern Quantum Chemistry - Introduction to Advanced Electronic Structure Theory*, Dover Publications, Inc., 1996.
- [55] D. J. Tannor, *Introduction to Quantum Mechanics: A Time-Dependent Perspective*, University Science Books, 2007.
- [56] T. Helgaker, P. Jorgensen and J. Olsen, *Molecular Electronic-Structure Theory*, John Wiley & Sons, 2014.
- [57] R. J. Bartlett and M. Musiał, *Rev. Mod. Phys.*, 2007, **79**, 291.
- [58] L. Kong, F. A. Bischoff and E. F. Valeev, *Chem. Rev.*, 2012, **112**, 75–107.
- [59] S. Ten-no and J. Noga, *Wiley Interdiscip. Rev. Comput. Mol. Sci.*, 2012, **2**, 114–125.
- [60] W. Koch and M. C. Holthausen, *A Chemist's Guide to Density Functional Theory*, Wiley-VCH Verlag GmbH, 2001.
- [61] A. Groß, *Theoretical Surface Science: A Microscopic Perspective*, Springer, 2003.
- [62] B. T. Sutcliffe, *J. Chem. Soc., Faraday Trans.*, 1993, **89**, 2321–2335.
- [63] A. G. Császár, C. Fábri, T. Szidarovszky, E. Mátyus, T. Furtenbacher and G. Czakó, *Phys. Chem. Chem. Phys.*, 2012, **14**, 1085–1106.
- [64] Z. Bačić and J. C. Light, *Annu. Rev. Phys. Chem.*, 1989, **40**, 469–498.
- [65] J. C. Light and T. Carrington Jr, *Adv. Chem. Phys.*, 2000, **114**, 263–310.

BIBLIOGRAPHY

- [66] J. M. Bowman, *J. Chem. Phys.*, 1978, **68**, 608–610.
- [67] J. M. Bowman, S. Carter and X. Huang, *Int. Rev. Phys. Chem.*, 2003, **22**, 533–549.
- [68] G. Rauhut, *J. Chem. Phys.*, 2004, **121**, 9313–9322.
- [69] M. Born and R. Oppenheimer, *Ann. Phys.*, 1927, **389**, 457–484.
- [70] C. C. J. Roothaan, *Rev. Mod. Phys.*, 1951, **23**, 69.
- [71] G. Hall, *Proc. R. Soc. Lond.*, 1951, **205**, 541–552.
- [72] J. Pople and R. Nesbet, *J. Chem. Phys.*, 1954, **22**, 571–572.
- [73] C. Ochsenfeld, J. Kussmann and D. S. Lambrecht, *Reviews in Computational Chemistry, Volume 23*, John Wiley & Sons, 2007.
- [74] D. Cremer, *Wiley Interdiscip. Rev. Comput. Mol. Sci.*, 2011, **1**, 509–530.
- [75] M. L. Leininger, W. D. Allen, H. F. Schaefer III and C. D. Sherrill, *J. Chem. Phys.*, 2000, **112**, 9213–9222.
- [76] K. Raghavachari, G. W. Trucks, J. A. Pople and M. Head-Gordon, *Chem. Phys. Lett.*, 1989, **157**, 479–483.
- [77] T. Kato, *Commun. Pure Appl. Math.*, 1957, **10**, 151–177.
- [78] J. C. Slater, *Phys. Rev.*, 1928, **31**, 333.
- [79] J. C. Slater, *Phys. Rev.*, 1928, **32**, 349.
- [80] E. A. Hylleraas, *Z. Phys.*, 1929, **54**, 347–366.
- [81] W. Kutzelnigg, *Theor. Chim. Acta*, 1985, **68**, 445–469.
- [82] A. J. May and F. R. Manby, *J. Chem. Phys.*, 2004, **121**, 4479–4485.
- [83] P. Hohenberg and W. Kohn, *Phys. Rev.*, 1964, **136**, B864.
- [84] W. Kohn and L. J. Sham, *Phys. Rev.*, 1965, **140**, A1133.
- [85] D. M. Ceperley and B. J. Alder, *Phys. Rev. Lett.*, 1980, **45**, 566.
- [86] S. H. Vosko, L. Wilk and M. Nusair, *Can. J. Phys.*, 1980, **58**, 1200–1211.

- [87] J. P. Perdew and Y. Wang, *Phys. Rev. B*, 1992, **45**, 13244.
- [88] J. P. Perdew, K. Burke and M. Ernzerhof, *Phys. Rev. Lett.*, 1996, **77**, 3865.
- [89] C. Lee, W. Yang and R. G. Parr, *Phys. Rev. B*, 1988, **37**, 785.
- [90] P. J. Stephens, F. J. Devlin, C. F. Chabalowski and M. J. Frisch, *J. Phys. Chem.*, 1994, **98**, 11623–11627.
- [91] C. Adamo and V. Barone, *J. Chem. Phys.*, 1999, **110**, 6158–6170.
- [92] M. Dion, H. Rydberg, E. Schröder, D. C. Langreth and B. I. Lundqvist, *Phys. Rev. Lett.*, 2004, **92**, 246401.
- [93] J. Klimeš, D. R. Bowler and A. Michaelides, *Phys. Rev. B*, 2011, **83**, 195131.
- [94] S. Grimme, *J. Comput. Chem.*, 2004, **25**, 1463–1473.
- [95] S. Grimme, J. Antony, S. Ehrlich and H. Krieg, *J. Chem. Phys.*, 2010, **132**, 154104.
- [96] E. Caldeweyher, S. Ehlert, A. Hansen, H. Neugebauer, S. Spicher, C. Bannwarth and S. Grimme, *J. Chem. Phys.*, 2019, **150**, 154122.
- [97] F. Bloch, *Z. Phys. A*, 1929, **52**, 555–600.
- [98] E. B. Wilson, J. C. Decius and P. C. Cross, *Molecular Vibrations: The Theory of Infrared and Raman Vibrational Spectra*, Courier Corporation, 1980.
- [99] H. B. Schlegel, *J. Comput. Chem.*, 2003, **24**, 1514–1527.
- [100] B. R. Johnson and W. P. Reinhardt, *J. Chem. Phys.*, 1986, **85**, 4538–4556.
- [101] R. T. Pack and G. A. Parker, *J. Chem. Phys.*, 1987, **87**, 3888–3921.
- [102] D. Petrascheck and F. Schwabl, *Elektrodynamik*, Springer Spektrum, 2019.
- [103] S. Carter and N. Handy, *Mol. Phys.*, 1982, **47**, 1445–1455.
- [104] T. Szidarovszky, A. G. Császár and G. Czakó, *Phys. Chem. Chem. Phys.*, 2010, **12**, 8373–8386.
- [105] J. K. Watson, *Mol. Phys.*, 1968, **15**, 479–490.
- [106] C. Eckart, *Phys. Rev.*, 1935, **47**, 552.

BIBLIOGRAPHY

- [107] C. Leforestier, *J. Chem. Phys.*, 1994, **101**, 7357–7363.
- [108] A. Chakraborty, D. G. Truhlar, J. M. Bowman and S. Carter, *J. Chem. Phys.*, 2004, **121**, 2071–2084.
- [109] V. Szalay, *J. Chem. Phys.*, 1993, **99**, 1978–1984.
- [110] D. T. Colbert and W. H. Miller, *J. Chem. Phys.*, 1992, **96**, 1982–1991.
- [111] J. Echave and D. C. Clary, *Chem. Phys. Lett.*, 1992, **190**, 225–230.
- [112] J. Tennyson, *J. Chem. Phys.*, 1993, **98**, 9658–9668.
- [113] J. M. Bowman, T. Carrington and H.-D. Meyer, *Mol. Phys.*, 2008, **106**, 2145–2182.
- [114] J. K. Cullum and R. A. Willoughby, *Lanczos Algorithms for Large Symmetric Eigenvalue Computations: Vol. I: Theory*, SIAM, 2002.
- [115] S.-W. Huang and T. Carrington Jr, *J. Chem. Phys.*, 2000, **112**, 8765–8771.
- [116] H. O. Karlsson and S. Holmgren, *J. Chem. Phys.*, 2002, **117**, 9116–9123.
- [117] I. Hamilton and J. Light, *J. Chem. Phys.*, 1986, **84**, 306–317.
- [118] S. Carter, J. M. Bowman and N. C. Handy, *Theor. Chem. Acc.*, 1998, **100**, 191–198.
- [119] L. S. Norris, M. A. Ratner, A. E. Roitberg and R. Gerber, *J. Chem. Phys.*, 1996, **105**, 11261–11267.
- [120] O. Christiansen, *J. Chem. Phys.*, 2004, **120**, 2149–2159.
- [121] L. Fredin, B. Nelander and G. Ribbegård, *J. Mol. Spectrosc.*, 1974, **53**, 410–416.
- [122] E. Knoezinger and P. Beichert, *J. Phys. Chem.*, 1995, **99**, 4906–4911.
- [123] A. Schriver, L. Schriver-Mazzuoli and A. A. Vigasin, *Vib. Spec.*, 2000, **23**, 83–94.
- [124] K. Jovan Jose and S. R. Gadre, *J. Chem. Phys.*, 2008, **128**, 124310.
- [125] M. W. Severson, *J. Chem. Phys.*, 1998, **109**, 1343–1351.
- [126] L. Wang and D. Xie, *J. Chem. Phys.*, 2012, **137**, 074308.
- [127] K. Mahjoubi, D. M. Benoit, N.-E. Jaidane, M. M. Al-Mogren and M. Hochlaf, *Phys. Chem. Chem. Phys.*, 2015, **17**, 17159–17168.

- [128] Y. Makina, K. Mahjoubi, D. M. Benoit, N.-E. Jaidane, M. M. Al-Mogren and M. Hochlaf, *J. Phys. Chem. A*, 2017, **121**, 4093–4102.
- [129] B. S. Ault and L. Andrews, *J. Am. Chem. Soc.*, 1976, **98**, 1591–1593.
- [130] B. S. Ault and L. Andrews, *Inorg. Chem.*, 1977, **16**, 2024–2028.
- [131] S. Riedel, T. Köchner, X. Wang and L. Andrews, *Inorg. Chem.*, 2010, **49**, 7156–7164.
- [132] F. A. Redeker, H. Beckers and S. Riedel, *RSC Adv.*, 2015, **5**, 106568–106573.
- [133] A. A. Tuinman, A. A. Gakh, R. J. Hinde and R. N. Compton, *J. Am. Chem. Soc.*, 1999, **121**, 8397–8398.
- [134] G. L. Heard, C. J. Marsden and G. E. Scuseria, *J. Phys. Chem.*, 1992, **96**, 4359–4366.
- [135] T. G. Wright and E. P. F. Lee, *Mol. Phys.*, 1993, **79**, 995–1009.
- [136] J. Czernek and O. Živný, *J. Chem. Phys.*, 2008, **129**, 194305.
- [137] P. A. Cahill, C. E. Dykstra and J. C. Martin, *J. Am. Chem. Soc.*, 1985, **107**, 6359–6362.
- [138] C. S. Ewig and J. R. Van Wazer, *J. Am. Chem. Soc.*, 1990, **112**, 109–114.
- [139] T. Kar and E. S. Marcos, *Chem. Phys. Lett.*, 1992, **192**, 14–20.
- [140] N. O. J. Malcolm and J. J. W. McDouall, *J. Phys. Chem.*, 1996, **100**, 10131–10134.
- [141] F. Mota and J. J. Novoa, *J. Chem. Phys.*, 1996, **105**, 8777–8784.
- [142] D. J. Tozer and P. Carlos, *Mol. Phys.*, 1997, **90**, 515–524.
- [143] B. Braïda and P. C. Hiberty, *J. Phys. Chem. A*, 2008, **112**, 13045–13052.
- [144] L. Andrews and X. Wang, *Phys. Chem. Chem. Phys.*, 2018, **20**, 23378–23385.
- [145] Z. Sun and H. F. Schaefer III, *Phys. Chem. Chem. Phys.*, 2018, **20**, 18986–18994.
- [146] D. Wang, D. Wang, L. Fu, J. Wang, G. Shi, Y. Li and X. Huang, *RSC Adv.*, 2019, **9**, 1929–1932.

BIBLIOGRAPHY

- [147] Z. Bihary, G. Chaban and R. Gerber, *J. Chem. Phys.*, 2002, **116**, 5521–5529.
- [148] A. Nakayama, K. Niimi, Y. Ono and T. Taketsugu, *J. Chem. Phys.*, 2012, **136**, 054506.
- [149] K. Niimi, A. Nakayama, Y. Ono and T. Taketsugu, *J. Phys. Chem. A*, 2014, **118**, 380–387.
- [150] M. Ryan, M. Collier, P. d. Pujo, C. Crépin and J. G. McCaffrey, *J. Phys. Chem. A*, 2010, **114**, 3011–3024.
- [151] J. Rezac and P. Hobza, *J. Chem. Theory Comput.*, 2013, **9**, 2151–2155.
- [152] J. Rezac and P. Hobza, *Chem. Rev.*, 2016, **116**, 5038–5071.
- [153] Z. Xie and J. M. Bowman, *J. Chem. Theory Comput.*, 2010, **6**, 26–34.
- [154] R. Hellmann, E. Bich and E. Vogel, *Mol. Phys.*, 2008, **106**, 133–140.
- [155] Z. Bihary, R. Gerber and V. Apkarian, *J. Chem. Phys.*, 2001, **115**, 2695–2701.
- [156] S. Goedecker, *J. Chem. Phys.*, 2004, **120**, 9911–9917.
- [157] F. E. Ben Mohamed, M. Slama, H. Hammami, M. Ben El Hadj Rhouma and M. Hochlaf, *J. Chem. Phys.*, 2015, **142**, 204309.
- [158] S. Jolkkonen, M. Pettersson and J. Lundell, *J. Chem. Phys.*, 2003, **119**, 7356–7364.
- [159] A. V. Bochenkova, V. E. Bochenkov and L. Khriachtchev, *J. Phys. Chem. A*, 2009, **113**, 7654–7659.
- [160] K. Patkowski and K. Szalewicz, *J. Chem. Phys.*, 2010, **133**, 094304.
- [161] K. Rościszewski, B. Paulus, P. Fulde and H. Stoll, *Phys. Rev. B*, 1999, **60**, 7905.
- [162] P. Schwerdtfeger, R. Tonner, G. E. Moyano and E. Pahl, *Angew. Chem. Int. Ed.*, 2016, **55**, 12200–12205.
- [163] A. C. Van Duin, S. Dasgupta, F. Lorant and W. A. Goddard, *J. Phys. Chem. A*, 2001, **105**, 9396–9409.
- [164] J. Behler and M. Parrinello, *Phys. Rev. Lett.*, 2007, **98**, 146401.
- [165] J. Behler, *Angew. Chem. Int. Ed.*, 2017, **56**, 12828–12840.

- [166] C. Schran, F. Uhl, J. Behler and D. Marx, *J. Chem. Phys.*, 2018, **148**, 102310.
- [167] B. Hartke, *Wiley Interdiscip. Rev. Comput. Mol. Sci.*, 2011, **1**, 879–887.
- [168] J. M. Dieterich and B. Hartke, *Mol. Phys.*, 2010, **108**, 279–291.
- [169] J. M. Dieterich and B. Hartke, *J. Comput. Chem.*, 2011, **32**, 1377–1385.
- [170] Z. Bacić and J. Light, *J. Chem. Phys.*, 1986, **85**, 4594–4604.
- [171] M. J. Bramley and N. C. Handy, *J. Chem. Phys.*, 1993, **98**, 1378–1397.
- [172] E. Catalano and D. E. Milligan, *J. Chem. Phys.*, 1959, **30**, 45–47.
- [173] J. Ceponkus, P. Uvdal and B. Nelander, *J. Chem. Phys.*, 2013, **138**, 244305.
- [174] P. M. Felker and Z. Bačić, *J. Chem. Phys.*, 2020, **152**, 014108.